The Dissertation Committee for **Kyriacos Agapiou** certifies that this is the approved version of the following dissertation:

Organometallic Precursors for Novel Material Design

COMMITTEE:

_____
Richard A. Jones, Supervisor

_____
Alan H. Cowley

_____
Bradley J. Holliday

_____
John G. Ekerdt

_____
Katherine A. Brown

Organometallic Precursors for Novel Material Design

by

Kyriacos Agapiou, B.S.; M.A.

Dissertation

Presented to the Faculty of the Graduate School

of The University of Texas at Austin

in Partial Fullfillment

of the Requirements

for the Degree of

Doctor of Philosophy

The University of Texas at Austin

December 2007

This dissertation is dedicated to my family

Acknowledgements

I wish to express my deepest gratitude to Professor Richard A. Jones who graciously provided me with the opportunity to complete my Ph.D. The guidance and mentorship he has provided during my time in his laboratories is truly priceless. Professor Jones's encouragement has assisted me greatly toward the completion of my studies. Additionally, I would like to thank Professors Bradley J. Holliday, Allan H. Cowley, John G. Ekerdt and Katherine A. Brown for all of their help and kind suggestions related to my research.

I would also like to thank my coworkers and others who assisted me on projects described in this thesis. These include Dr. Xiaoping Yang, Joseph Rivers, Jeffrey McCarty, Lauren DePue, Michelle Mejia and Jinhong Shin.

I give many thanks to all of the good friends I have made during my time in Austin, TX. I will never forget the great times we have spent together here and the encouragement you all have given me.

Finally, I am grateful to my father and mother, Agapios K. and Ana Agapiou, and my sister, Teresa, who have continually supported me through my studies at The University.

Organometallic Precursors for Novel Material Design

Kyriacos Agapiou, Ph.D.

The University of Texas at Austin, 2007

Supervisor: Richard A. Jones

As part of a broad program directed toward the discovery of inorganic and inorganic-organic hybrid materials that exhibit interesting and/or useful properties (e.g. electronic, photonic, magnetic, etc.), several distinct projects dealing with the identification and synthesis of novel organometallic complexes have arisen. The unveiling of such metal-complexes or new applications for existing complexes adds to the repertoire of candidates that may be incorporated into or used to generate new materials. The research conducted addresses (1) the design of precursors for the chemical vapor deposition (CVD) growth of amorphous metallic alloys, (2) the design, synthesis, and study of a novel class of polymerizable organometallic precursors for heterocomposite photovoltaic materials and (3) the preparation of triazolato ruthenium complexes *vis-à-vis* "click" cycloaddition chemistry.

Table of Contents

List of Figures

List of Schemes

List of Tables

Chapter 1: The Synthesis and X-ray Crystal Structures of Polymerizable Schiff Base Metal Complexes: Precursors for Hybrid Photovoltaic Materials

1.1. Introduction

Efforts to relieve our emerging local, national and global energy crisis are of great importance as the demand for fossil-fuel based resources increases and supplies diminish. Reliance on such resources has profound environmental and political consequences among other significant impacts. Renewable energy sources, which utilize naturally replenished resources such as sunlight, wind, tides and geothermal heat, provide a potentially powerful and environmentally benign alternative. Renewable energy technologies range from hydroelectricity and wind power to biomass and biofuels, however, none of these show more promise than solar power. Enough energy (4.3×10^{20} J) to power the world for a year strikes the Earth each hour in the form of solar energy.[1] The conversion of solar energy has direct implications for several avenues of energy use, and none are more promising than the direct conversion of sunlight into electricity. This process may be achieved through a process known as the photovoltaic effect. Currently, electricity generated from photovoltaic devices accounts for a very small percentage of the total electricity produced, and also

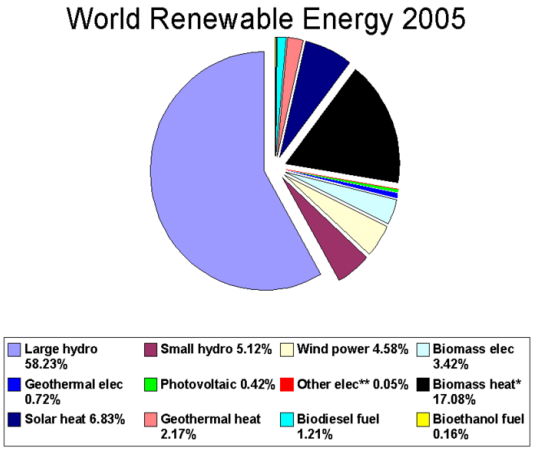

Figure 1.1. Renewable energy sources worldwide in 2005 (2004 for items marked * or **).

represents a small percentage of energy derived from all renewable sources (Fig. 1.1). This is primarily a result of the high cost and low overall efficiency of existing photovoltaic materials and devices. The energy conversion efficiency (ECE) is the most important parameter with which to measure the overall performance of a PV device. The ECE is the ratio between the amount of electrical power collected and converted and the possible energy available. At the present, the best commercially available PV cells are made from polycrystalline silicon and have an energy conversion efficiency of approximately 12 %. The cost of these cells is $3 per Watt of power generated under terrestrial standard solar conditions (AM 1.5G).[2] These costs must be reduced by an order of magnitude to near $0.3 per Watt in order for PV devices to compete with other energy generation systems and to be manufactured on a large scale.[2] Despite such limitations, the solar electricity market commands a $7.5 billion industry that is growing at a rate of 35-40% each year.[1] Thus, there is substantial motivation toward the development of efficient, inexpensive PV devices that can exploit solar power.

1.1.2. General Structure and Operating Principles

The general structure used for solar cells resembles that of a light emitting diode (LED). The devices are constructed in a "sandwich" geometry (Fig. 1.2). The substrate electrode, or back contact, covers the entire back surface and acts as a conductor. This can be made of metal, but may also be plastic or glass covered with a suitable material. The active layer is a specially treated, light absorbing semiconductor material that absorbs photons and generates electrons via the photovoltaic effect. The materials utilized in PV cells have the ability to preferentially absorb the wavelengths of solar light

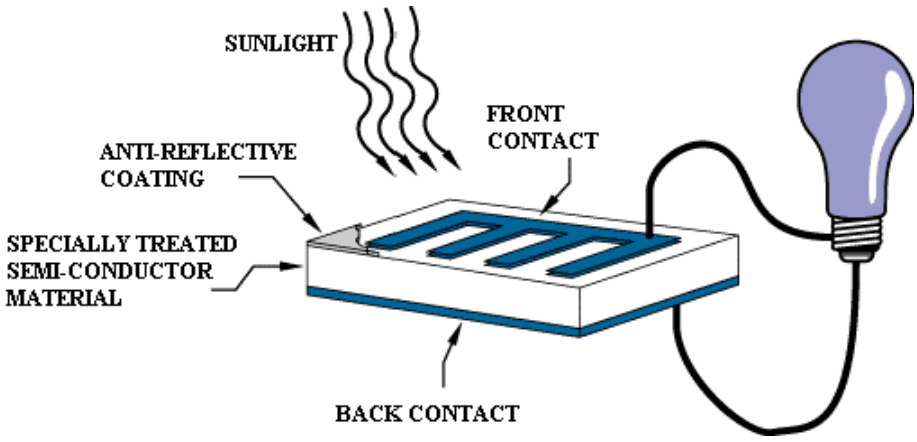

Figure 1.2. Basic structure of a photovoltaic device.

that can reach the surface of the Earth. Some solar cells, however, are optimized for light absorption beyond Earth's atmosphere as well. The region in the solar cell where the n- and p-type layers meet, the p-n junction, is found in the active layer. At the p-n junction, current will flow readily in one direction (forward bias) but not in the other (reverse bias). Common PV cells utilize bulk semiconducting material such as silicon in the active layer; however, combinations of semiconducting materials, used by heterojunction PV cells, offer an interesting alternative. The active layers are typically coated using solution or vacuum deposition techniques. The anti-reflective coating (AR coating) above the active layer serves to guide light into the PV cell through a combination of a favorable refractive index and thickness. Without this layer, much of the light entering the PV cell would bounce off the surface prior to being absorbed. The front contact is made of a good conductor, such as a metal, and it serves as a collector of electrons. In general, a lower work-function metal (as compared to the back contact) is used. Not shown in

Figure 1.2 is the encapsulate which is typically made of glass or another transparent material such as plastic and seals the PV cell from the external environment.

A number of PV cells, like those described above, electrically connected to each other and mounted in a support structure or a frame is referred to as a photovoltaic module (Fig. 1.3). Modules are designed to provide electricity at a certain voltage, such as a common 12 volt system. The current supplied is directly dependent on how much light strikes the module. Wiring multiple modules together forms an array. In general, the larger the area of a module or array, the greater the amount of electric power generated. Photovoltaic modules and arrays produce direct-current (dc) electricity, and can be connected in both series and parallel electrical arrangements to produce a number of voltage and current combinations.

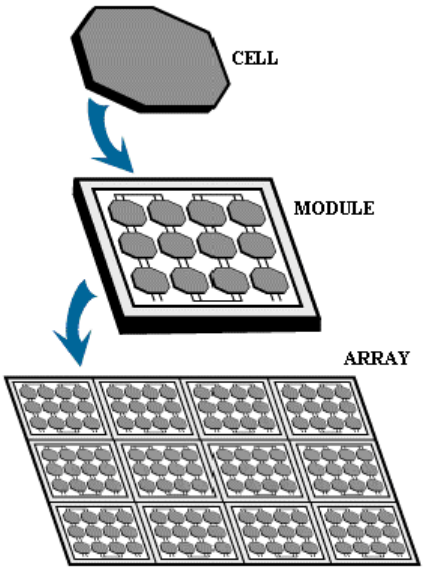

Figure 1.3. PV cell, module and array used to generate electricity.

The process involved to convert light to electricity by a PV cell can be described by the following steps: (1) absorption of a photon leading to the formation of an excited state, or generation of the bound electron-hole pair commonly referred to as an exciton, (2) exciton diffusion to a region where the exciton dissociates, i.e. charge separation occurs, and (3) transport of charge within the semiconductor to the respective electrodes.[3] The sun's energy arrives on Earth as radiation distributed across the spectrum from

infrared to ultraviolet. The energy of this radiation can be captured as excited electron-hole pairs in a semiconductor, a dye, or a chromophore, or as heat in a thermal storage medium. Excited electrons and holes can be tapped off for immediate conversion to electrical power. To optimize the performance of PV cells, the desirable processes: *1*. light absorption, *2*. exciton diffusion, *3*. forward electron transfer, and *4*. charge transport to the electrodes (Fig. 1.4a) must be maximized, and the undesirable recombination processes: *5*. geminate recombination and *6*. back electron transfer (Fig. 1.4b) should be

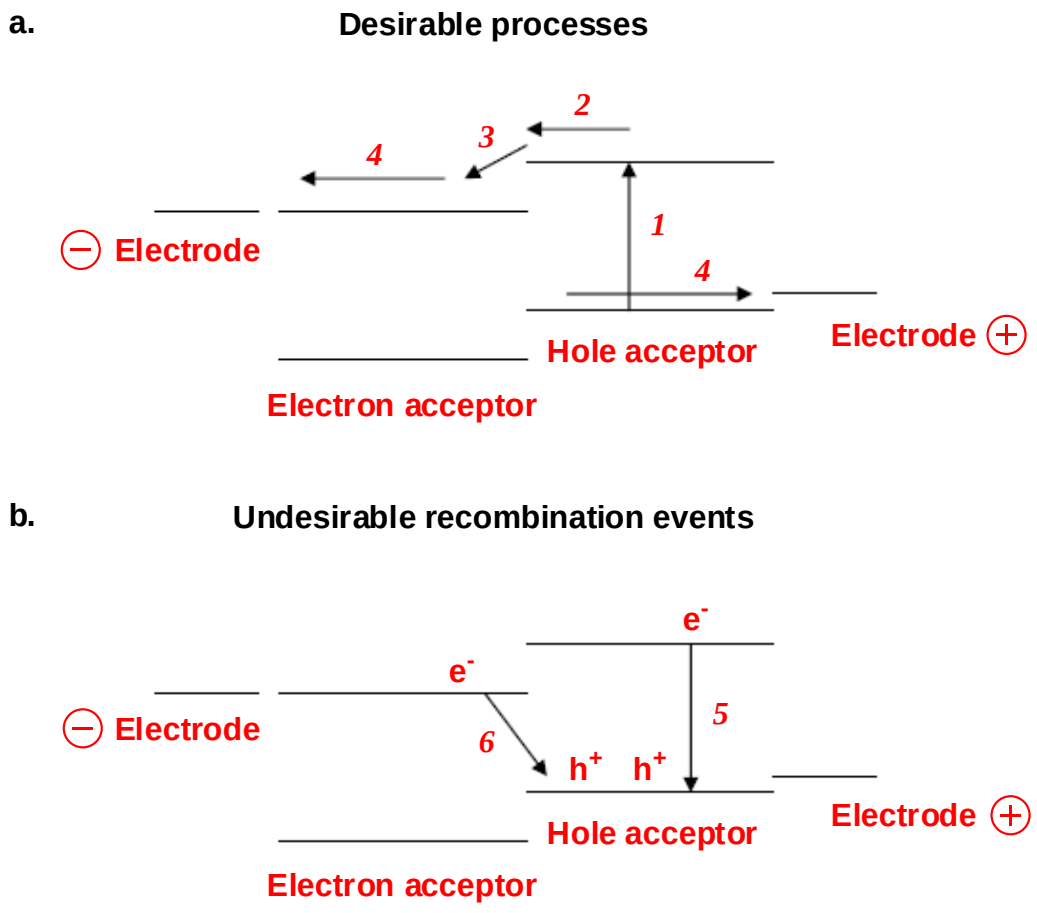

Figure 1.4. Schematic diagram of the energy levels in a heterojunction PV cell and the electronic processes (*1-6*, defined in the text) that occur.

minimized.[2] This kind of optimization may be obtained through improvement of charge carrier mobility and by slowing the rate of back electron transfer so that photogenterated charge carriers can escape from the film prior to recombination, while maintaining proper layer dimensions. A thick enough film must be maintained to allow most of the light to be absorbed. In a typical heterojunction PV cell, dimensions of phase separation between the active materials have to be within the exciton diffusion length (~10 nm) in order to avoid undesirable recombinations.

1.1.3. Semiconducting PV Materials

All PV cells must employ a light absorbing material contained within the structure of the cell to absorb photons and then generate electrons via the photovoltaic effect. Materials used in PV cells preferentially absorb the wavelengths of solar light that reach the surface of the earth. Much effort has gone into and is currently going into the pursuit of new materials. The ideal PV cell requirements are:[4]

- bandgap between 1.1 and 1.7eV;
- direct band gap structure;
- consisits of readily available, nontoxic materials;
- easy, reproducible deposition technique, suitable for large area production;
- good photovoltaic conversion efficiency;
- long-term stability

Multiple physical configurations of light absorbing materials can be used to take advantage of different light absorption and charge separation mechanisms. Many PV cells currently available are configured as *bulk* materials that are subsequently cut into wafers. These wafers are typically connected together to form a PV cell module. *Thin-film* configurations can also be utilized and are commonly associated to inorganic layer,

organic dye and organic polymer PV cells deposited on supporting substrates. Other materials are configured as *nanocrystals* and harness quantum dots contained within a supporting matrix.

Bulk Material PV Cells: Silicon. Crystalline silicon (*c*-Si), also referred to as "solar grade silicon" is, by far, the most prevalent bulk material used for PV cells. Despite the complicated manufacture and the high cost, crystalline *c*-Si still dominates the market and will probably continue to do so in the near future.[4] This is primarily a consequence of the abundant supply of raw silicon, the feasibility of high efficiencies and low environmental impact. Furthermore, *c*-Si exhibits little to no degradation. Together, the various forms of *c*-Si account for 87.6% of the market share of different PV materials - significantly more than the combined share of non-crystalline forms of silicon and other materials such as cadmium telluride (CdTe).[4] One major drawback to silicon is that it is an indirect band gap semiconductor. Semiconductors with an indirect band gap have valence band maximum and conduction band minimum that are not opposite to each other across the band gap (Fig. 1.5). Because of this, silicon and other indirect semiconductors are inefficient at emitting light. Furthermore, light absorption is weaker than in a direct band gap semiconductor, the

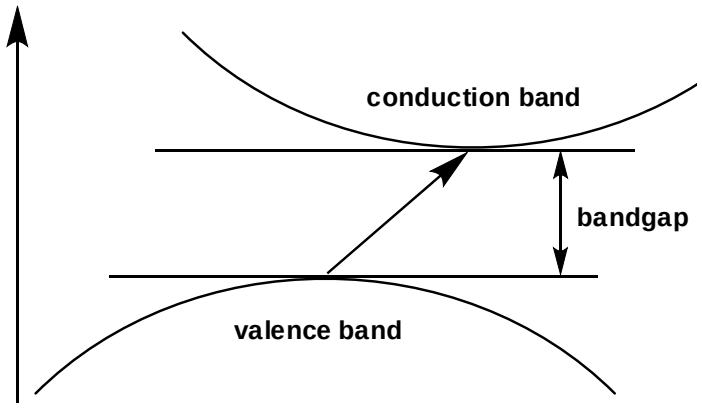

Figure 1.5. Indirect bandgap semiconductor.

valence band maximum and conduction band minimum of which are directly opposite one another. This has serious consequences from a PV materials point of view.

Organic Solar Cells: Conjugated Polymers. Alternatives to silicon PV cells include cells made from organic materials, such as conjugated organic polymers, and cells containing inorganic-organic blend materials. Devices from these types of materials offer the potential for high efficiencies, can be produced on flexible substrates, and are comparatively inexpensive. Organic solar cells are built from thin films (~ 100 nm) of organic semiconductors such as conjugated polymers and small-molecule compounds like polyphenylene vinylene, poly-hexylthiophene, copper phthalocyanine (a blue or green organic pigment) and carbon fullerenes. The main structural feature present in these materials is an extended π-system in the backbone. Solution-processable conjugated polymer-based solar cells are attractive for the production of inexpensive alternatives with solar power efficiencies up to 2.5%.[5] Conventional inorganic solar cells, however, commonly exhibit solar power conversion efficiencies of 10%.[5] Further, the external quantum efficiency (EQE) of single-layer organic PV cells is only up to 1%.[6] The poor efficiency has been attributed to the low dissociation probability of excitons and the inefficient hopping carrier transport.[7] Bilayer organic PV cells have been reported, but typically show only slight improvements over pure polymer films, mostly owing to problems regarding exciton diffusion.[6]

Bulk Heterojunction PV Cells. One way to resolve such problems is found through the use of bulk heterojunction PV cells. Bulk heterojunction cells incorporate an interpenetrating network of electron-accepting and hole-accepting components within the

device (Fig. 1.6).[8] In such a blended network, the donor-acceptor phase separation is small and, thus, each interface lies within a distance less than the exciton diffusion length from the absorbing site. As a result, these types of cells exhibit a large donor-acceptor interfacial area that facilitates the dissociation of photogenerated excitons by electron transfer and gives improved efficencies. Bulk heterojunction PV cells of regioregular poly(3-hexylthiophene) (RR-P3HT) and (6,6)-phenyl C_{61}-butyric acid methyl ester (PCBM) (PCMB) have been reported to give EQE near 75% and power conversion efficiencies up to 5%.[9,10] It is worth noting that, as a result of the importance of the blended interface, bulk heterojunction devices are sensitive to the nanoscale morphology of the interpenetrating network.

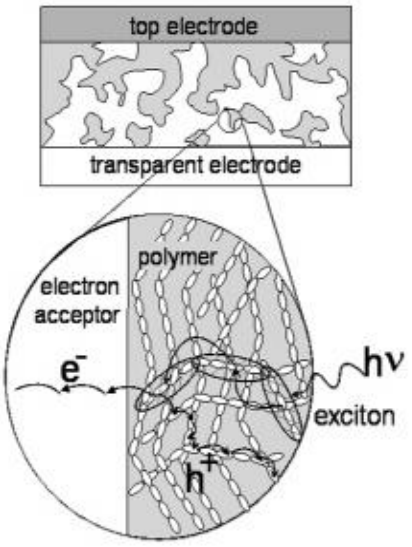

Figure 1.6. Disordered bulk heterojunction PV cell.

Two types of materials utilized in heterojunction cells are (a) polymer-polymer blends and (b) polymer-nanoparticle blends. Bulk heterojunction cells made up of two conjugated polymers are advantageous for several reasons. Both components of the conjugated polymer blend can exhibit a high optical absorption coefficient and cover complementary parts of the solar spectrum. Additionally, both components can relatively easily and individually be tuned to optimize optical properties, charge transfer, and

charge collection processes. A drawback, however, is that the phases in these polymer blends have an intrinsic tendency to separate. These phase-separated domains typically have dimensions of several micrometers making them too large in comparison to exciton diffusion length limitations for polymeric cells. It is therefore necessary for the polymer/polymer bulk heterojunction concept to identify appropriate n-type polymers with electron-acceptor properties and good stability.[11]

Polymer-nanoparticle blends known as hybrid solar cells consist of a combination of both organic and inorganic semiconducting materials. Hybrid cells combine the advantageous properties of both inorganic semiconductors and organic polymers.[12] Organic materials, such as conjugated polymers, are typically inexpensive, adaptable through molecular design and chemical synthesis, and can be processed easily. Inorganic nanoparticle semiconductors offer the ability for band gap and absorption/emission spectra modification by varying the size and shape of the individual nanoparticles. Utilizing blends of nanocrystals with semiconductive polymers as the bulk heterojunction material is an effective strategy for hybrid solar cell fabrication.[3] In a hybrid composite thin film, photogenerated excitons dissociate into free charge carriers very efficiently at the polymer-nanoparticle interface. Hybrid solar cells containing several types of nanocrystals including CdSe, CdS, $CuInS_2$, and PbS in conjugated polymer blends have been demonstrated.[7,8,13]

One problem inherent to hybrid PV cells involves the solubility of the n-type and p-type components.[3] While organic semiconductors are commonly dissolved in organic solvents, aqueous solvents are typically used to dissolve inorganic semiconducting

nanoparticles. By incorporating suitable organic ligands, however, the solubility of the nanoparticles in common organic solvents can be enhanced. These organic capping ligands, typically introduced during synthesis, are also employed to prevent aggregation and oxidation by shielding the nanoparticles. Consequently, solution properties and dispersion of the nanoparticles in the polymer matrices are affected by such incorporation.[14,15] Furthermore, the organic ligand impedes charge transport from nanoparticle to nanoparticle. Thus, for the hybrid cell to achieve intimate electrical contact between the nanoparticles, the capping ligands must be removed. [16,17]

To overcome the interface limitations exhibited by conventional polymer-nanoparticle heterojunction PV cells it is necessary to consider the device architecture. The bulk heterojunction devices discussed above contain mixtures of conjugated polymer and electron acceptor that are randomly interspersed throughout the film. This random distribution of materials can lead to electron trapping processes and incomplete exciton dissociation in regions of the polymer that are longer than an exciton diffusion length (10-20 nm)[3] from the acceptor material. These negative processes reduce efficiencies overall. Researchers have attempted to resolve these issues by developing well-ordered conjugated polymer-electron acceptor materials (Fig. 1.7). An ideal well-ordered structure would allow each exciton formed in the donor to be within a diffusion length of the electron

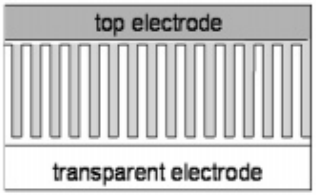

Figure 1.7. Well-ordered bulkheterojunction PV cell. The donor-acceptor phase interspaced distance must be near 10-20 nm or less than the exciton diffusion length.

acceptor. Additionally, all charge carriers have an uninterrupted pathway to the electrodes, and polymer chains are aligned to increase their charge carrier mobility. A well-ordered nanostructure, however, is difficult to achieve in typical polymer mixtures due to disorder. Highly interdisciplinary research amongst various areas of chemistry, physics and process engineering must be employed to take full advantage of this well-ordered strategy.

Nanoparticle-containing Conjugated Polymers. In order to take full advantage of the potential held by bulk heterojunction devices issues regarding the donor-acceptor interface must be addressed. One strategy adopted to remedy or even eliminate such interfacial limitations seeks to design new semiconducting materials which embed inorganic nanoparticles directly bonded into the conjugated polymer. A π-conjugated polymer or molecule serving as a linker between nanoparticles can act as a "molecular wire" and enhance coupling between adjacent particles.[18] Peng, et al. and Wolf, et al. have independently reported polythiophene-Au nanoparticle systems that showed increased conductivity when compared to the conjugated polymer alone (Fig. 1.8).[19]

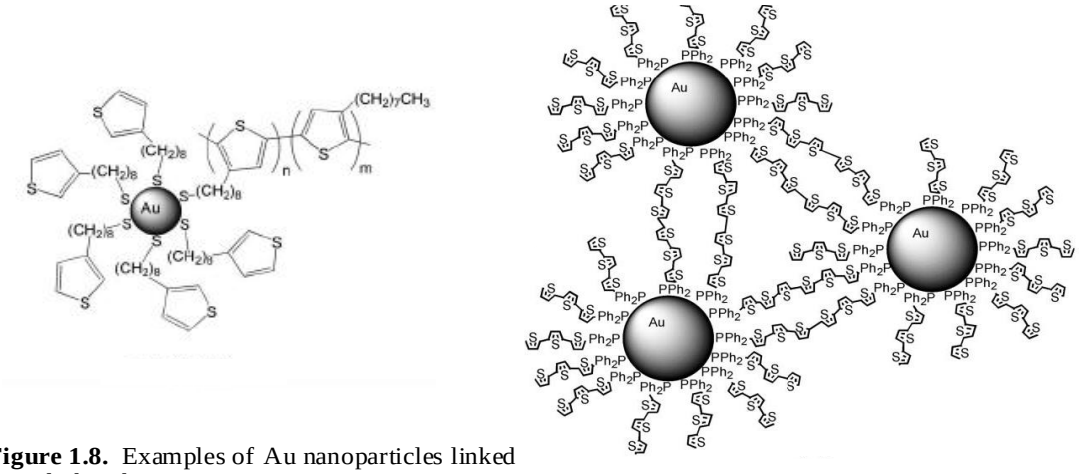

Figure 1.8. Examples of Au nanoparticles linked by polythiophene matrices

These Au nanoparticle-polythiophene systems where generated by capping the Au nanoparticles with oligothiophene units upon formation. Another way to implement such a strategy requires the design of metal complexes incorporating polymerizable organic ligands. Nanocrystals can subsequently be grown at the metal nucleation sites embedded directly within the polymer backbone. This technique hinges on the ability to synthesize and isolate stable complexes of metals which can lead to the growth of usable nanocrystals for the purpose of harvesting solar energy. The organic ligands should contain polymerizable moieties and exhibit suitable conjugation to enable charge transport.

A broad program conceived by Professor Bradley J. Holliday addresses the design and testing of new photovoltaic devices based on the "seeded growth" of semiconductor nanoparticles within a conducting polymer matrix. Specifically, several novel Schiff base metal complexes have been discovered that contain polymerizable thiophene and bithiophene moieties in their ligand system. Complexes of cadmium (Cd) and copper (Cu) will be described herein although complementary work by Joe Rivers has produced interesting complexes of gallium (Ga) and lead (Pb). The Cd and Cu systems have been shown to undergo suitable electropolymerizations to provide metal-containing polythiophenyl films and evidence has been obtained demonstrating the "seeded growth" of CdS nanocrystals and the ternary nanomaterial $CuGaS_2$ respectively. This work, performed by Michelle Mejia, in the Holliday group will not be described in detail in this thesis. This methodology should lead to materials with *no interfaces* between the key components, thus differentiating themselves from conventional systems based on organic

polymers and inorganic semiconductors. Upon optimization, devices incorporating these materials should exhibit superior photovoltaic properties.

1.2. Results and Discussion

One of the key goals *en route* to the development of the above described class of PV materials is the preparation of molecules which have both metal binding sites as well as functional groups that are capable of undergoing appropriate polymerization reactions. The "salen" class of Schiff base (SB) ligands was initially chosen for binding to metal ions since our research group already has expertise with this type of ligand (Scheme 1.1).[20] Indeed, SB ligands have proven to be an excellent choice for demonstrating the feasibility of this approach.

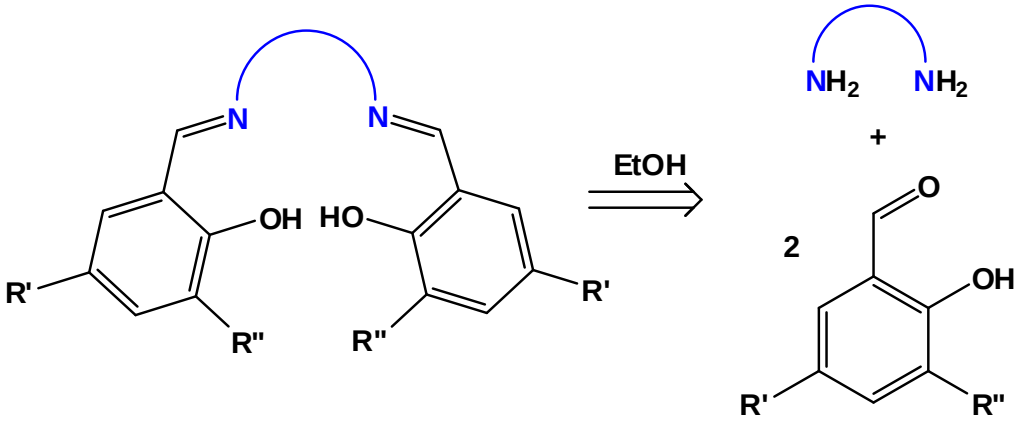

Scheme 1.1. Retrosynthetic scheme for the preparation of "salen" Schiff base ligands.

Schiff base ligands are inexpensive, easy to prepare and many variations in their metal binding properties can be achieved through synthetic means. They may be readily

obtained in good yield as a precipitate from the condensation of a suitable diamine with the corresponding salicylaldehyde derivative in alcoholic solvent, as shown in Scheme 1.1. Since several SB complexes of Cd^{2+}, Ga^{3+} and Pb^{2+} have already been reported [21,22,23] it was reasonable to assume that metal complexes of the ligands suitably modified for subsequent electropolymerizations could be prepared.

Metal complexes incorporating polymerizable substituents such as thiophene or bithiophene groups can be converted to conducting polymeric films by careful potentiodynamic electropolymerizations. Thiophene moieties were selected to append to the SB-metal complexes because they are easily polymerizable through electrochemical means, the resulting polymer chains are electrically conductive and the thiophene groups may be incorporated into the ligand framework through established synthetic methods such as Pd-catalyzed aryl-aryl couplings (i.e. Stille, Suzuki reactions). The formation of nanocrystals of CdS and CdSe by a variety of methods is now fairly well-established. Therefore the preparation of Cd-SB complexes was initially undertaken with the intention of demonstrating nanocrystalline CdS growth at the metal sites. The metal atoms situated within the polymerized films are firmly bound by the surrounding ligand framework which establishes excellent electrical contact with the conducting polymer. The metal sites can therefore serve as nucleation centers or "seed points" for the growth of nanocrystals of the desired semiconductors. Upon growth, nanocrystals of inorganic semiconducting materials are “directly wired” into the conducting polymer matrix. Due to this direct wiring, the formation of an interface between the organic conducting polymer and the inorganic nanocrystals is avoided. The donor-acceptor interface is often

considered to be a problematic issue and a major limitation in the performance of conventional heterocomposite organic polymer/inorganic nanocrystal-based PV devices.[5,24]

1.2.1. Model Cadmium-Schiff Base Complexes

A series of model SB complexes of Cd^{2+} of general formula $L^n{}_xCd_y$ (**1-I** – **1-III)** was initially prepared. The SB ligands lack polymerizable bithiophene substituents

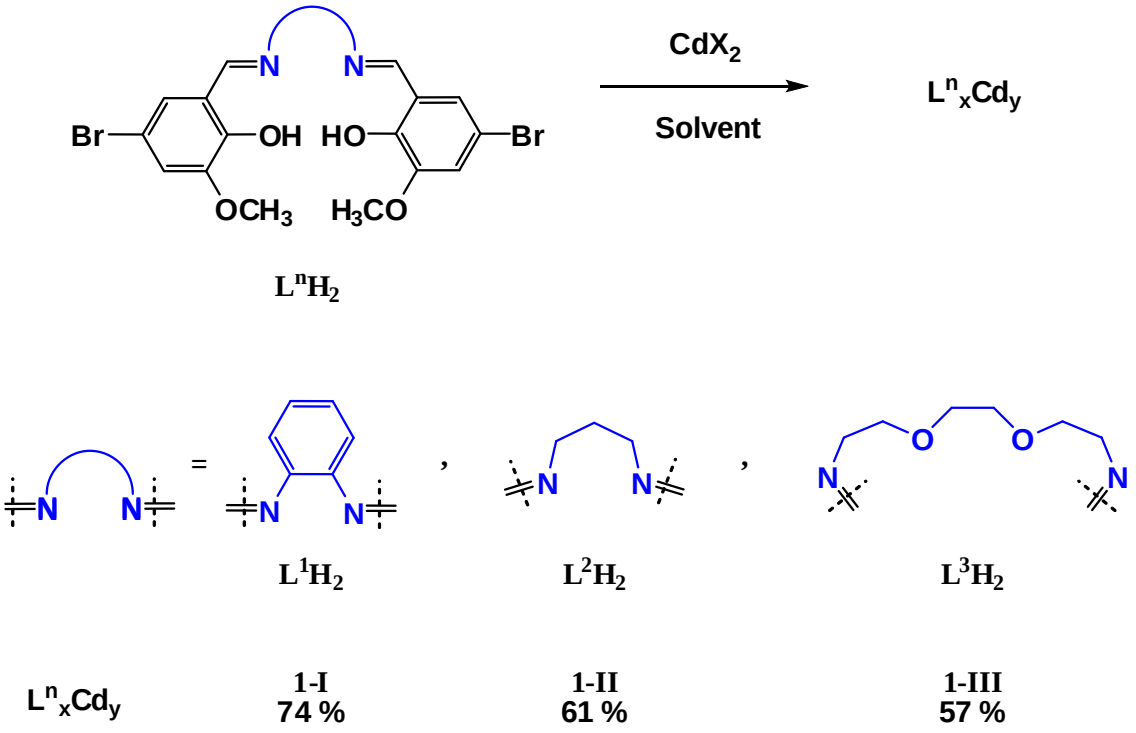

Scheme 1.2. Synthetic route to nonpolymerizable Cd-SB complexes **1-I** - **1-III**.

(Scheme 1.2, Table 1.1). These complexes were intended to provide key information regarding the coordination environments and geometries required by Schiff bases that feature electro-polymerizable bithiophene groups. Additionally, spectroscopic studies on

Table 1.1. Conditions for the preparation of nonpolymerizable Cd-SB complexes **1-I – 1-III**.

$L^n_xCd_y$	L^nH_2	CdX_2	Solvent	[ ]	T	t	Xtals obtained by…
1-I	L^1H_2	$Cd(OAc)_2$	EtOH	0.01 M	78 ºC	15 min	slow evaporation
1-II	L^2H_2	$Cd(OAc)_2$	MeOH	0.01 M	65 ºC	1 h	vapor diffusion
1-III	L^3H_2	$Cd(OAc)_2$	MeOH	0.01 M	65 ºC	1 h	vapor diffusion

these complexes should provide valuable benchmark data from which to compare the subsequent characterization of metal containing conducting polymer films. For the prepared Cd^{2+} complexes, compounds containing two, three and four metal ions have been isolated and characterized illustrating the very versatile nature of Schiff base complex chemistry.

$L^1_2Cd_2$·2(MeOH) (1-I). Reacting Schiff base **L^2H_2** with $Cd(OAc)_2$·$2H_2O$ (1:1) in EtOH under reflux gave the dinuclear complex $L^1_2Cd_2$·2(MeOH), **1-I**, in 74% yield. Adjusting the stoichiometry of the reaction to match the L:Cd ratio found in the product had no affect on the yield. The complex is sparingly soluble in polar organic solvents such as $CHCl_3$, MeOH and MeCN. Spectroscopic data is consistent with the structure observed in the solid state. Thus the ^{1}H NMR spectrum in CD_3CN shows peaks assigned to both L and MeOH protons.

Numerous crystallization techniques were explored in order to obtain X-ray quality crystals of this dinuclear Cd_2 complex. The most successful of these was found to be slow evaporation of the reaction filtrate over several days. Compound **1-I** crystallizes in the triclinic space group P1 with one molecule per unit cell (Fig. 1.9). Crystallographic

details are given in Table 1.2 and key bond lengths and angles in Table 1.3. The overall molecular framework contains a central Cd_2 core in which the Cd atoms are coordinated by the N_2O_2 atoms of the Schiff base ligands and by one methoxy (OMe) group of each ligand. The Schiff base ligands contain a planar benzene backbone which enforces near planarity throughout each ligand framework. The Cd atoms are located between the Schiff base ligands deviating from the N_2O_2 plane by 0.963 Å. The Cd…Cd distance is 3.497 Å. The structural configuration of **1-I** results in each Cd atom adopting a seven-coordinate distorted pentagonal bipyramidal geometry. The average Cd-N and Cd-O(phenolic) distances are 2.333 and 2.261 Å respectively and are comparable to those found in other Schiff base complexes of Cd.[25] The two coordinated MeOH molecules point away from one another on opposite sides of the ligand framework in an *anti* fashion. The average Cd-O(HMe) distance is 2.436 Å.

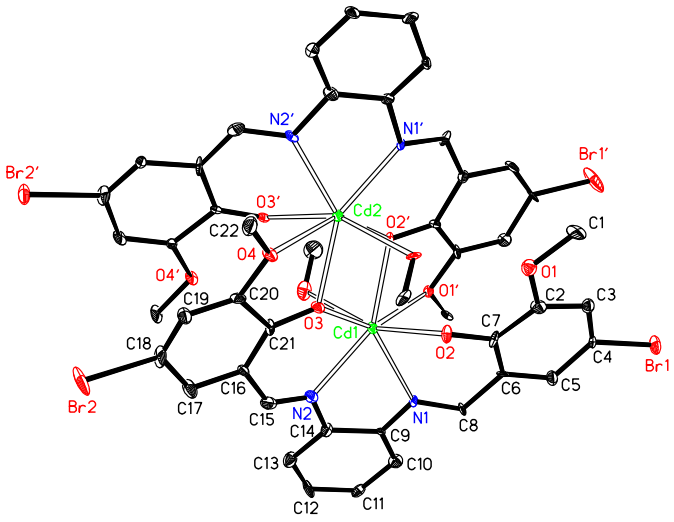

Figure 1.9. Crystal structure of **1-I** with hydrogen atoms omitted for clarity. Thermal ellipsoids are drawn at the 25 % probability level.

$L^2_2Cd_3(OAc)_2\cdot(Et_2O)\cdot2(MeOH)$ (1-II). Reaction of the dibromo substituted Schiff base **L^2H_2**, featuring a propylene backbone, with $Cd(OAc)_2\cdot2H_2O$ (1:1) in MeOH under reflux gave good yields of the trinuclear complex $L^2_2Cd_3(OAc)_2\cdot(Et_2O)\cdot2(CH_3OH)$, **1-II**. Changing the stoichiometry of the reaction to match the L:Cd ratio found in the

product did not affect the yield. The complex is sparingly soluble in polar organic solvents such as CH_2Cl_2, MeOH and MeCN. Spectroscopic data is consistent with the structure observed in the solid state. Thus the ^1H NMR spectrum in CD_3CN shows peaks assigned to both L and OAc protons.

Several different crystallization techniques were screened in order to obtain X-ray quality crystals of this complex. The most successful of these involved vapor diffusion of Et_2O into saturated MeOH solutions. The structure described here crystallized with two MeOH and one Et_2O. Compound **1-II** crystallizes in the monoclinic space group P2(1)/n with four independent molecules per unit cell (Fig. 1.10). Crystallographic details are given in Table 1.2 and key bond lengths and angles in Table 1.4. The molecular framework contains a central Cd_3 core in which the terminal Cd atoms are coordinated by the N_2O_2 atoms of the Schiff base ligands. Additionally, one OMe group from each ligand coordinates to the central Cd atom through their oxygen atoms. The Cd_3 core is nearly linear with a Cd(1)-Cd(3)-Cd(2) angle of 171.1° and exhibits a Cd…Cd distance of 3.571 Å.. The Schiff base ligands contain a relatively flexible three carbon backbone and are folded about the central CH_2 group so that they have a V-shaped configuration. The terminal Cd atoms are

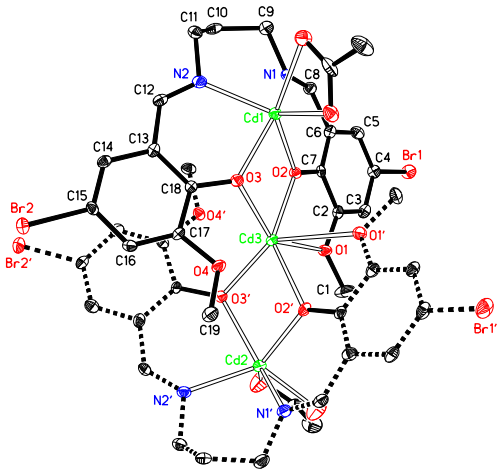

Figure 1.10. Crystal structure of **1-II** with hydrogen atoms omitted for clarity. Thermal ellipsoids are drawn at the 25 % probability level.

located slightly above the N_2O_2 plane by 0.887 Å and the dihedral angle between each half of the ligand is 130.3°. The terminal Cd atoms are each bonded to a bidentate acetate unit. This configuration results in a six-coordinate trigonal prismatic geometry for the terminal Cd atoms. The central Cd atom also resides in a six-coordiante trigonal prismatic coordination environment. The average Cd-N and Cd-O(phenolic) distances are 2.280 and 2.266 Å respectively and are comparable to those found in other Schiff base complexes of Cd.[21] The average Cd-O(OAc^-) distance is 2.358 Å.

$L^3{}_2Cd_4(OAc)_4$ (1-III). Reaction of the Schiff base **L^3H_2** with $Cd(OAc)_2{\cdot}2H_2O$ (1:1) in MeOH under reflux gives the tetranuclear complex $L^2{}_2Cd_4(OAc)_4$, **1-III**, in 57% yield. The complex was found to be sparingly soluble in polar organic solvents such as $CHCl_3$ and MeOH. Spectroscopic data is consistent with structure observed in the solid state. Thus the ^1H NMR spectrum in $CDCl_3$ shows peaks assigned to both L and OAc protons. The IR spectrum features bands corresponding to both bridging and bidentate OAc groups at 1646 and 1533 cm^{-1}, respectively.

A variety of different crystallization techniques to obtain X-ray quality crystals were explored. The best method was found to be vapor diffusion of Et_2O into saturated MeOH solutions. The structure described here crystallized with an additional unidentifiable moiety in the unit cell which prevented the complete assignment of crystallographic parameters (Fig. 1.11). However, structural features were determined for the Cd_4-containing unit and are reported here. Key bond lengths and angles are given in Table 1.5. The molecular framework contains a central Cd_4 core in which the Cd atoms are engaged in a complex coordination environment by the N_2O_2 atoms of the Schiff base

moieties and the OMe groups of the ligands. The Cd_4 core is essentially planar and exhibits an average Cd…Cd distance of 3.585 Å. The Schiff base ligands contain a flexible acyclic $C_6H_{12}O_2$ backbone which bends about the central OC_2H_4O group. Two bidentate and two bridging acetate groups are present in the complex. The average Cd-O(OAc^-)$_{bidentate}$ distance is 2.479 Å and the average Cd-O(OAc^-)$_{bridging}$ distance is 2.321 Å. This configuration results in a seven-coordinate pentagonal biprismatic geometry for the core Cd atoms. The average Cd-N and Cd-O(phenolic) distances are 2.272 and 2.283 Å respectively and are comparable to those found in other Schiff base complexes of Cd.[21]

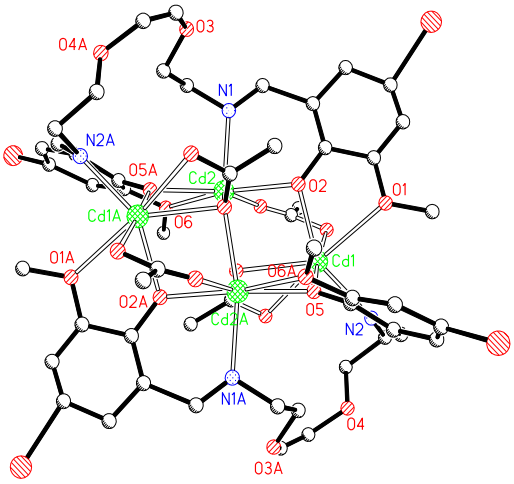

Figure 1.11. Crystal structure of **1-III** with hydrogen atoms omitted for clarity. Thermal ellipsoids are drawn at the 25 % probability level.

1.2.2. Bithiophene Substituted Cadmium-Schiff Base Complexes

The synthesis and isolation of polymerizable Cd-SB complexes was pursued next. Michelle Mejia of the Holliday group found success in employing Pd-catalyzed Stille aryl-aryl coupling chemistry to functionalize salicylaldehyde derivatives with polymerizable bithiophene substituents (Scheme 1.3). Thus, 5-bromosalicylaldehyde reacts with 2-(tributylstannyl)bithiophene under Stille conditions using $PdCl_2(PPh_3)_2$ as a catalyst to give the 5-substituted bithiophene-salicylaldehyde adduct **1-IV** in 79% yield.

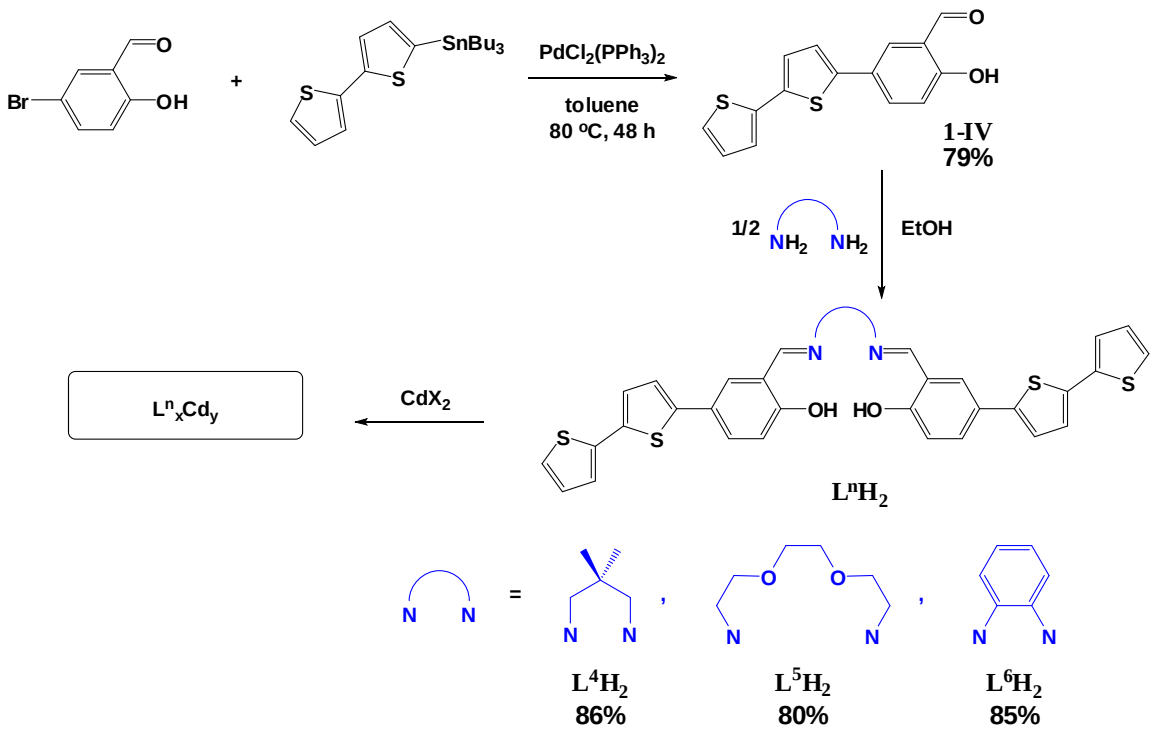

Scheme 1.3. Preparation of bithiophene substituted SB ligands.

Good yields of ligands $\mathbf{L^4H_2}$-$\mathbf{L^6H_2}$ were obtained upon condensation of two equivalents of **1-IV** with the appropriate diamine. Reacting these bithiophene-SB ligands with suitable Cd^{2+} salts gave polymerizable Cd-SB complexes that are described hereafter. Polymerizable Cd-SB complexes were obtained from reactions utilizing $\mathbf{L^4H_2}$ and $\mathbf{L^5H_2}$. We were not able to isolate polymerizable Cd-SB complexes in reactions employing $\mathbf{L^6H_2}$.

$L^4_2Cd_3(OAc)_2{\cdot}4(Et_2O)$ (1-V). Reaction of the bithiophene substituted Schiff base $\mathbf{L^4H_2}$ with $Cd(OAc)_2{\cdot}2H_2O$ (1:1) in CH_2Cl_2 under reflux gave good yields of the trinuclear complex $L_2Cd_3(OAc)_2$ (Scheme 1.4). Changing the stoichiometry of the

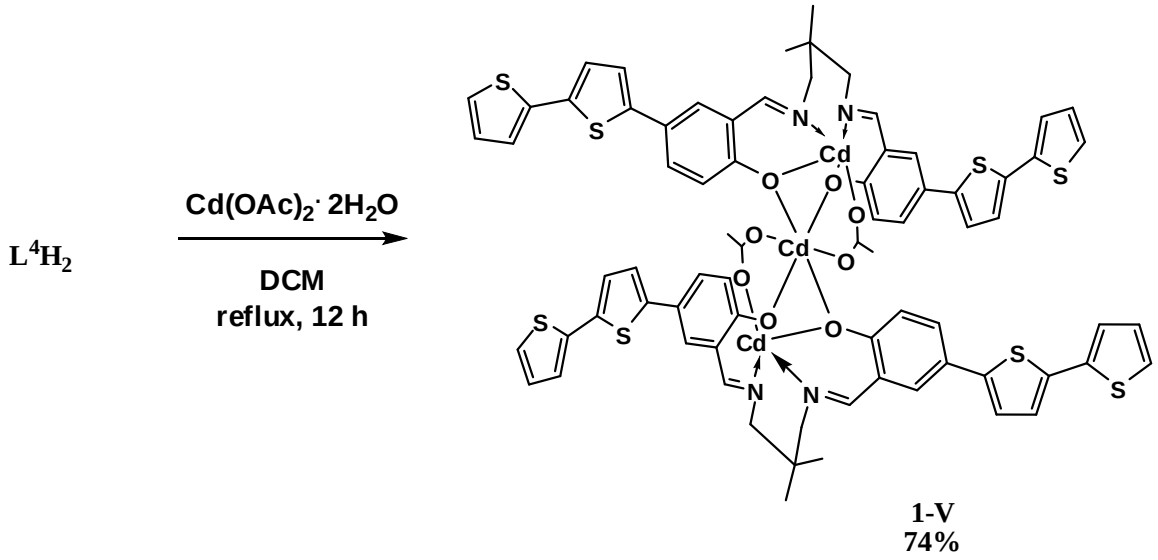

Scheme 1.4. Preparation of bithiophene containing trinuclear Cd-SB complex **1-V**.

reaction to match the L:Cd ratio found in the product did not affect the yield. The complex is sparingly soluble in polar organic solvents such as CH_2Cl_2 and MeOH. Spectroscopic data is consistent with the structure observed in the solid state. Thus the ^1H NMR spectrum in CD_2Cl_2 shows peaks assigned to both L and OAc protons. Solvent molecules which crystallize with the complex are readily removed under vacuum and the high resolution mass spectrum shows a peak for the molecular ion (M+) 751.0145 amu (calcd. 751.0146).

In order to obtain X-ray quality crystals of the trinuclear Cd_3 complex a variety of different crystallization techniques were tried. The most successful of these involved vapor diffusion of Et_2O into saturated methylene chloride solutions. Several structures were obtained which differed only in the nature of the solvent molecules which co-crystallized with the Cd_3 unit. We report here details on the structure which crystallized

with four Et_2O. Two other structures were obtained with stoichiometries $L_2Cd_3(OAc)_2 \cdot 2(Et_2O)$ and $L_2Cd_3(OAc)_2 \cdot 2(Et_2O)(MeOH)$. The metrical parameters of the Cd_3 units in these compounds were similar to those found in **1-V**. Compound **1-V** crystallizes in the monoclinic space group P2(1)/n with two independent molecules per unit cell (Fig. 1.12). Crystallographic details are given in Table 1.2 and key bond lengths and angles in Table 1.6. The overall molecular framework contains a central linear Cd_3 core in which the terminal Cd atoms are coordinated by the N_2O_2 atoms of the Schiff base ligands. The Schiff base ligands contain a relatively flexible three carbon backbone and are folded about the central $C(Me)_2$ group so that they have a V-shaped configuration. The terminal Cd atoms are located slightly above the N_2O_2 plane by 0.720 Å and the dihedral angle between each half of the ligand is 111.1°. A similar ligand arrangement is found in trinuclear Zn_3 Schiff base (SB) complexes with formula $(SB)_2Zn_3(OAc)_2$.[26] Each Cd_3 unit resides on a center of inversion at Cd(2) with a Cd…Cd distance of 3.266 Å. The central Cd atom is bonded to two acetate units which also bridge to the terminal Cd atoms. This configuration results

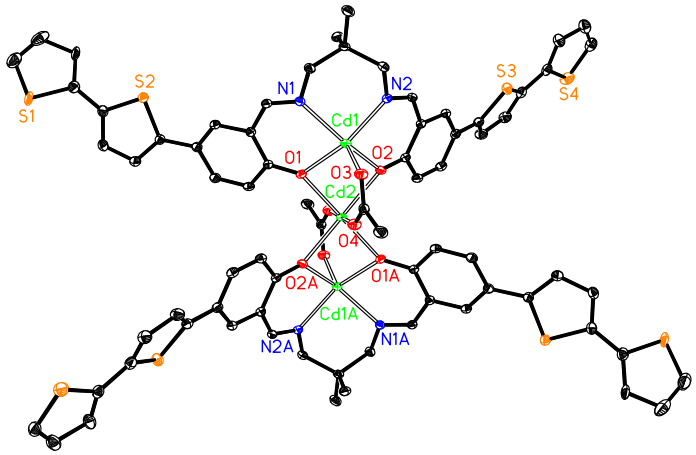

Figure 1.12. Crystal structure of **1-V** with hydrogen atoms omitted for clarity. Thermal ellipsoids are drawn at the 25 % probability level.

in a five-coordinate square-based pyramidal geometry for the terminal Cd atoms while the central Cd atom has a pseudo-octahedral coordination environment. The average Cd-N and Cd-O(phenolic) distances are 2.242 and 2.228 Å respectively and are comparable to those found in other Schiff base complexes of Cd.[21] The average Cd-O(OAc^-) distance is 2.237 Å.

$L^5Cd{\cdot}2(MeOH)$ (1-VI). The reaction of ligand **L^5H_2** with $Cd(NO_3)_2{\cdot}4H_2O$ (1:1) in MeOH under reflux gave the mononuclear bithiophene-substituted Cd-SB complex **1-VI** in 41% yield (Scheme 1.5). The complex is sparingly soluble in polar organic

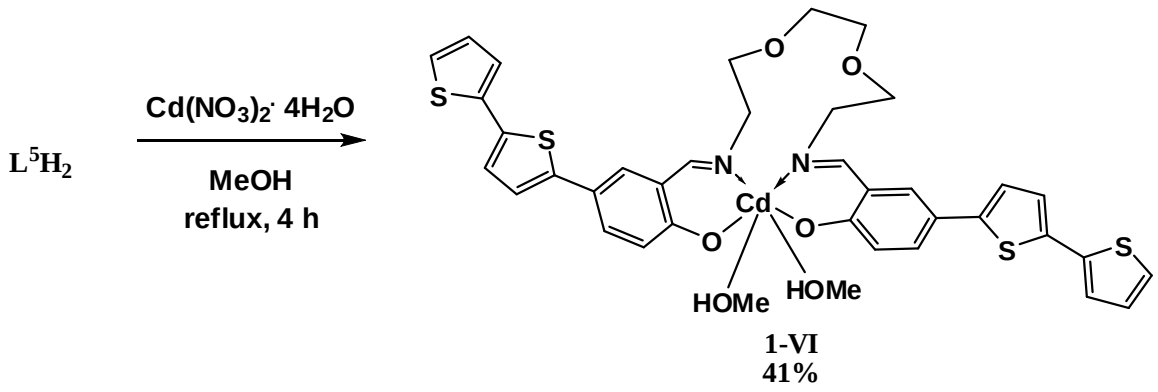

Scheme 1.5. Preparation of bithiophene containing mononuclear Cd-SB complex **1-VI**.

solvents such as $CHCl_3$ and MeOH. Spectroscopic data is consistent with retention of the MeOH groups in solution. Thus the ^1H NMR spectrum in $CDCl_3$ shows peaks assigned to both L and MeOH protons. Solvent molecules which crystallize with the complex are readily removed under vacuum and the high resolution mass spectrum shows a peak for the molecular ion (M+) 796.0121 amu (calcd. 796.0122).

X-ray quality crystals of the mononuclear Cd complex **1-VI** were obtained through slow evaporation of the reaction filtrate over several days. Compound **1-V1**

crystallizes in the monoclinic space group P2(1)/n with four independent molecules per unit cell (Fig. 1.13). Crystallographic details are given in Table 1.2 and key bond lengths

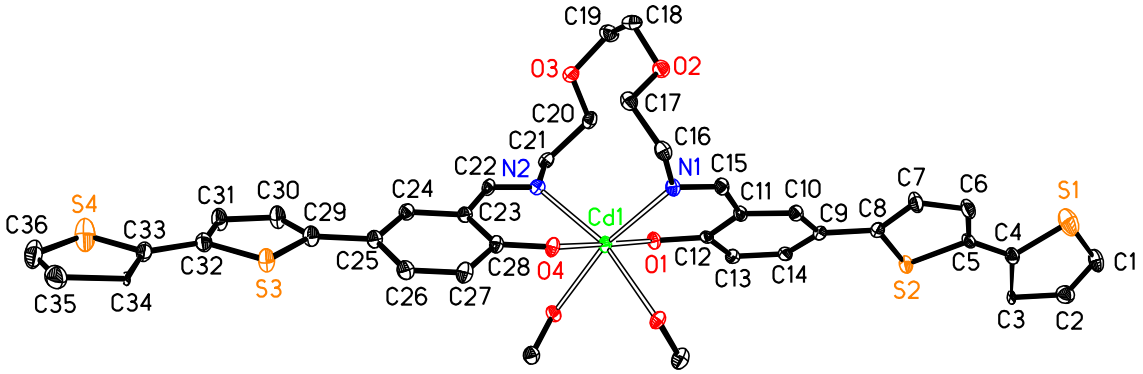

Figure 1.13. Crystal structure of **1-VI** with hydrogen atoms omitted for clarity. Thermal ellipsoids are drawn at the 25 % probability level.

and angles in Table 1.7. The overall molecular framework contains a central Cd atom core which is coordinated by the N_2O_2 atoms of the Schiff base ligand. The Schiff base ligands contain a flexible acyclic $C_6H_{12}O_2$ backbone which bends about the central OC_2H_4O group. Each half of the ligand is tilted away from one another at an angle of 115.3º. The central Cd atom is bonded to two MeOH units with a Cd-O(HMe) distance of 2.360 Å. This configuration results in a six-coordinate pseudo-octahedral geometry with the MeOH groups occupying *cis* coordination sites. The average Cd-N and Cd-O(phenolic) distances are 2.292 and 2.226 Å respectively and are comparable to those found in other Schiff base complexes of Cd.[21]

1.2.3. Bithiophene Substituted Copper-Schiff Base Complexes

Photovoltaic devices based on chalcopyrite materials of the general form $[Cu(In:Ga)(S:Se)_2]$ (CIGS) have been investigated by space researchers for several

years.[27] Semiconducting materials of these types show great promise for achieving high efficiencies. In fact, efficiencies of 12.5% and 18.8% have been reported for thin-film $CuInS_2$- and $Cu(In:Ga)Se_2$-based cells, respectively.[28] The band gaps of the ternary and quaternary CIGS materials range from 1.5 eV for $CuInS_2$ to 1.1 eV for $CuInSe_2$ and are well suited for the extraterrestrial AM 0 solar spectrum.[24] Additional material properties such as high absorption coefficients, structural defect tolerance and inexpensive thin-film deposition methods enhance the promise of the materials for PV device applications.

Building on efforts to identify useful metal-SB complexes from which to grow semiconducting nanocrystals, a polymerizable copper-SB complex was prepared. It is envisioned that promising PV cells may be generated upon growth of ternary and/or quaternary CIGS nanocrystals at the copper nucleation sites.

$L^4Cu{\cdot}CH_2Cl_2$ (1-VII). Upon refluxing ligand **L^4H_2** with $Cu(OAc)_2{\cdot}H_2O$ (1:1) in MeOH, the bithiophene-substituted mononuclear Cu-SB complex $L^4Cu{\cdot}2(CH_2Cl_2)$**, 1-VII**, was obtained in 78% yield (Scheme 1.6). Changing the stoichiometry of the reaction. to match the L:Cd ratio found in the product did not affect the yield. The complex is sparingly soluble in polar organic solvents such as $CHCl_3$ and MeOH. Solvent molecules which crystallize with the complex are readily removed under vacuum and the high resolution mass spectrum shows a peak for the molecular ion (M+) 700.0408 amu (calcd.700.0408).

A variety of different crystallization techniques were explored in order to obtain X-ray quality crystals of the mononuclear Cu complex **1-VII**. The most successful of these involved vapor diffusion of Et_2O into saturated methylene chloride solutions.

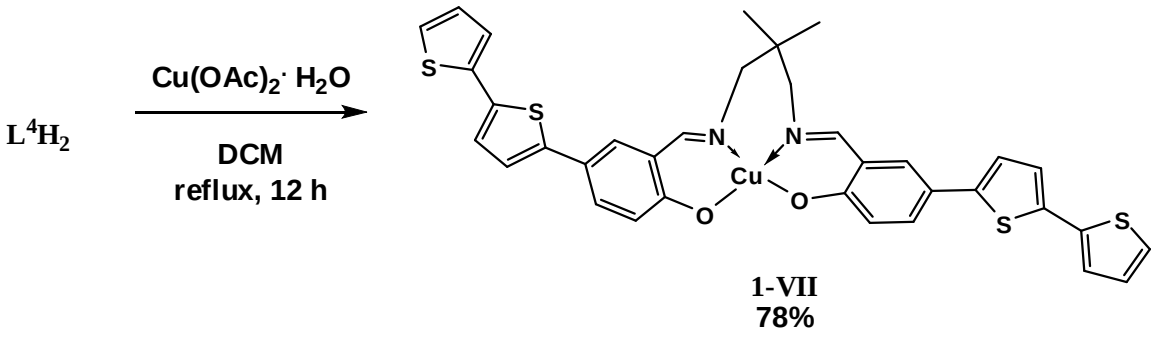

Scheme 1.6. Preparation of bithiophene containing mononuclear Cu-SB complex **1-VII**.

Compound **1-VII** crystallizes in the triclinic space group P1 with two independent molecules per unit cell (Fig. 1.14). The structure shown in Figure 1.14 crystallized with

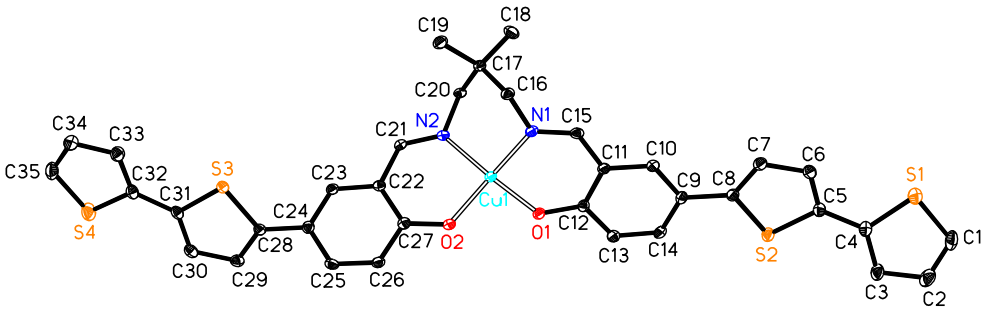

Figure 1.14. Crystal structure of **1-VII** with hydrogen atoms omitted for clarity. Thermal ellipsoids are drawn at the 25 % probability level.

one molecule of dichlormethane per Cu complex. Crystallographic details are given in Table 1.2 and key bond lengths and angles in Table 1.8. The overall molecular framework contains a central Cu atom core which is coordinated by the N_2O_2 atoms of the Schiff base ligand. The Schiff base ligands contain a relatively flexible three carbon backbone. This backbone and the attached N_2Cu unit comprise a 6-membered

metallocyclic core that resembles a twist-boat conformation. The central Cu atom resides in a four-coordinate distorted square planar environment with average bond angles around Cu of 93.2 º. The average Cu-N and Cu-O(phenolic) distances are 1.942 and 1.899 Å respectively.

1.3. Future Studies

With bithiophene-substituted Cd-and Cu-SB complexes in hand, the next phase of this project seeks to obtain conducting polymeric films through careful potentiodynamic electropolymerizations followed by subsequent growth of desired nanoparticles in the polymer matrix. It is envisioned that the metal atoms held in the films by the salen ligand cavities will establish excellent electrical contact with the conducting polymer. As mentioned earlier, these Cd and/or Cu sites will serve as "seed points" for the growth of semiconducting nanoparticles. By doing so the semiconductiong materials are wired directly into the conducting polymer, which eliminates an interface between organic and inorganic components (Fig. 1.15). Such interfaces typically present problems and are

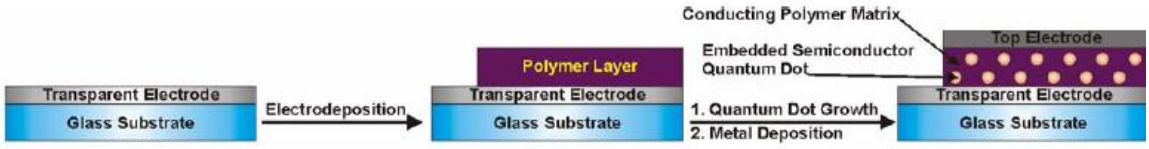

Figure 1.15. Fabrication of our hybrid solar cell.

seen as a major drawback in the performance of conventional heterojunction PV devices. Furthermore, by employing a controlled seed growth process, it should be possible to control the size and shape (and therefore the optoelectronic properties) of the desired nano-particles.

Michelle Mejia has successfully performed controlled electropolymerizations with bithiophene-containing SB complexes of Cd and Cu and characterized the resulting thin films. These experiments indicate that bithiophene-substituted SB complexes may be readily electropolymerized with either themselves or with additionally bithiophene in copolymerizations (Scheme 1.7).

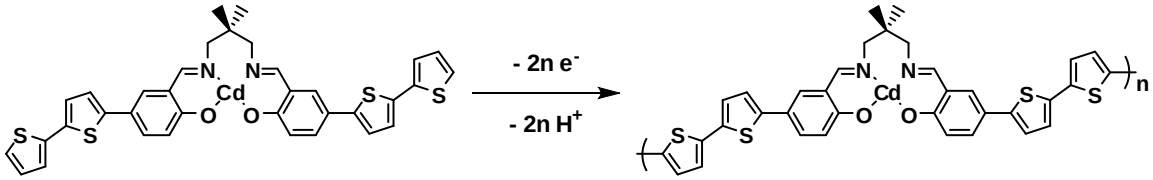

Scheme 1.7. Example of the electrochemical polymerization of a Cd-SB complex.

Furthermore, Michelle has clearly shown that the thin films of metal-containing conducting polymers are suitable substrates for the subsequent growth of semiconductor nanoparticles. Thus nanoparticles of CdS and $CuGaS_2$ have been identified on thin films of the respective Cd- and Cu-containing polymeric films (Fig. 1.16). There is limited precedent for the conversion of metal sites in polymers to inorganic nanoparticles of CdS and PbS,[29] and to our knowledge no reports exist with thin film polythiophene systems. Work is being conducted in our labs by Joseph Rivers to prepare analogous bithiophene-

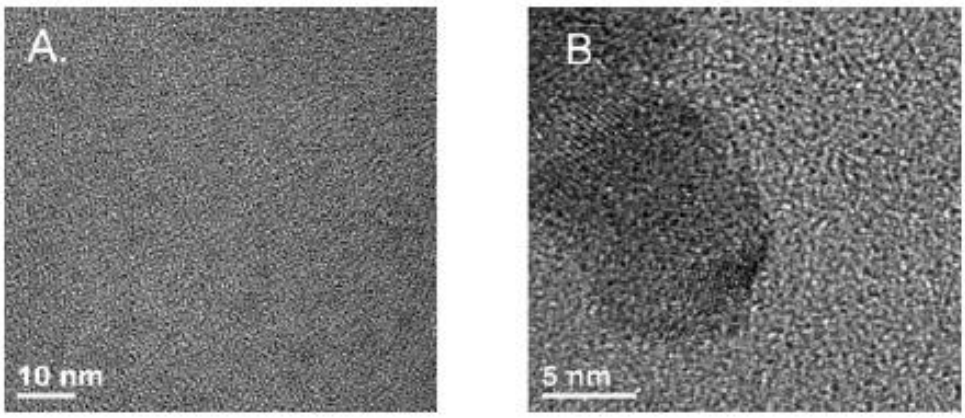

Figure 1.16. TEM images: Electropolymerized film on carbon coated Au grids (a) without copolymerizaed Cd-SB, and (b) with Cd-SB complex. Both were treated sequentially with Cd^{2+} and S^{2-} under similar conditions.

containing Ga- and Pb-SB complexes. With these in hand, similar electropolymerizations may be performed and subsequent growth of useful semiconducting nanomaterials such as GaAs, GaP and PbS can be explored. A number of additional metals may be incorporated into polymerizable SB complexes that will lead to interesting, light-harvesting PV materials.

1.4. Conclusion

In summary, a number of metal-SB complexes of Cd and Cu have been prepared. Initially, model Cd systems lacking polymerizable bithiophene substituents were synthesized demonstrating the feasibility of obtaining such metal-SB complexes. Subsequently, bithiophene-substituented systems of Cd and Cu were prepared. These polymerizable Cd- and Cu-SB complexes have been shown to participate in successful electropolymerizations to give thin films of conducting polymers. Additionally, the

seeded growth of Cd- and Cu-containing nanoparticles has been performed on the respective films. Further studies are to be performed in order to identify and prepare a range of useful metal-containing SB systems that can be subjected to electropolymerizations and seeded nanoparticle growth.

1.5. Experimental

General. Unless otherwise noted, all reactions and manipulations were carried out under a dry, oxygen-free nitrogen atmosphere using standard Schlenk techniques or in an inert atmosphere glove-box. All solvents were dried prior to use by distillation from CaH_2 (toluene, dichloromethane), magnesium (methanol) or by using an Innovative Technology, Pure Solv solvent purifier with a double purifying column. The following chemicals were used as received: 5-bromosalcyladehyde (Alfa), 5-bromo-2-hydroxy-3-methoxybenzaldehyde (Aldrich), 2,2'-bithiophene (Aldrich), tributyltin chloride (Alfa), 2,2-dimethyl-1,3-propanediamine (TCI), 1,3-propanediamine (Aldrich), 1,2-phenylenediamine (TCI), 2,2'-(ethylenedioxy)bis(ethylamine) (Aldrich), $Cd(OAc)_2{\cdot}2H_2O$ (OAc = acetate) (Aldrich), triethylamine (Fisher).

Instrumental Details. NMR spectra were recorded on a Mercury 400 MHz spectrometer and/or Varian 300 Unity Plus spectrometer (^{1}H, 300 MHz) at 25 °C. ^{1}H NMR signals are reported relative to residual proton resonances in deuterated solvents. Electrospray ionization (ESI) and Fast atom bombardment (FAB) mass spectra were recorded on a Finnigan MAT TSQ 700. High-resolution mass spectra (HRMS) were obtained on a VG Analytical ZAB-VE sector instrument and are reported as *m/z* (relative intensity). Low-

resolution chemical ionization (CI) mass spectra were collected on a Micromass Autospec Ultima mass spectrometer. Infrared spectra were recorded using a Nicolet IR 200 FTIR spectrometer. TEM pictures were taken using JEOL 2010F. Gold Melting points were obtained in sealed glass capillaries under dinitrogen and are uncorrected.

X-Ray Crystallography. The crystallographic data and structure refinement for complexes **1-I**, **1-II**, **1-V** – **1-VII** are listed in Table 1.2. Selected bond lengths (Å) and angles (°) for **1-I**, **1-II, 1-III, 1-V**, **1-VI** and **1-VII** are given in Tables 1.3, 1.4, 1.5, 1.6, 1.7 and 1.8, respectively. Data were collected on a Nonius Kappa CCD diffractometer with graphite monochromated Mo-Kα radiation (λ = 0.71073 Å) at 153 K. Absorption corrections were applied using GAUSSIAN. The structures were solved by direct methods and refined anisotropically using full-matrix least-squares methods with the SHELX 97 program package.[30] The coordinates of the non-hydrogen atoms were refined anisotropically, while hydrogen atoms were included in the calculation isotropically but not refined. Neutral atom scattering factors were taken from Cromer and Waber.[31]

***N,N'*-(1,2-phenylenyl)-bis(5-bromo-2-hydroxy-3-methoxybenzaldimine) (L^1H_2).** To a solution of 5-bromo-2-hydroxy-3-methoxybenzaldehyde (2.31 g, 10 mmol) in ethanol (125 mL) was added dropwise to a solution of 1,2-phenylenediamine (0.540 g, 5 mmol) in ethanol (125 mL). The mixture was stirred at 25 °C for 12 h. The reaction mixture was filtered, to give $\mathbf{L^1H_2}$ as a reddish orange solid. This solid was washed with cold ethanol and then dried under vacuum. Isolated: $\mathbf{L^1H_2}$, 2.35 g, 88%; m.p.144-148 °C; ^{1}H NMR (400 MHz, $CDCl_3$): δ 13.78 (br s, -O*H*, 2H), 8.49 (s, -C*H*N-, 2H), 7.32 (d, Ar*H*,

2H, *J* = 5.4 Hz), 7.19 (d, ArH, 2H, *J* = 5.1), 7.04 (s, Ar*H*, 4H), 6.94 (s, Ar*H*, 4H), 6.92 (s, Ar*H*, 4H), 3.79 (s, -OCH_3, 6H); ^{13}C NMR (100 MHz, $CDCl_3$): δ 162.6, 151.3, 149.4, 141.5, 128.1, 125.2, 119.9, 119.6, 117.7, 109.7, 56.1; FTIR (Nujol, cm^{-1}): 3579 (w), 3051 (m), 2974 (m), 2839 (w), 1613 (m), 1568 (w), 1462 (m), 1437 (m), 1421 (m), 1262 (s), 739 (s), 710 (s).

***N,N'*-(propyl)-bis(5-bromo-2-hydroxy-3-methoxybenzaldimine) (L^2H_2).** Ligand L^2H_2 was prepared in a similar manner as described above for L^1H_2 from 5-bromo-2-hydroxy-3-methoxybenzaldehyde (2.31 g, 10 mmol) and 1,3-propanediamine (0.371 g, 5 mmol) in ethanol (250 mL). The mixture was stirred at 25 °C for 12 h. After filtering, washing with cold ethanol, and drying under vacuum, L^1H_2 was isolated as a yellow solid. Isolated: L^2H_2, 2.27 g, 91%; m.p. 126-128 °C; ^{1}H NMR (400 MHz, $CDCl_3$): δ 13.68 (br s, -O*H*, 2H), 8.24 (s, -C*H*N-, 2H), 6.95 (s, Ar*H*, 4H), 3.86 (s, -OCH_3, 6H), 3.70 (t, -CH_2-, 4H, *J* = 6.3 Hz), 2.08 (qn, -CH_2-, 2H, *J* = 6.5 Hz); ^{13}C NMR (100 MHz, $CDCl_3$): δ 164.5, 151.5, 149.4, 124.7, 118.9, 116.9, 109.2, 55.8, 38.8, 31.3; FTIR (Nujol, cm^{-1}): 3579 (w), 3081 (w), 2933 (m), 2892 (w), 2843 (m), 1634 (s), 1573 (m), 1471 (s), 1442 (s), 1392 (m), 1324 (m), 1294 (s), 759 (m).

***N,N'*-(2,2'-ethylenedioxybis(ethyl))-bis(5-bromo-2-hydroxy-3-methoxybenzaldimine) (L^3H_2).** Ligand L^3H_2 was prepared in a similar manner as described above for $L^1H_2$from 5-bromo-2-hydroxy-3-methoxybenzaldehyde (2.31 g, 10 mmol) and 2,2'-(ethylenedioxy)-bis(ethylamine) (0.742 g, 5 mmol) in ethanol (250 mL). The mixture was stirred at 25 °C

for 8 h. After filtering, washing with cold ethanol, and drying under vacuum, **L^3H_2** was isolated as a yellow solid. Isolated: **L^3H_2,** 2.70 g, 94%; m.p. 174-178 °C; ^{1}H NMR (400 MHz, $CDCl_3$): δ 13.98 (br s, -O*H*, 2H), 8.17 (s, -C*H*N-, 2H), 6.94 (s, Ar*H*, 4H), 6.92 (s, Ar*H*, 4H), 3.84 (s, -OCH_3, 6H), 3.69 (t, -CH_2-, 8H, *J* = 3.1 Hz), 3.56 (s, -CH_2-, 4H); ^{13}C NMR (100 MHz, $CDCl_3$): δ 165.2, 152.6, 149.6, 124.8, 118.8, 116.7, 108.6, 70.6, 70.1, 57.8, 56.2; FTIR (Nujol, cm^{-1}): 3583 (w), 3051 (m), 2986 (m), 2868 (w), 1638 (w), 1535 (w), 1471 (w), 1442 (m), 1421 (m), 1266 (s), 1098 (w), 743 (s), 702 (s).

$L^1_2Cd_2$·2(MeOH) (1-I). To a solution of ligand**,** **L^1H_2** (0.053 g, 0.1 mmol) in ethanol (10 mL) was added a solution of $Cd(OAc)_2·2H_2O$ (0.027 g, 0.1 mmol) in ethanol (1 mL). The reaction mixture was heated to reflux and stirred for 15 min. After cooling to room temperature, the mixture was filtered. The solid collected upon filtering was taken up in a 1:1 mixture of dichloromethane:methanol (5 mL), and allowed to stand at room temperature in air. Reddish orange crystals of **$L^1_2Cd_2$·2(MeOH)** were obtained by slow evaporation.. Isolated: **$L^1_2Cd_2$·2(MeOH),** 0.048 g, 74% yield; dec 276-280 °C; ^{1}H NMR (400 MHz, CD_3CN): δ 8.44 (s, -C*H*N-, 2H), 7.25 (m, Ar *H*, 2H), 7.16 (m, Ar *H*, 4H), 7.07 (m, Ar *H*, 2H), 3.69 (s, -OCH_3, 6H), 3.35 (br s, -CH_3, 6H), 2.15 (s, -O*H*, 2H); FTIR (Nujol, cm^{-1}): 3052 (m), 2972 (m), 2841 (w), 1613 (m), 1568 (w), 1461 (m), 1437 (m), 1423 (m), 1260 (s), 739 (s), 710 (s); MS (chemical ionization, CH_3CN) *m/z* 1292 [M^+- 2 (CH_3OH)].

$L^2_2Cd_3(OAc)_2·(Et_2O)·2(CH_3OH)$ (1-II). To a solution of ligand**,** **L^2H_2** (0.050 g, 0.1

mmol) in methanol (10 mL) was added a solution of $Cd(OAc)_2 \cdot 2H_2O$ (0.027 g, 0.1 mmol) in methanol (1 mL). The reaction mixture was heated to reflux and stirred for 1 h. After cooling to room temperature, the mixture was filtered. The filtrate was subjected to slow vapor diffusion in diethyl-ether to provide **$L^2_2Cd_3(OAc)_2 \cdot (Et_2O) \cdot 2(CH_3OH)$** as bright yellow crystals. Isolated: **$L^2_2Cd_3(OAc)_2 \cdot (Et_2O) \cdot 2(CH_3OH)$,** 0.037 g, 61% yield; dec 302-306°C; ^{1}H NMR (400 MHz, CD_2Cl_2): δ 8.13 (s, -C*H*N-, 2H), 7.17-6.84 (s, Ar *H*, 4H), 4.26 (br, CH_3O*H*, 2H), 3.80 (s, -OCH_3, 6H), 3.66 (m, CH_3OH, 6H), 3.54 (t, -CH_2-, 4H, J = 6.3 Hz), 3.41 (q, -CH_2CH_3, 8H, J = 7.2 Hz), 1.80 (qn, -CH_2-, 2H, J = 2.5 Hz), 1.26 (s, CO_2CH_3, 6H), 1.11 (t, -CH_2CH_3-, 6H, J = 7.1 Hz); FTIR (Nujol, cm^{-1}): 3081 (w), 2932 (s), 2895 (s), 2845 (s), 1633 (s), 1573 (w), 1522 (w), 1516 (w), 1460 (s), 1381 (s), 1303 (m), 1190 (w), 1175 (m), 841 (m), 792 (m), 691 (m); MS (electrospray ionization, CH_3CN) *m/z* 1392 [M$^+$- OAc].

$L^3_2Cd_4(OAc)_4$ (1-III). To a solution of ligand**, L^3H_2** (0.057 g, 0.1 mmol) in methanol (10 mL) was added a solution of $Cd(OAc)_2 \cdot 2H_2O$ (0.027 g, 0.1 mmol) in methanol (1 mL). The reaction mixture was heated to reflux and stirred for 1 h. After cooling to room temperature, the mixture was filtered. The filtrate was subjected to slow vapor diffusion in diethyl-ether to provide **$L^3_2Cd_4(OAc)_4$** as bright yellow crystals. Isolated: **$L^3_2Cd_4(OAc)_4$,** 0.039 g, 57% yield; m.p 252-255 °C, dec 280-282 °C; ^{1}H NMR (400 MHz, $CDCl_3$): δ 8.20 (s, -C*H*N-, 4H), 7.17-6.97 (m, Ar *H*, 8H), 3.78 (s, -OCH_3, 12H), 3.44 (dt, -CH_2-, 8H, J_1 = 1.7, J_2 = 3.2 Hz), 3.16 (dt, -CH_2-, 8H, J_1 = 1.7, J_2 = 3.4 Hz), 1.93 (s, -CH_2-, 8H), 1.26 (s, -CH_3, 12H); FTIR (Nujol, cm^{-1}): 3051 (m), 2988 (m), 2867

(w), 1646 (m), 1638 (w), 1533 (w), 1468 (w), 1442 (m), 1420 (m), 1264 (s), 1098 (w), 743 (s), 702 (s); MS (chemical ionization, $CHCl_3$) *m/z* 1371 [M^+- 2 ($Cd(OAc)_2$)].

5-(2,2'-bithiophene-5-yl)-2-hydroxybenzaldehyde (1-IV). To a mixture of 5-bromosalicylaldehyde (3.5 g, 17.4 mmol), and $Pd(PPh_3)_2Cl_2$ (0.613 g, 0.88 mmol) in toluene (40 mL) was added 2-(tri-butylstannyl)bithiophene (9.56 g, 21 mmol). The reaction mixture was added heated to 80°C for 48 h under argon. The reaction was cooled and dried in vacuo to give a yellow solid. The solid was dissolved in dichloromethane, and then filtered through a silica plug. Filtrate was washed with dilute aqueous NH_4Cl, and then dried over $MgSO_4$. Solvent was removed in vacuo to give a yellow solid that was then washed with hexanes. The yellow solid was recrystallized from dichloromethane and hexanes, then dried in vacuo to give **1-IV**. Isolated: **1-IV**, 3.96g, 79%; m.p. 164-170 °C; ^{1}H NMR (300 MHz, DMSO-d^6) δ 10.96 (s, -O*H*, 1H), 10.29 (s, -C*H*O, 1H), 7.84 (m, Ar*H*, 2H), 7.51 (d, Ar*H*, 1H, J = 5.7 Hz), 7.40 (d, Ar*H*, 1H, J = 3.9 Hz), 7.30 (d, Ar*H*, 1H, J = 18.3), 7.28 (d, Ar*H*, 1H, J = 3.6), 7.08 (m, Ar*H*, 2H); UV-Vis (CH_2Cl_2) 36031 $cm^{-1}M^{-1}$ (352 nm); MS (chemical ionization, CH_2Cl_2) *m/z* calc'd: 287.0200, found: 287.0199 (M^+).

***N,N'*-((2,2'-dimethyl)propyl)-bis(5-(2,2'-bithiophene-5-yl)salcylidenimine) (L^4H_2).** To a solution of **1-IV** (1.00g, 3.49 mmol) dissolved in dichloromethane (200 mL) was added ethanol (200 mL), and 1,3-diamino-2,2'-dimethylpropane (0.1784 g,1.75 mmol). The mixture was stirred at 25 °C for 8 h, and then dichloromethane was removed under

vacuum. The reaction mixture was filtered to give $\mathbf{L^4H_2}$ as an orange solid that was then dried under vacuum. Isolated: $\mathbf{L^4H_2}$, 0.954g, 86%; m.p. 167-174 °C; ^{1}H NMR (300MHz, CD_2Cl_2): δ 13.65 (s, -O*H*, 2H), 8.40 (s, -C*H*N-, 2H), 7.57 (dd, Ar *H*, 2H, *J* = 8.4 Hz), 7.51 (d, Ar *H*, 2H, *J* = 2.1 Hz), 7.23 (d, Ar *H*, 2H, *J* = 5.1 Hz), 7.18 (d, Ar *H*, 2H, *J* = 3.6 Hz), 7.12 (m, Ar *H*, 2H,), 7.03 (d, Ar *H*, 2H, *J* = 9 Hz), 7.03 (d, Ar *H*, 2H, *J* = 1.2 Hz), 6.97 (d, Ar *H*, 2H, *J* = 8.7 Hz), 3.54 (s, -CH_2-, 4H), 1.11 (s, -CH_3, 6H); UV-Vis 23768 $cm^{-1}M^{-1}$ (349 nm); FTIR (Nujol, cm^{-1}): 3579 (w), 3051 (m), 2986 (m), 2835 (w), 1634 (m), 1580 (w), 1491 (w), 1417 (m), 1266 (s), 1176 (w), 894 (m) (MS (chemical ionization, CH_2Cl_2) *m/z* calc'd: 638.1190, found: 638.1188 *m/z* 638 (M^+).

***N,N'*-(2,2'-ethylenedioxybis(ethyl))-bis(5-(2,2'-bithiophene-5-yl)salcylidenimine) ($\mathbf{L^5H_2}$).** To a solution of **1-IV** (1.00g, 3.49 mmol) dissolved in dichloromethane (200 mL) was added ethanol (200 mL), and 2,2'-(ethylenedioxy)-bis(ethylamine) (0.282 mL, 1.75 mmol). The reaction mixture was stirred at 25 °C for 8 h, then dichloromethane was removed under vacuum. The reaction mixture was filtered to give $\mathbf{L^5H_2}$ as an orange solid which was dried under vacuum. Isolated: $\mathbf{L^5H_2}$, 0.900 g, 80% yield; m.p. 131-135°C; ^{1}H NMR (300MHz, CD_2Cl_2): δ 13.58 (s, -O*H*, 2H), 8.36 (s, -C*H*N-, 2H), 7.54 (d, Ar *H*, 2H, *J* = 8.4 Hz), 7.48 (d, 2H, *J* = 2.4 Hz), 7.23 (d, 2H, *J* = 5.1 Hz), 7.18 (d, 2H, *J* = 3.45 Hz), 7.11 (q, Ar *H*, 4H, *J* = 3.9), 7.02 (m, Ar *H*, 2H), 6.94 (d, Ar *H*, 2H, *J* = 8.4 Hz), 3.71 (s, -CH_2-, 4H), 3.61 (s, -CH_2-, 4H), 2.15 (s, -CH_2-, 4H); UV-Vis: 81588 $cm^{-1}M^{-1}$ (349 nm); FTIR (Nujol, cm^{-1}): 3583 (w), 3056 (m), 2986 (m), 2827 (w), 1638 (m), 1548 (w), 1487 (w), 1421 (m), 1266 (s), 1160 (w), 894 (m); MS (chemical ionization, CH_2Cl_2)

m/z calc'd: 684.1245, found: 684.1249 (M^+).

***N,N'*-((1,2-phenylenyl)-bis(5-(2,2'-bithiophene-5-yl)salcylidenimine) (L^6H_2).** To a solution of **1-IV** (1.00g, 3.49 mmol) dissolved in dichloromethane (200 mL) was added ethanol (200 mL), and 1,2-phenylenediamine (0.188 g, 1.75 mmol). The reaction mixture was stirred at 25 °C for 8 h, and then dichloromethane was removed under vacuum. The reaction mixture was filtered to give $\mathbf{L^6H_2}$ as a brown solid which was dried under vacuum**.** Isolated: $\mathbf{L^6H_2}$**,** 1.02 g, 85% yield; m.p. 204-208 °C; ^{1}H NMR (300MHz, CD_2Cl_2): δ 13.19 (s, -O*H*, 2H), 8.73 (s, -C*H*N-, 2H), 7.66 (m, Ar *H*, 4H), 7.42 (m, Ar *H*, 2H), 7.32 (m, Ar *H*, 2H), 7.20 (m, Ar *H*, 8H), 7.05 (m, Ar *H*, 4H); FTIR (Nujol, cm^{-1}): 3579 (w), 3051 (m), 2987 (m), 2823 (w), 1617 (m), 1572 (w), 1487 (m), 1421 (m), 1262 (s), 1168 (s), 899 (m); UV-Vis (CH_2Cl_2): 48664 $cm^{-1}M^{-1}$ (350 nm) MS (chemical ionization, CH_2Cl_2) *m/z* calc'd: 644.0721, found: 644.0722 (M^+).

$L^4_2Cd_3(OAc)_2{\cdot}4(Et_2O)$ (1-V). To a solution of the ligand $\mathbf{L^4H_2}$ (0.064 g, 0.1 mmol)**,** in dichloromethane (10 mL) was added $Cd(OAc)_2{\cdot}2H_2O$ (0.027 g, 0.1 mmol) in methanol (1 mL). The mixture was stirred under reflux for 12 h. After cooling to room temperature, the mixture was filtered. The filtrate was subjected to slow vapor diffusion in diethyl-ether to provide $\mathbf{L^4_2Cd_3(OAc)_2{\cdot}4(Et_2O)}$ as reddish orange crystals. Isolated: $\mathbf{L^4_2Cd_3(OAc)_2{\cdot}4(Et_2O)}$, 0.150 g, 74% yield; m.p. 300-304 °C, (dec 328-330 °C); ^{1}H NMR (400 MHz, CD_2Cl_2): δ 8.40 (s, -C*H*N-, 4H), 7.59-6.97 (m, Ar *H*, 32H), 3.54 (s, -CH_2-, 8H), 3.43 (q, -CH_2CH$_3$, 16 H, *J* = 7.1 Hz), 1.26 (s, CO_2CH_3, 6H), 1.14 (t, -

CH_2CH_3, 24 H, *J* = 7.1 Hz), 1.10 (s, -CH_3, 12H); FTIR (Nujol, cm^{-1}): 3068 (w), 2921 (s), 2950 (s), 2844 (s), 2725 (w), 2672 (w), 1744 (m), 1641 (m), 1634 (m), 1565 (w), 1532 (w), 1511 (w), 1462 (s), 1381 (s), 1365 (w), 1303 (m), 1193 (w), 1172 (m), 1106 (w), 972 (w), 837 (m), 796 (m), 690 (m); HRMS (chemical ionization, CH_2Cl_2): *m/z* calcd for $C_{35}H_{28}CdN_2O_2S_4$ 751.0146 (M^+), found 751.0145; MS (chemical ionization, CH_2Cl_2): *m/z* calcd for $Cd(OAc)_2$ 231.9, found 231.3; UV-Vis: 363 nm, 153949 $L \cdot cm^{-1} \cdot mol^{-1}$.

$L^5Cd \cdot 2(MeOH)$ (1-VI). To a solution of the ligand **L^5H_2** (0.068 g, 0.1 mmol) and triethylamine (0.051 g, 0.5 mmol) in methanol (10 mL) was added $Cd(NO_3)_2 \cdot 4H_2O$ (0.031 g, 0.1 mmol) in methanol (1 mL). The mixture was stirred under reflux for 4 h. After cooling to room temperature, the mixture was filtered. The filtrate was subjected to slow vapor diffusion in diethyl-ether to provide **$L^5Cd \cdot 2(MeOH)$** as yellow needles. Isolated: **$L^5Cd \cdot 2(MeOH)$**, 0.035 g, 41%; m.p. 146-150 °C; ^1H NMR (400 MHz, CD_2Cl_2): δ 8.28 (s, -C*H*N-, 2H), 7.59-6.99 (m, Ar *H*, 16H), 3.90 (br s, CH_3OH, 2H), 3.72 (m, -CH_2-, 4H), 3.65 (m, -CH_2-, 4H), 3.46 (s, HOCH_3, 6H), 2.91(s, CH_2, 4H); FTIR (Nujol, cm^{-1}): 3406 (br), 3014 (w), 2954 (w), 2917 (m), 2845 (w), 1633 (m), 1598 (m), 1532 (w), 1418 (m), 1279 (m), 1256 (m), 1218 (s), 1124 (m), 1041 (m); HRMS (chemical ionization, CH_2Cl_2): *m/z* calcd for $C_{36}H_{30}CdN_2O_4S_4$ 796.0122 (M^+), found 796.0121.

$L^4Cu \cdot 2(CH_2Cl_2)$ (1-VII). To a solution of the ligand **L^4H_2** (0.064 g, 0.1 mmol) in dichloromethane (10 mL) was added $Cu(OAc)_2 \cdot H_2O$ (0.020 g, 0.1 mmol) in methanol (1

mL). The mixture was stirred under reflux for 12 h. After cooling to room temperature, the mixture was filtered to give **$L^4Cu{\cdot}2(CH_2Cl_2)$** as a green solid. Dark green crystals suitable for X-ray diffraction were obtained by subjecting the filtrate to slow vapor diffusion in diethyl-ether. Isolated: **$L^4Cu{\cdot}2(CH_2Cl_2)$**, 0.055 g, 78%; m.p. 184-188 °C; ^{1}H NMR (400 MHz, $CDCl_3$): δ 8.18 (s, -C*H*N-, 2H), 7.30-6.78 (m, Ar *H*, 16H), 5.24 (s, C*H*$_2$Cl$_2$, 2H), 3.61 (s, -C*H*$_2$-, 4H), 1.35 (s, -C*H*$_3$, 6H); FTIR (Nujol, cm^{-1}): 3023 (s), 2974 (m), 2924 (m), 2896 (w), 1625 (m), 1523 (m), 1474 (m), 1416 (m), 1388 (w), 1261 (s), 1044 (s), 926 (m), 873 (m), 775 (s), 669 (s); HRMS (chemical ionization, CH_2Cl_2): *m/z* calcd for $C_{35}H_{29}CdN_2O_4S_4$ 700.0408 (M^+), found 700.0408.

Table 1.2. Crystal data and structure refinement for complexes **1-I, 1-II, 1-V, 1-VI** and **1-VII**.

	1-I	**1-II**	**1-V**	**1-VI**	**1-VII**
Formula	$C_{47}H_{46}Br_2N_4O_{12}Cd_2$	$C_{48}H_{60}Br_4N_4O_{15}Cd_{32}$	$C_{90}H_{102}N_4O_{12}S_8Cd_3$	$C_{38}H_{38}N_2O_6S_4Cd$	$C_{36}H_{30}Cl_2N_2O_2S_4Cu$
Fw	1403.25	1589.78	2025.44	857.33	785.30
Cryst syst.	triclinic	monoclinic	monoclinic	monoclinic	triclinic
Space group	P1	P2(1)/n	P2(1)/n	P2(1)/n	P1
a, Å	9.6620(19)	17.088(3)	14.900(3)	10.407(2)	10.282(2)
b, Å	11.490(2)	13.312(3)	9.3764(19)	10.261(2)	13.176(3)
c, Å	12.405 (3)	25.861(5)	32.033(6)	35.010(7)	13.204(3)
α, deg	70.93(3)	90	90	90	107.65(3)
β, deg	71.84(3)	103.27(3)	92.21(3)	90.10(3)	97.12(3)
γ, deg	71.28(4)	90	90	90	90.65(3)
V, $Å^3$	1199.4(4)	5726.7(2)	4471.9(16)	3738.6(13)	1689.1(6)
Z	1	4	2	4	2
D_{calc}, g cm^{-3}	1.932	1. 835	1.504	1.523	1.544
temp, K	153(1)	153(1)	153(1)	153(1)	153(1)
F(000)	680	3088	2076	1752	806
μ, mm^{-1}	4.285	3.960	0.955	0.856	1.089
θ rang, deg	2.94-27.49	2.96-27.54	2.97-25.00	3.02-27.49	3.12-27.52
reflns meads	7951	22284	14365	14137	11372
reflns used	7951	13010	7762	7156	7686
params	622	667	535	461	424
R^a ($I > 2\sigma(I)$)	R1 = 0.0493	R1 = 0.0569	R1 = 0.0368	R1 = 0.0732	R1 = 0.0455
	wR2 = 0.1164	wR2 = 0.1060	wR2 = 0.0856	wR2 = 0.1631	wR2 = 0.1095
R^a (all data)	R1 = 0.0707	R1 = 0.1525	R1 = 0.0513	R1 = 0.1208	R1 = 0.0733
	wR2 = 0.1292	wR2 = 0.1326	wR2 = 0.0923	wR2 = 0.1847	wR2 = 0.1260
S	1.010	0.935	1.076	1.069	1.051

[a] $R1 = \Sigma||F_o| - |F_c||\Sigma|F_o|$. $wR2 = [\Sigma w[(F_o^2 - F_c^2)^2]/\Sigma|[w(F_o^2)^2]]^{1/2}$. $w=1/[\sigma^2(F_o^2)+(0.075P)^2]$, where $P = [\max(F_o^2,0)+2F_c^2]/3$.

Table 1.3. Selected Bond Lengths (Å) and Angles (°) for **1-I**.

Cd(2)-O(2')	2.267(2)	N(1')-Cd(2)-O(2W)	80.10(10)
Cd(2)-O(3')	2.275(3)	O(2')-Cd(2)-O(4)	143.93(8)
Cd(2)-N(2')	2.316(3)	O(3')-Cd(2)-O(4)	86.15(10)
Cd(2)-O(3)	2.320(2)	N(2')-Cd(2)-O(4)	77.78(10)
Cd(2)-N(1')	2.326(3)	O(3)-Cd(2)-O(4)	64.23(8)
Cd(2)-O(2W)	2.453(3)	N(1')-Cd(2)-O(4)	131.08(9)
Cd(2)-O(4)	2.601(3)	O(2W)-Cd(2)-O(4)	83.03(9)
Cd(1)-O(3)	2.226(2)	O(3)-Cd(1)-O(2)	91.28(10)
Cd(1)-O(2)	2.275(3)	O(3)-Cd(1)-N(1)	135.91(11)
Cd(1)-N(1)	2.332(2)	O(2)-Cd(1)-N(1)	77.74(10)
Cd(1)-O(2')	2.334(2)	O(3)-Cd(1)-O(2')	80.49(8)
Cd(1)-N(2)	2.360(3)	O(2)-Cd(1)-O(2')	83.20(9)
Cd(1)-O(1W)	2.417(3)	N(1)-Cd(1)-O(2')	138.41(8)
Cd(1)-O(1')	2.527(3)	O(3)-Cd(1)-N(2)	79.92(9)
O(2')-Cd(2)-O(3')	90.37(9)	O(2)-Cd(1)-N(2)	119.91(11)
O(2')-Cd(2)-N(2')	136.72(11)	N(1)-Cd(1)-N(2)	69.81(9)
O(3')-Cd(2)-N(2')	79.54(10)	O(2')-Cd(1)-N(2)	149.83(9)
O(2')-Cd(2)-O(3)	79.94(8)	O(3)-Cd(1)-O(1W)	83.76(10)
O(3')-Cd(2)-O(3)	77.78(10)	O(2)-Cd(1)-O(1W)	159.56(9)
N(2')-Cd(2)-O(3)	136.58(9)	N(1)-Cd(1)-O(1W)	119.16(10)
O(2')-Cd(2)-N(1')	79.86(8)	O(2')-Cd(1)-O(1W)	76.43(9)
O(3')-Cd(2)-N(1')	122.87(11)	N(2)-Cd(1)-O(1W)	78.82(11)
N(2')-Cd(2)-N(1')	71.32(10)	O(3)-Cd(1)-O(1')	143.70(8)
O(3)-Cd(2)-N(1')	151.00(9)	O(2)-Cd(1)-O(1')	89.38(9)
O(2')-Cd(2)-O(2W)	85.70(9)	N(1)-Cd(1)-O(1')	79.49(9)
O(3')-Cd(2)-O(2W)	155.62(8)	O(2')-Cd(1)-O(1')	63.56(7)
N(2')-Cd(2)-O(2W)	119.02(10)	N(2)-Cd(1)-O(1')	129.90(9)
O(3)-Cd(2)-O(2W)	77.84(9)	O(1W)-Cd(1)-O(1')	83.16(10)

Table 1.4. Selected Bond Lengths (Å) and Angles (°) for **1-II**.

Cd(2)-O(2')	2.241(5)	N(1')-Cd(2)-C(4W)	109.0(2)
Cd(2)-N(2')	2.261(7)	O(8)-Cd(2)-C(4W)	26.1(2)
Cd(2)-O(3')	2.290(5)	O(3)-Cd(1)-O(6)	92.1(2)
Cd(2)-O(7)	2.312(6)	O(3)-Cd(1)-N(1)	140.8(2)
Cd(2)-N(1')	2.320(7)	O(6)-Cd(1)-N(1)	123.2(2)
Cd(2)-O(8)	2.371(6)	O(3)-Cd(1)-N(2)	82.4(2)
Cd(2)-C(4W)	2.709(8)	O(6)-Cd(1)-N(2)	122.9(2)
Cd(1)-O(3)	2.245(5)	N(1)-Cd(1)-N(2)	90.6(2)
Cd(1)-O(6)	2.248(6)	O(3)-Cd(1)-O(2)	74.32(17)
Cd(1)-N(1)	2.267(6)	O(6)-Cd(1)-O(2)	107.6(2)
Cd(1)-N(2)	2.268(7)	N(1)-Cd(1)-O(2)	78.55(19)
Cd(1)-O(2)	2.287(5)	N(2)-Cd(1)-O(2)	124.7(2)
Cd(1)-O(5)	2.500(6)	O(3)-Cd(1)-O(5)	128.20(18)
Cd(1)-C(2W)	2.706(9)	O(6)-Cd(1)-O(5)	54.7(2)
Cd(3)-O(2')	2.242(5)	N(1)-Cd(1)-O(5)	89.2(2)
Cd(3)-O(2)	2.251(5)	N(2)-Cd(1)-O(5)	85.4(2)
Cd(3)-O(3')	2.263(5)	O(2)-Cd(1)-O(5)	147.06(19)
Cd(3)-O(3)	2.274(5)	O(3)-Cd(1)-C(2W)	111.1(2)
Cd(3)-O(1)	2.528(5)	O(6)-Cd(1)-C(2W)	27.3(3)
Cd(3)-O(1')	2.572(5)	N(1)-Cd(1)-C(2W)	108.0(2)
O(2')-Cd(2)-N(2')	131.5(2)	N(2)-Cd(1)-C(2W)	104.6(3)
O(2')-Cd(2)-O(3')	74.34(17)	O(2)-Cd(1)-C(2W)	130.4(3)
N(2')-Cd(2)-O(3')	82.1(2)	O(5)-Cd(1)-C(2W)	27.4(2)
O(2')-Cd(2)-O(7)	124.6(3)	O(2')-Cd(3)-O(2)	138.97(18)
N(2')-Cd(2)-O(7)	97.2(3)	O(2')-Cd(3)-O(3')	74.85(18)
O(3')-Cd(2)-O(7)	91.2(2)	O(2)-Cd(3)-O(3')	133.63(18)
O(2')-Cd(2)-N(1')	81.0(2)	O(2')-Cd(3)-O(3)	126.82(18)
N(2')-Cd(2)-N(1')	87.4(2)	O(2)-Cd(3)-O(3)	74.45(17)
O(3')-Cd(2)-N(1')	135.4(2)	O(3')-Cd(3)-O(3)	113.64(18)
O(7)-Cd(2)-N(1')	133.2(2)	O(2')-Cd(3)-O(1)	84.96(17)
O(2')-Cd(2)-O(8)	102.1(2)	O(2)-Cd(3)-O(1)	66.47(16)
N(2')-Cd(2)-O(8)	123.9(3)	O(3')-Cd(3)-O(1)	94.87(18)
O(3')-Cd(2)-O(8)	135.1(2)	O(3)-Cd(3)-O(1)	140.90(17)
O(7)-Cd(2)-O(8)	53.2(2)	O(2')-Cd(3)-O(1')	64.74(18)
N(1')-Cd(2)-O(8)	85.8(2)	O(2)-Cd(3)-O(1')	78.87(17)
O(2')-Cd(2)-C(4W)	116.7(2)	O(3')-Cd(3)-O(1')	138.63(17)
N(2')-Cd(2)-C(4W)	111.7(2)	O(3)-Cd(3)-O(1')	97.95(17)
O(3')-Cd(2)-C(4W)	115.2(2)	O(1)-Cd(3)-O(1')	73.81(18)
O(7)-Cd(2)-C(4W)	27.2(2)		

Table 1.5. Selected Bond Lengths (Å) and Angles (°) for **1-III**.

Cd(1)-O(10)	2.22(4)	O(2)-Cd(1)-Cd(2)	97.2(7)
Cd(1)-N(1)	2.22(4)	O(8)-Cd(1)-Cd(2)	42.8(7)
Cd(1)-O(5)	2.30(3)	O(7)-Cd(1)-Cd(2)	82.4(7)
Cd(1)-O(2)	2.30(4)	O(2)#1-Cd(2)-N(2)	91.9(13)
Cd(1)-O(8)	2.51(3)	O(2)#1-Cd(2)-O(5)	146.7(12)
Cd(1)-O(7)	2.51(3)	N(2)-Cd(2)-O(5)	83.4(11)
Cd(1)-Cd(2)	3.421(4)	O(2)#1-Cd(2)-O(9)	136.4(12)
Cd(2)-O(2)#1	2.24(3)	N(2)-Cd(2)-O(9)	96.7(17)
Cd(2)-N(2)	2.25(4)	O(5)-Cd(2)-O(9)	76.9(12)
Cd(2)-O(5)	2.29(3)	O(2)#1-Cd(2)-O(8)	95.6(11)
Cd(2)-O(9)	2.43(4)	N(2)-Cd(2)-O(8)	165.5(12)
Cd(2)-O(8)	2.33(3)	O(5)-Cd(2)-O(8)	83.6(10)
Cd(2)-O(8)#1	2.48(3)	O(9)-Cd(2)-O(8)	86.4(15)
Cd(2)-O(1)	2.61(3)	O(2)#1-Cd(2)-O(8)#1	75.6(11)
O(10)-Cd(1)-N(1)	95.9(14)	N(2)-Cd(2)-O(8)#1	101.1(13)
O(10)-Cd(1)-O(5)	85.1(12)	O(5)-Cd(2)-O(8)#1	73.0(11)
N(1)-Cd(1)-O(5)	147.4(12)	O(9)-Cd(2)-O(8)#1	142.7(11)
O(10)-Cd(1)-O(2)	173.0(11)	O(8)-Cd(2)-O(8)#1	68.9(11)
N(1)-Cd(1)-O(2)	82.1(13)	O(2)#1-Cd(2)-O(1)	62.4(10)
O(5)-Cd(1)-O(2)	93.0(11)	N(2)-Cd(2)-O(1)	100.9(12)
O(10)-Cd(1)-O(8)	112.1(11)	O(5)-Cd(2)-O(1)	150.9(11)
N(1)-Cd(1)-O(8)	128.9(12)	O(9)-Cd(2)-O(1)	74.0(10)
O(5)-Cd(1)-O(8)	79.4(10)	O(8)-Cd(2)-O(1)	93.6(10)
O(2)-Cd(1)-O(8)	74.1(10)	O(8)#1-Cd(2)-O(1)	132.8(9)
O(10)-Cd(1)-O(7)	87.1(12)	O(2)#1-Cd(2)-Cd(1)	141.7(8)
N(1)-Cd(1)-O(7)	88.6(12)	N(2)-Cd(2)-Cd(1)	122.7(9)
O(5)-Cd(1)-O(7)	123.9(10)	O(5)-Cd(2)-Cd(1)	42.0(7)
O(2)-Cd(1)-O(7)	99.5(10)	O(9)-Cd(2)-Cd(1)	61.5(10)
O(8)-Cd(1)-O(7)	53.0(9)	O(8)-Cd(2)-Cd(1)	47.1(7)
O(10)-Cd(1)-Cd(2)	85.9(9)	O(8)#1-Cd(2)-Cd(1)	81.4(7)
N(1)-Cd(1)-Cd(2)	170.8(10)	O(1)-Cd(2)-Cd(1)	119.0(7)
O(5)-Cd(1)-Cd(2)	41.7(7)		

Table 1.6. Selected Bond Lengths (Å) and Angles (°) for **1-V**.

Cd(3)-O(5)	2.228(2)	O(1)-Cd(3)-Cd(2)	137.80(6)
Cd(3)-O(4)	2.284(2)	O(5)-Cd(3)-Cd(1)	114.81(6)
Cd(3)-O(2)	2.2864(19)	O(4)-Cd(3)-Cd(1)	66.35(6)
Cd(3)-O(1')	2.293(2)	O(2)-Cd(3)-Cd(1)	42.38(6)
Cd(3)-O(2')	2.292(2)	O(1')-Cd(3)-Cd(1)	137.36(5)
Cd(3)-O(1)	2.306(2)	O(2')-Cd(3)-Cd(1)	138.00(7)
Cd(3)-Cd(2)	3.3104(16)	O(1)-Cd(3)-Cd(1)	42.19(5)
Cd(3)-Cd(1)	3.3112(16)	Cd(2)-Cd(3)-Cd(1)	179.84(2)
Cd(2)-O(6)	2.162(2)	O(6)-Cd(2)-N(1')	124.86(10)
Cd(2)-N(1')	2.214(2)	O(6)-Cd(2)-O(2')	97.33(9)
Cd(2)-O(2')	2.225(2)	N(1')-Cd(2)-O(2')	137.53(8)
Cd(2)-O(1')	2.2477(19)	O(6)-Cd(2)-O(1')	106.53(8)
Cd(2)-N(2')	2.286(2)	N(1')-Cd(2)-O(1')	83.47(8)
Cd(1)-O(3)	2.163(2)	O(2')-Cd(2)-O(1')	79.55(8)
Cd(1)-O(1)	2.228(2)	O(6)-Cd(2)-N(2')	108.37(9)
Cd(1)-O(2)	2.237(2)	N(1')-Cd(2)-N(2')	87.52(9)
Cd(1)-N(2)	2.246(2)	O(2')-Cd(2)-N(2')	83.06(9)
Cd(1)-N(1)	2.272(3)	O(1')-Cd(2)-N(2')	142.59(8)
O(5)-Cd(3)-O(4)	178.20(8)	O(6)-Cd(2)-Cd(3)	85.86(6)
O(5)-Cd(3)-O(2)	94.73(8)	N(1')-Cd(2)-Cd(3)	126.50(6)
O(4)-Cd(3)-O(2)	87.04(8)	O(2')-Cd(2)-Cd(3)	43.68(5)
O(5)-Cd(3)-O(1')	86.59(9)	O(1')-Cd(2)-Cd(3)	43.73(6)
O(4)-Cd(3)-O(1')	93.36(9)	N(2')-Cd(2)-Cd(3)	126.63(7)
O(2)-Cd(3)-O(1')	103.00(8)	O(3)-Cd(1)-O(1)	105.08(8)
O(5)-Cd(3)-O(2')	84.11(8)	O(3)-Cd(1)-O(2)	98.16(8)
O(4)-Cd(3)-O(2')	94.13(8)	O(1)-Cd(1)-O(2)	79.86(9)
O(2)-Cd(3)-O(2')	178.80(8)	O(3)-Cd(1)-N(2)	108.34(9)
O(1')-Cd(3)-O(2')	77.24(8)	O(1)-Cd(1)-N(2)	144.52(9)
O(5)-Cd(3)-O(1)	94.73(9)	O(2)-Cd(1)-N(2)	83.95(9)
O(4)-Cd(3)-O(1)	85.30(9)	O(3)-Cd(1)-N(1)	124.58(10)
O(2)-Cd(3)-O(1)	77.23(8)	O(1)-Cd(1)-N(1)	83.03(9)
O(1')-Cd(3)-O(1)	178.64(9)	O(2)-Cd(1)-N(1)	136.82(9)
O(2')-Cd(3)-O(1)	102.56(9)	N(2)-Cd(1)-N(1)	87.69(10)
O(5)-Cd(3)-Cd(2)	65.04(6)	O(3)-Cd(1)-Cd(3)	85.58(6)
O(4)-Cd(3)-Cd(2)	113.80(6)	O(1)-Cd(1)-Cd(3)	44.03(6)
O(2)-Cd(3)-Cd(2)	137.53(7)	O(2)-Cd(1)-Cd(3)	43.53(5)
O(1')-Cd(3)-Cd(2)	42.66(5)	N(2)-Cd(1)-Cd(3)	127.44(7)
O(2')-Cd(3)-Cd(2)	42.09(6)	N(1)-Cd(1)-Cd(3)	126.18(6)

Table 1.7. Selected Bond Lengths (Å) and Angles (°) for **1-VI**.

Cd(1)-O(4)	2.2226(18)	N(1)-Cd(1)-N(2)	104.20(8)
Cd(1)-O(1)	2.2277(17)	O(4)-Cd(1)-O(1W)	90.90(6)
Cd(1)-N(1)	2.282(2)	O(1)-Cd(1)-O(1W)	89.45(6)
Cd(1)-N(2)	2.301(2)	N(1)-Cd(1)-O(1W)	167.17(7)
Cd(1)-O(1W)	2.3536(18)	N(2)-Cd(1)-O(1W)	86.69(7)
Cd(1)-O(2W)	2.3643(17)	O(4)-Cd(1)-O(2W)	89.96(6)
O(4)-Cd(1)-O(1)	179.11(7)	O(1)-Cd(1)-O(2W)	90.91(7)
O(4)-Cd(1)-N(1)	97.22(7)	N(1)-Cd(1)-O(2W)	88.52(7)
O(1)-Cd(1)-N(1)	82.58(7)	N(2)-Cd(1)-O(2W)	165.76(7)
O(4)-Cd(1)-N(2)	82.20(7)	O(1W)-Cd(1)-O(2W)	81.54(6)
O(1)-Cd(1)-N(2)	97.00(7)		

Table 1.8. Selected Bond Lengths (Å) and Angles (°) for **1-VII**.

Cu(1)-O(1)	1.892(2)	O(1)-Cu(1)-N(2)	152.07(9)
Cu(1)-O(2)	1.9045(19)	O(2)-Cu(1)-N(2)	94.71(9)
Cu(1)-N(2)	1.941(2)	O(1)-Cu(1)-N(1)	94.81(9)
Cu(1)-N(1)	1.944(2)	O(2)-Cu(1)-N(1)	153.44(9)
O(1)-Cu(1)-O(2)	91.46(9)	N(2)-Cu(1)-N(1)	91.74(9)

1.6. References

[1] "Basic Research Needs for Solar Energy Utilization", *Report of the Basic Energy Sciences Workshop on Solar Energy Utilization*, **April 18-21, 2005**. Available on the web at http://www.sc.doe.gov/bes/reports/files/SEU_rpt.pdf (accessed Oct 28, 2006).

[2] McGehee, M. D.; Liu, Y.; Gowrishankar, V.; Goh, C.; Srinivasan, B.; Rowell, M. "Nanaostructured Photovoltaic Cells", *GCEP Technical Report*. **2005**. Available on the web at http://gcep.stanford.edu (accessed March 24, 2007)

[3] Günes, S.; Neugebauer, H.; Niyazi, S. S. "Conjugated Polymer-Based Organic Solar Cells", *Chem. Rev.* **2007**, *107*, 1324.

[4] Goetzberger, A.; Hebling, C.; Schock, H.-W. "Photovoltaic materials, history, status and outlook", *Materials Science and Engineering*. **2003**, *R 40*, 1.

[5] Huynh, W. U.; Dittmer, J. J.; Alivisatos, P. "Hybrid Nanorod-Polymer Solar Cells', *Science* **2002**, *295*, 2425.

[6] Coakley, K. M.; McGehee, M. D. "Conjugated Polymer Photovoltaic Cells", *Chem. Mater.* **2004**, *16*, 4533.

[7] Kang, Y.; Kim, D. "Well-aligned CdS Nanorod/Conjugated Polymer Solar Cells", *Solar Energy Materials & Solar Cells* **2006**, *90*, 166.

[8] Sun, B.; Marx, E.; Greenham, N. C. 'Photovolatic Devices Using Blends of Branched CdSe Nanopartivles and Conjugated Polymers" *Nano Lett.* **2003**, *3*, 962.

[9] Padinger, F.; Rittberger, R. S.; Sariciftci, N. S. "Effects of Postproduction Treatment on Plastic Solar Cells**",** *Adv. Funct. Mater.* **2003**, *13*, 85; Kim, J.

[10] Kim, S.; Lee, H.; Lee, K.; Ma, W.; Huong, X.; Heeger, A. J. "New Architecture for High-Efficiency Polymer Photovoltaic Cells Using Solution-Based Titanium Oxide as an Optical Spacer"**,** *Adv. Mater.* **2006**, *18*, 572.

[11] Kroon, J.M.; Wienk, M.M.; Verhees, W.J.H.;. Hummelen, J.C. "Accurate efficiency determination and stability studies of conjugated polymer / fullerene solar cells", *Thin Solid Films* **2002**, *403-404*, 223.

[12] Sih, B. C.; Wolf, M.O. "Metal nanoparticle-conjugated polymer nanocomposites", *Chem. Commun.* **2005**, 3375.

[13] (a) Bereznev, S.; Koeppe, R.; Konovalov, I.; Kois, J.; Günes, S.; Öpik, A.; Mellikov, E.; and Sariciftci, N.S. "Hybrid solar cells based on $CuInS_2$ and organic buffer–

sensitizer layers", *Thin Solid Films*, **2007**, *515*, 5759; (b) Arici, E.; Sariciftci, N. S.; Meissner, D. "Hybrid Solar Cells Based on Nanoparticles of $CuInS_2$ in Organic Matrices", *Adv. Funct. Mater.* **2003**, *2*,13; (c) Günes, S.; Fritz, K.; Neugebauer, H.; Sariciftci, N. S.; Kumar, S.; Scholes, G. "Hybrid solar cells using PbS nanoparticles", *Sol. Energy Mater. Sol. Cells* **2007**, *91*, 420.

[14] Arici, E.; Sariciftci, N. S.; Meissner, D. "Hybrid Solar Cells Based on Nanoparticles of CuInS2 in Organic Matrices**",** *Adv. Funct. Mat.*, **2003**, *13*, 165.

[15] Arici, E.; Meissner, D.; Schaffler, F.; Sariciftci, N. S. "Core/shell nanomaterials in photovoltaics",*Int. J. Photoenergy* **2003**, *5*, 199.

[16] Gűnes, S.; Fritz, K.; Neugebauer, H.; Sariciftci, N. S.; Kumar, S.; Scholes, G. "Hybrid solar cells using PbS nanoparticles", *Sol. Energy Mater. Sol. Cells* **2006**, *91*, 420.

[17] Empedocles, S. A.; Bavendi, M. G. "Spectroscopy of Single CdSe Nanocrystallites", *Acc. Chem. Res.* **1999**, *32*, 389.

[18] Andres, R. P.; Bielefeld, J. D.; Henderson, J. I.; Janes, D. B.; Kolagunta, V. R.; Kubiak, C. P.; Mahoney, W. J.; Oscifchin, R. G. "Self-assembly of a Two-Dimensional Superlattice of Molecularly Linked Metal Clusters", *Science* **1996**, *273*, 1690.

[19] (a) Peng, Z.; Wang, E.; Dong, S. "Incorporation of surface-derivatized gold nanoparticles into electrochemically generated polymer films", *Electrochem. Commun.* **2002,** *4*, 210; (b) Moorlag, C.; Sih, B. C. Scott, T. L.; Wolf, M. O. "Metal-containing conjugated materials: oligomers, polymers, and nonomaterials", *J. Mater. Chem.* **2005**, *15*, 2433.

[20] (a) Yang, X.-P.; Jones, R. A.; Lynch, V.; Oye, M. M.; Holmes, A. L. "Synthesis and Near Infrared Luminescence of a Tetrametallic Zn_2Yb_2 Architecture from a Trinuclear Zn_3L_2 Schiff Base Complex," *Dalton Trans.* **2005**, 849; (b) Yang, X.-P.; Jones, R. A.; Wiester, M. J. "A Nanoscale Slipped Sandwich of Tb_{10} - Stabilization of a Benzaldehyde Methyl Hemiacetyl," *Dalton Trans.* **2004**, 1787; (c) Jones, R. A.; Yang, X.-P.; Waheed, A.;Wiester, M.; Zhang, L. "New Complexes of Lanthanides with Unusual Main Group Ligands," ACS Symposium Series No. 917 Modern Aspects of Main Group Chemistry, **2005**, *917*, 221; (d) Yang, X.-P.; Jones, R. A. "Anion Dependant Self-Assembly of 'Tetra-Decker' and 'Triple-Decker' Luminescent Tb(III) Salen Complexes," *J. Am. Chem. Soc.* **2005**, *127*, 7686; (e). Yang, X-P.; Jones, R. A.; Wu, Q.; Oye, M. M.; Holmes, A. L.; Lo, W-K.; Wong, W-K. "Synthesis, Crystal Structures and Antenna-Like Sensitization of Visible and Near Infrared Emission in Heterobimetallic Zn-Eu and Zn-Nd Schiff Base Compounds" *Polyhedron*, **2006**, *25(2)*, 271; (f) Wong, W-K.; Yang, X. P.; Jones, R. A.; Rivers, J. H.; Lynch, V.; Lo, W-K.; Xiao, D.; Oye, M. M.; Holmes, A. L. "Multinuclear Luminescent Schiff-Base Zn-Nd

Sandwich Complexes" *Inorg. Chem*., **2006**, *45*, 4340; (g) Yang, X-P.; Jones, R. A.; Oye, M. M.; Holmes, A. L.; Wong, W-K. "Near Infrared Luminescence and Supramolecular Structure of a Helical Triple-decker Yb (III) Schiff Base Cluster", *Crystal Growth and Design*, **2006**, *6*, 2122; (h) Lo, W-K.; Wong, W. K.; Wong, W- Y.; Guo, J.; Yeung, K-T.; Cheng, Y-K.; Yang, X-P.; Jones, R. A. "Heterobimetallic Zn(II)-Ln(III) Phenylene-Bridged Schiff Base Complexes, Computational Studies and Evidence for Singlet Energy Transfer as the Main Pathway in the Sensitization of Near-Infrared Nd^{3+} Luminescence" *Inorg Chem*. **2006**, *45*, 9315.

[21] (a) Ganjali, M. R.; Poursaberi, T.; Basiripour, F.; Niassari, M. S.; Yousefi, M.; Shamsipur, M. "Highly Selective Thiocyanate Poly(vinyl chloride) Membrane Electrode Based on a Cadmium-Schiff's Base Complex," *Fresenius J. Anal. Chem.* **2001**, *370*, 1091; (b) Duran, M. L.; Rodriguez, A.; Romero, J.; Sousa, A. "Electrochemical Synthesis of Zinc and Cadmium Complexes with Schiff Bases Obtained from Salicylaldehyde Derivatives and 2-Aminoethylpyridine," *Synth. React. Inorg. Met. Org. Chem.* **1987**, *17*, 681; (c) Keypour, H.; Salehzadeh, S.; Pritchard, R. G.; Parish, R.V. "Cadmium(II) Complexes of Fully Condensed Schiff-base Ligands Derived From Two Different Symmetrical and Asymmetrical Tripodal Tetraamines and 2-Acetylpyridine: the Novel Observations for Heptadentate Mono-capped Trigonal Antiprismatic Schiff-base Complexes," *Polyhedron*, **2000**, *19*, 1633; (d) Lindoy, L. F.; Busch, D. H.; Goedken, V. "Helical Co-ordination: Five-Co-ordinate Zinc and Cadmium Complexes Formed by Metal-ion-induced Ligand Reactions," *J. Chem. Soc. Chem. Comm.* **1972**, 683; (e) Jantti, A.; Wagner, M.; Suontamo, R.; Kolehmainen, E.; Rissanen, K. "Schiff-base Podates-X-ray, NMR and Ab Initio Molecular-Orbital Studies of the Cadmium(II) Complexes of Linear and Three-Armed Podands in Solution and Solid State," *Eur. J. Inorg. Chem.* **1998**, 1555.

[22] (a) Prasad, R. N.; Tandon, J. P. "Gallium(III) Complexes of Monofunctional Bidentate Schiff Bases," *J. Less -Common Met.* **1974**, *37*, 141; (b) Prasad, R. N.; Tandon, J. P. "Schiff Base Complexes of Gallium," *J. Inorg. Nucl. Chem.* **1975**, *37*, 35; (c) Munoz-Hernandez, M-A.; Keizer, T. S.; Parkin, S.; Patrick, B.; Atwood, D. A. "Group 13 Cation Formation with a Potentially Tridentate Ligand," *Organometallics*, **2000**, *19*, 4416; (d) Qiao, J.; Wang, L. D.; Duan, L.; Li, Y.; Zhang, D. Q.; Qiu, Y. "Synthesis, Crystal Structure, and Luminescent Properties of a Binuclear Gallium Complex with Mixed Ligands," *Inorg. Chem.* **2004**, *43*, 5096; (e) Darensbourg, D. J.; Billodeaux, D. R. "Five-coordinate Schiff Base Complexes of Gallium. Potential for the Copolymerization of Carbon Dioxide and Epoxides," *Comp. Rend. Chim*. **2004**, *7*, 755; (f) Hill, M. S.; Atwood, D. A. "Formation and Reactivity of Five-coordinate Gallium Supported by Salen Ligands," *Eur. J. Inorg. Chem*. **1998**, *1*, 67; (g) Hill, M. S.; Hutchinson, A. R.; Keizer, T. S.; Parkin, S.; VanAelstyn, M. A.; Atwood, D. A. "Monomeric Group 13 Compounds with Bidentate (N,O) Ligands," *J. Organomet. Chem*. **2001**, *628*, 71; (h) Atwood, D. A.; Jegier, J. A.; Rutherford, D. "The First Structurally Characterized Salen-Indium Complexes," *Bull. Chem. Soc. Jpn*. **1997**, *70*,

2093; (i) Hill, M. S.; Atwood, D. A. "Synthesis and Reactivity of Five-coordinate Indium Halides and Alkyls," *Main Group Chem*. **1998**, *2*, 191.

[23] (a) Prasad, R. N.; Tandon, J. P. "Gallium(III) Complexes of Monofunctional Bidentate Schiff Bases," *J. Less -Common Met.* **1974**, *37*, 141; (b) Prasad, R. N.; Tandon, J. P. "Schiff Base Complexes of Gallium," *J. Inorg. Nucl. Chem.* **1975**, *37*, 35; (c) Munoz-Hernandez, M-A.; Keizer, T. S.; Parkin, S.; Patrick, B.; Atwood, D. A. "Group 13 Cation Formation with a Potentially Tridentate Ligand," *Organometallics*, **2000**, *19*, 4416; (d) Qiao, J.; Wang, L. D.; Duan, L.; Li, Y.; Zhang, D. Q.; Qiu, Y. "Synthesis, Crystal Structure, and Luminescent Properties of a Binuclear Gallium Complex with Mixed Ligands," *Inorg. Chem.* **2004**, *43*, 5096; (e) Darensbourg, D. J.; Billodeaux, D. R. "Five-coordinate Schiff Base Complexes of Gallium. Potential for the Copolymerization of Carbon Dioxide and Epoxides," *Comp. Rend. Chim*. **2004**, *7*, 755; (f) Hill, M. S.; Atwood, D. A. "Formation and Reactivity of Five-coordinate Gallium Supported by Salen Ligands," *Eur. J. Inorg. Chem*. **1998**, *1*, 67; (g) Hill, M. S.; Hutchinson, A. R.; Keizer, T. S.; Parkin, S.; VanAelstyn, M. A.; Atwood, D. A. "Monomeric Group 13 Compounds with Bidentate (N,O) Ligands," *J. Organomet. Chem*. **2001**, *628*, 71; (h) Atwood, D. A.; Jegier, J. A.; Rutherford, D. "The First Structurally Characterized Salen-Indium Complexes," *Bull. Chem. Soc. Jpn*. **1997**, *70*, 2093; (i) Hill, M. S.; Atwood, D. A. "Synthesis and Reactivity of Five-coordinate Indium Halides and Alkyls," *Main Group Chem*. **1998**, *2*, 191.

[24] Huynh, W. U.; Dittmer, J. J.; Alivisatos, A. P. "A Hybrid Planar-Mixed Molecular Heterojunction Photovoltaic Cell," *Adv. Mater.*, **2005**, *17*, 66.

[25] (a) Ganjali, M. R.; Poursaberi, T.; Basiripour, F.; Niassari, M. S.; Yousefi, M.; Shamsipur, M. *Fresenius J. Anal. Chem.* **2001**, *370*, 1091; (b) Duran, M. L.; Rodriguez, A.; Romero, J.; Sousa, A. *Synth. React. Inorg. Met. Org. Chem.* **1987**, *17*, 681; (c) Keypour, H.; Salehzadeh, S.; Pritchard, R. G.; Parish, R.V. *Polyhedron*, **2000**, *19*, 1633; (d) Lindoy, L. F.; Busch, D. H.; Goedken, V. *J. Chem. Soc. Chem. Comm.* **1972**, 683; (e) Jantti, A.; Wagner, M.; Suontamo, R.; Kolehmainen, E.; Rissanen, K. *Eur. J. Inorg. Chem.* **1998**, 1555.

[26] Zhang, L.; Jones, R. A.; Lynch, V. M. "Synthesis and structure of a novel supramolecular Zn3Co8 assembly containing a linear Zn3 core", *Chem. Comm.*, **2002**, 2986-2987.

[27] (a) Bailey, S. G.; Flood, D. J. *Prog. Photovolt. Res. Appl.* **1998**, *6*, 1; (b) Schock, H. W.; Noufi, R. *Prog. Photovolt. Res. Appl.* **2000**, *8*, 151.

[28] Castro, S. L.; Bailey, S. G.; Raffaelle, R. P.; Banger, K. K.; Hepp, A. F. "Synthesis and Characterization of Colloidal $CuInS_2$ Nanoparticles from a Molecular Single-Source Precursor", *J. Phys. Chem. B* **2004**, *108*, 12429.

[29] (a) Cummins, C. C.; Schrock, R. R.; Cohen, R. E. "Synthesis of ZnS and CdS within ROMP Block Copolymer Microdomains," *Chem. Mater.* **1992**, *4*, 27; (b) Sone, E. D.; Zubarev, E. R.; Stupp, S. I. "Semiconductor Nanohelices Templated by Supramolecular Ribbons," *Angew. Chem., Int. Ed.* **2002**, *41*, 1705; (c) Sone, E. D.; Stupp, S. I. "Semiconductor-Encapsulated Peptide-Amphiphile Nanofibers," *J. Am. Chem. Soc.* **2004**, *126*, 12756; (d) Sone, E. D.; Zubarev, E. R.; Stupp, S. I. "Supramolecular Templating of Single and Double Nanohelices of Cadmium Sulfide," *Small*, **2005**, *1*, 694; (e) Tassoni, R.; Schrock, R. R. "Synthesis of PbS Nanoclusters within Microphase-Separated Diblock Copolymer Films," *Chem. Mater.* **1994**, *6*, 744-749.

[30] Sheldrick, G. M. SHELX 97, *A software package for the solution and refinement of X-ray data*; University of Göttingen: Göttingen, Germany, **1997**.

[31] Cromer, D. T.; Waber, J. T. *International Tables for X-Ray Crystallography*, Kynoch Press, Birmingham, vol. 4, **1974**, Table 2.2A.

Chapter 2: Design and CVD Growth of Amorphous Metallic Alloys from Single Source Precursors

2.1. Overview of Chemical Vapor Deposition

Chemical Vapor Deposition (CVD) is a process used to generate thin films of high-purity, high-performance materials by a chemical reaction of fluid, gaseous reactant(s) on a solid surface. In a typical CVD procedure, the solid surface, or substrate, is exposed to one or more volatile precursors, which may react and/or decompose on the substrate surface to produce the desired mateial. Because the reactant fluid surrounds the solid object, deposition occurs on every surface, with little regard to direction. Therefore, thin films produced from chemical deposition techniques tend to be conformal, rather than directional as is the case with physical deposition methods. Control of layer thickness for films deposited by CVD can be within a few tens of a nanometer. A familiar example is the formation of soot on a cool object when placed inside a flame. The ability to rapidly and economically coat non-planar objects has contributed to a rise in the use of CVD methods.[1] Solar cells and layers, for example, are now commonly fabricated by CVD processes. Furthermore, coatings of Ti_xN_y, (known as "synthetic gold") are used on a great volume of personal jewelry for cosmetic purposes and to provide a tough, scratch-resistant outer shell at an attractive economic cost.[1]

One of the earliest examples of CVD was reported by Baker and Morris in 1961 describing the deposition of thin films of tin and lead by electron beam decomposition of vaporized metal alkyls.[2] Shortly after, Sterling and Swann patented a method for

depositing SiO_2 onto a heated lens from silane and nitrous oxide.[3] Since these seminal reports, a number of forms of CVD have been developed and are frequently referenced in the literature. These techniques differ in the activation processes that initiate the relevant chemical reactions and process conditions. Depostions by Organometallic Chemical Vapor Deposition (OMCVD), for example, employ precursors that contain a direct metal-carbon interaction, regardless of whether its nature is σ or π, and there is considerable flexibility in the design of deposition precursors. Modification of the organic ligands comprising the precursor complex can impart various steric and/or electronic features that affect the mechanisms by which reactions or decompositons occur. Ultimately, deposition properties may be affected by such modifications.

CVD is well suited for the generation of thin films of various compositions on a wide range of planar *and* non-planar substrates. CVD processes may be run under mild conditions (i.e. low temperatures), offer control over microstructure and composition, provide high deposition rates, and allow for large-scale processing. The critical factor for any CVD process, however, is selection of suitable precursors. A CVD experiment can employ a precursor molecule for each element in the resulting film, or a single precursor molecule that contains all of the desired elements. The precursor(s) are delivered to the substrate in the vapor phase. The vaporization of a low-volatility precursor is commonly achieved by using a combination of heat, reduced pressure, and/or a carrier gas. Typically, the precursor delivery lines and other sections of the deposition apparatus must be heated to avoid condensation of the precursor prior to reaching the substrate. This issue may be resolved by placing the precursor and its delivery lines inside an oven. The

chemical reaction or decomposition of the precursor(s) to form the film is usually induced thermally by heating or photochemically by illumination of the substrate surface.

At the outset, rsearchers were restricted to precursors that were readily known and commericially available. This led practioners of CVD for semiconducting materials to regularly use highly toxic and pyrophoric compounds (e.g. AsH_3, PH_3, H_2Se, Me_3Al). Use of such reagents may be avoided by considering the intrinsic properties of the compounds containing the elements of interest. When selecting suitable candidates for a CVD precursor, the following characteristics are among those that should be considered:[1,4]

1. The precursor should deposit the desired elements upon decomposition and the deposition of undesired elements should be avoided.
2. In most cases the precursor is either a liquid or a solid with sufficient vapor pressure and mass transport at the preferred temperature (ideally below 200 °C).
3. The precursor must be oxidatively, hydrolytically, thermally, and photochemically stable under normal storage conditions, but exhibit sufficient reactivity to permit decomposition at a reasonably low temperature.
4. The precursor should be relatively easy to prepare and purify.

Controlled deposition of the required elements for the intended film is not entirely straightforward and, consequently, not easily obtainable. This has been illustrated in the

attempted use of gallium amide complexes as single-source precursors for gallium nitride, GaN.[4] Often, upon decomposition, gallium metal is deposited and nitrogen remains unincorporated as a volatile by-product. Deposition of undesired elements has also proven to be problematic. Attempts to employ trimethyl gallium as a gallium precursor have yielded films contaminated with high levels of carbon.[4]

Volatility issues must be addressed as well. Compounds that cannot be transported to the substrate at reasonable rates in the vapor phase perform poorly as precursors. Expensive and difficult-to-handle high vacuum equipment must often be used to vaporize nonvolatile precursor molecules. Fluctuations in vapor pressure may also be a problem. Researchers attempting the CVD of high temperature superconducting materials have shown that the vapor pressures of fluorinated β-diketonate alkali earth complexes of calcium, barium and strontium steadily decrease during the deposition experiments.[5] Such vapor phase instability leads to uneven delivery rates. Precursors that are likely to be oligomeric should be avoided as large molecules tend to have low vapor pressures.

A delicate balance must be achieved between stability and reactivity of the precursor. Poor stability results in unwanted decomposition during synthesis, purification and/or storage. Conversely, the compound(s) must exhibit sufficient reactivity at a reasonable temperature to be useful. This is necessary in order to prevent diffusion processes between the substrate and film that often occur for deposition at higher temperatures. Poor quality layers typically result from such diffusion. In a multi-precursor system, the precursors should require heating or photolysis to initiate the

reaction with each other. This is to avoid gas-phase reactions between the precursors that can lead to deposition on surfaces other than the substrate. These undesirable gas-phase processes also prematurely consume the precursor.

In order to ensure that there is sufficient availability of the material for testing and fabrication, the synthesis of the precursor should be relatively simple and reproducible. The preparation must allow for purification of the compound to a relatively high level of purity. All of this must hold true for large-scale preparations as well as for smaller scale syntheses. Ideally the precursor should be derived from readily available starting reagents and require the minimum number of chemical transformations in order to minimize cost.

2.2. CVD of Thin Film Materials

Microfabrication processes routinely employ CVD to deposit materials in various forms, including: monocrystalline, polycrystalline, epitaxial and amorphous. These materials include: silicon, carbon fiber, carbon nanofibers, carbon nanotubes, filaments, SiO_2, silicon-germanium, tungsten, silicon carbide, silicon nitride, silicon oxynitride, titanium nitride, and a number of high-*k* dielectrics. In fact, CVD is also used to produce synthetic diamonds. The work discussed herein focuses primarily on the CVD growth of metallic-based *amorphous* thin films.

2.2.1. Background: Amorphous Materials

A great number of thin film materials incorporate metal atoms derived from metal-containing precursors. Most metals are crystalline in their normal state, having a

highly ordered arrangement of atoms. In contrast, amorphous metals and alloys are *non*-crystalline metallic materials with a disordered atomic-scale structure. Amorphous materials lack the long-rang order exhibited by normal, crystalline metals. However, the attractive interactions and difference in sizes of atoms of different types in amorphous metallic alloys do lead to a short-range order that can be characterized by clusters of "solute" atoms of one type surrounded by "solvent" atoms of a more numerous type.[6] Materials that exhibit a disordered structure produced directly from the liquid state during cooling are referred to as "glasses", and so amorphous metals are routinely called "metallic glasses" or "glassy metals". There are, however, a number of other ways to produce amorphous metals including physical vapor deposition (PVD), solid-state reactions, ion irradiation, and mechanical alloying. Relatively, few examples of thin film growth of amorphous metallic alloys by CVD have been reported.

Amorphous materials that do not exhibit long range order at the atomic level are well known. Optically clear glasses derived from oxides of silicon, metalloids and metals have been known for thousands of years. Amorphous silicon is used in the microelectronics industry for solar cell technologies and amorphous thin films of Si and Si/Ge alloys have applications as semiconductors. More recently amorphous films of transition metal nitrides like WN and TaN have been explored for barrier layer applications and diffusion barriers. Due to its amorphous nature, among other characteristics, SiO_2 has held a central role as the gate dielectric in microelectronics. The most common glass forming alloy combinations are (a) transition metal-metalloid systems such as Fe-B and Fe-P, (b) early transition metal-late transition metal alloys such

as FeZr and FeTi, or (c) simple metallic glass such as MgZn.[7] A number of binary systems such as CaAl, CuZr, and CuHf have been reported to form a glassy phase with high stability.[8]

Although amorphous alloys have received considerable interest in recent years, the issues regarding glass formation as well as atomic-level structure are still not well understood. A number of studies have been directed toward investigating the mechanism of glass formation. Researchers have attributed several factors to the formation of an amorphous state such as eutectic composition, atomic size mismatch and a large negative heat of mixing.[9] Formation in metal-metal binary alloys such as CuMg is favored by large negative heat of formation, nondirectional bonds and a tendency to maximize packing fraction.[10] Kinetic parameters have also been considered to play an important role in glass forming ability. Turnbull has noted the importance of the ratio of the glass transition temperature T_g to the liquidus temperature T_l in determining glass forming ability.[11] Greater glass forming ability can be obtained when there is a small difference between the liquidus temperature and the glass transition temperature. This provides an explanation for the high glass forming ability exhibited by transition metal–metalloid metallic glasses near compositions corresponding to deep eutectics. Additionally, it has been reported by Lu *et al.* that, because glass formation processes compete with the liquid phase and the resulting crystalline phase, the system's crystallization temperature may play a critical role in determining glass formation.[12] Glass formation would be facilitated if the liquid phase is stabilized upon cooling and the competing crystalline phases precipitate with difficulty.

Multicomponent systems that exhibit great stability with respect to crystallization, generally referred to as bulk metallic glasses (BMG), have been discovered and have renewed interest in this field. BMG are predominantly metallic in nature and have been known since 1960.[13] Due to the amorphous nature of the BMG, crystalline defects such as grain boundaries, dislocations and stacking faults, which are typical of metals, are absent. They have therefore attracted significant attention for their extraordinary engineering properties like strength, hardness, toughness and elasticity. Other useful properties exhibited by BMG include soft magnetic behavior and high corrosion resistance. Still others have been explored as catalysts. Much of the interest in thin films of amorphous metallic alloys stems from their potential utilization as catalysts, in ultra large scale microelectronics devices (ULSIs) and as diffusion barriers.

A variety of methods used to convert BMG into thin films based on physical methods have been reported including PVD, magnetron sputtering and ion beam assisted deposition (IBAD). Growth of thin films by CVD offers several important advantages over physical growth. These include (a) economical scale-up, (b) ease of operation, (c) mild growth conditions and (d) the ability to achieve conformal coverage on features with high aspect ratios. While examples of chemical growth during electrochemical deposition have been reported, there are very few examples of thin film growth of amorphous metallic alloys by CVD.[14] This may be a result from the fact that the chemical nature of the precursor is critical to the outcome of the CVD process and suitable precursors for such materials have simply not been developed. The few documented examples of amorphous metallic alloys grown by CVD include nitrides (WN,[15] TaN,[16] CrMoN[17]),

borides (FeB,[18] NiB_x[19]), carbides (TiC[20]), and oxides ($FeCo_xO_y$[21]).

2.3. CVD Growth of Amorphous Ru-P Alloy Films from a Single Source Precursor

Ultra-large-scale integrated microelectronic devices have seen continued improvement in functionality, operating speed and circuit density over the past decades. This has led to the use of Cu-based interconnects in these systems. Cu presents several advantages over the Al metal it displaced including lower resistivity and higher electromigration resistance. However, a diffusion barrier must be incorporated into the design since Cu readily diffuses into silicon resulting in impurities and/or the formation of silicides. Currently, Ta or a TaN/Ta multilayer stack deposited by physical vapor deposition (PVD) onto an interlayer dielectric serves as the Cu diffusion barrier. A Cu seed layer is deposited on the Ta barrier layer for subsequent Cu electroplating.[22] However, the PVD technology employed to grow Ta or the TaN/Ta multilayer stack may not be well suited for the production of 32-nm generation of devices and beyond where an ultra-thin (< 3 nm) and conformal barrier/cladding layer multilayer stack is required in order to maintain a low effective interconnect resistivity.[23] This has stimulated investigations into new barrier/cladding layer materials including $TiSi_xN_y$,[24] WN_xC_y [25] and Ru [26], and on alternate deposition technologies, such as CVD and atomic layer deposition (ALD).

2.3.1. Introduction

Ruthenium has been considered for numerous microelectronics applications, including utilization as a Cu diffusion barrier and Cu seed layer owing to its low

resistivity (~ 7 μΩ cm), chemical stability, and low solubility with Cu.[26a] Recent studies, however, indicate some barrier limitations exhibited by Ru films. It has been shown that Cu diffusion persisted through a 20 nm Ru film at temperatures above 450 °C, and a 5 nm Ru film lost its barrier property at temperatures above only 300 °C.[27] Films of ruthenium can be grown by CVD or ALD methods from precursors including Ru carbonyl ($Ru_3(CO)_{12}$) [26b], cyclopentadienyl or substituted cyclopentadienyl derivatives such as Cp_2Ru [26c] or $(EtCp)_2Ru$ [26d], and β-diketonates such as $Ru(thd)_3$ [26e], (Cp = η^5-C_5H_5, EtCp = η^5-C_5H_4Et, thd = 2,2,6,6-tetramethyl-3,5-heptanedione). Generally, Ru films deposited by CVD or PVD methods lead to polycrystalline, columnar films. Cu diffusion can occur rapidly across grain boundaries because of the much greater diffusion at these features than in the bulk.[28] If formation of columnar structures in thin Ru films leads to poor barrier properties, controlling the microstructure of Ru films may provide improvements in barrier capabilities. Elimination or suppression of fast Cu diffusion through grain boundaries may be achieved by modifying the Ru film microstructure from polycrystalline to nanocrystalline, or even further to an amorphous state.

The work discussed in this chapter describes the CVD growth of ultra-thin films of *amorphous* ruthenium-phosphorous (Ru-P) alloy metal films employing *cis*-$RuH_2(PMe_3)_4$ (Me = CH_3), **2-I**, as a single-source precursor.[29] Interestingly, all of the precursors employed previously for the CVD growth of Ru films (noted above) carry either hydrocarbon, carbon monoxide (CO) or oxygen donor ligands bound to Ru. Therefore, they all contain Ru-C or Ru-O bond

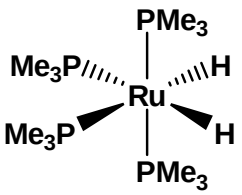

2-I

connectivities. Since ligand selection can often have a significant effect on the outcome of a CVD process, **2-I**, which contains Ru-H and Ru-P bonds, was explored. Choice of the Ru-H bond was driven by the desire to facilitate dissociative adsorption of *cis*-$H_2Ru(PMe_3)_4$, and the PMe_3 ligands were selected as potentially stable, volatile leaving groups. To our surprise, under the growth conditions employed, highly conformal, smooth films of amorphous RuP alloys (P 15-20 %) were obtained.[30] Growth of RuP may have been anticipated since complete demethylation of adsorbed PMe_3 has been shown on Ru(0001) by 227 °C and the adsorbed P subsequently reacted to form Ru_xP above 327 °C.[31] In fact, in separate experiments performed by members of the Ekerdt group, **2-I** was found to undergo demethylation at 287 °C when adsorbed at 182 °C.

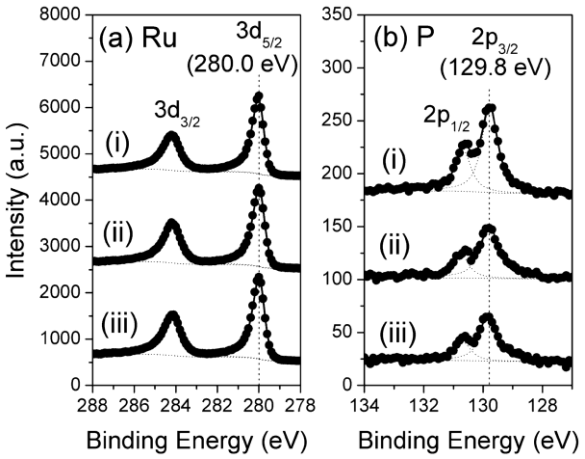

Figure 2.1. High resolution XPS result of the (a) Ru 3d and (b) P 2p peaks for a film deposited at 300 °C. The spectra (i), (ii), and (iii) correspond to sputtering times of 5, 45, and 105 s, respectively. Attenuation of the P 2p peaks with depth profiling (sputtering) illustrates the concentration changing from 28% at the surface to ~15% within the bulk.

2.3.2. Results and Discussion

Amorphous RuP films were grown in a cold-wall CVD reactor on thermally grown SiO_2 substrates at growth temperatures of 250-300 °C and a pressure of 200 mTorr. Argon was used as a carrier gas. The films have been characterized by X-ray photoelectron spectroscopy (XPS), tunneling electron microscopy (TEM) and X-ray diffraction (XRD) methods. XPS measurements revealed the presence of Ru and P both in the zero oxidation state (Fig. 2.1). Thus, for the films grown at 250 and 300

°C, the binding energy of the Ru $3d_{5/2}$ peak is observed at 280.0 eV. The P $2p_{3/2}$ peak is at 129.8eV indicating the presence of phosphorus in elemental form and, therefore, not donating or accepting electrons with Ru.[32]

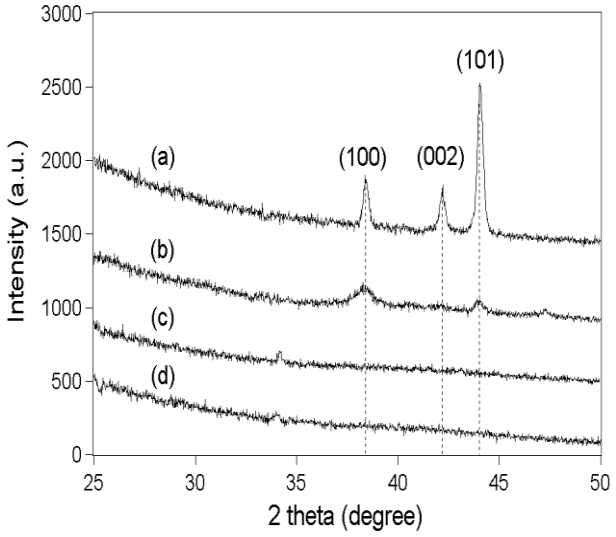

Figure 2.2. XRD of ~30 nm RuP deposited at 300 °C from **2-I**: (a) after annealing to 700 °C for 30 min, (b) after annealing to 500 °C for 30 min, (c) after annealing to 300 °C for 30 min, and (d) after growth. The (100), (002), and (101) diffraction features at 38.6, 42.4, and 44.2°, respectively, are associated with hcp Ru.

The presence of elemental Ru and P therefore distinguishes these materials from the well known binary phosphides of Ru such as Ru_2P, RuP_4 and RuP_2, which exhibit precise stoichiometries and contain the P^{3-} phosphide anion and related species.[33] X-ray diffraction (XRD) data reveal that the films lack long-range order (Fig. 2.2) and the amorphous nature of the films is confirmed by selected area diffraction (SAD) studies (Fig. 2.3).

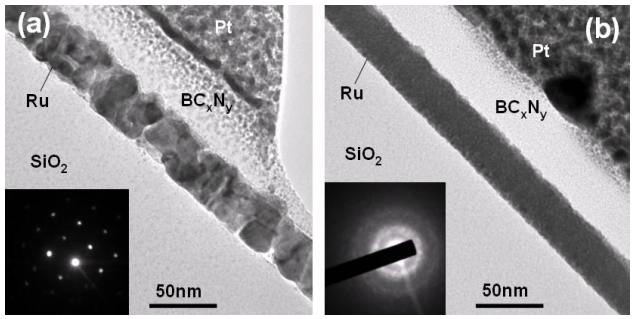

Figure 2.3. SAD patterns and cross section transmission electron micrographs of (a) a PVD Ru film, and (b) a CVD RuP film grown at 300 °C.

High resolution transmission electron microscopy (TEM) images also confirm the non-crystalline character of the films although a few small Ru crystallites ~5 nm in size were

observed adjacent to the SiO_2 substrate. The films remain amorphous upon heating for 3 hr at 350 °C, and then begin to crystallize upon annealing at 500 °C for 30 min under vacuum, though they are still predominantly amorphous. This was revealed in SAD images, the XRD annealing series in Fig. 2.2, and separately in TEM images. Crystallization of the metastable amorphous phase after annealing to these higher temperatures is expected.[34]

Ab initio molecular dynamics (MD) studies, performed by members of the Hwang group, show that a glassy structure exhibiting topological and strong chemical short-range order can result from Ru-P alloys with moderate P content. The $Ru_{80}P_{20}$ structure (Fig. 2.4) exhibits medium-range order arising from packing the "quasi-equivalent" P-centered Ru clusters in three-dimensional space. Indeed the short-to-medium range order is seen in other transition metal-metalloid systems where the chemical short-range-order is significant.[13b] These MD simulation results sufficiently provide insight into the nature of local packing in Ru-P amorphous structures.

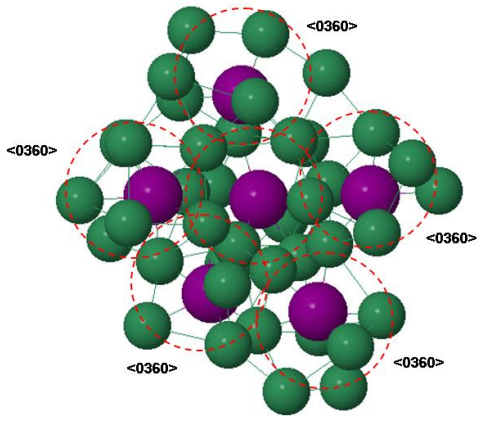

Figure 2.4. Modeling results for the packing of the solute-centered polyhedra for a Ru_{80}:P_{20} mixture. Large (purple) and small (green) balls represent P and Ru atoms, respectively.

2.3.3. Future Studies

The results described above create a number of fundamental questions. For

example, in the precursor molecule **2-I**, both Ru and P have non-zero formal oxidation states (+2 and +3, respectively). How does this compound decompose to give an alloy containing Ru(0) and P(0)? It is evident that detailed mechanistic studies of the CVD growth process should be performed in order to address this issue. Understanding these processes will be essential to the identification and/or development of precursors for the CVD of amorphous metallic alloys. Thin films of amorphous metal–phosphorus alloys grown by CVD are apparently uncommon and very little is known of their chemical and physical properties. With the exception of the studies on the RuP system described above it seems that it is actually quite challenging to grow other amorphous metal-phosphorus alloys by CVD. For example, under similar growth conditions Choi *et al*. have shown that the Fe analog of **2-I**, $H_2Fe(PMe_3)_4$, produces thin films of Fe metal and the liberated PMe_3 does not decompose.[35] Trialkylphosphite derivatives of Co and Ni also produced thin films of pure polycrystalline metals.[36,37] Ru may be a special case since it is also known that adsorbed PMe_3 undergoes complete demethylation on Ru(0001) on heating to 500 K and the adsorbed P then reacts to form Ru_xP above 600 K.[32] This suggests that under the conditions of our film growth **2-I** initially decomposes to produce Ru metal which then catalyzes the demethylation of PMe_3 present in the reaction chamber and this allows the eventual formation of the RuP alloys. This leads to the intriguing possibility that the combination of Ru with PMe_3 is key to the formation of thin films of other novel amorphous metal-phosphorus alloys by CVD. Thus, growth of thin films of Fe_xP_y, for example, may be accessible through CVD using $H_2Fe(PMe_3)_4$ in combination with a catalytic quantity of *cis*-$H_2Ru(PMe_3)_4$ (**2-I**). The resulting thin films of Fe_xP_y (containing

trace levels of Ru) should be amorphous, due to the presence of elemental P generated by the catalytic quantity of **2-I**.

Subsequent research should be directed toward: (1) Detailed mechanistic studies on the decomposition pathways of **2-I**. These will aid the ensuing development of precursors for the CVD growth of other novel amorphous metal-phosphorus alloys. (2) Investigations into the use of **2-I** to serve as a catalyst for the CVD growth of thin films of other transition metal-phosphorus alloys (M_xP_y) which are not otherwise accessible. (3) The design and synthesis of new volatile precursors for the CVD growth of amorphous metal-phosphorus alloys. (4) Preliminary investigations into the use of these materials for meaningful processes in the microelectronics and/or petroleum refining industries.

Perhaps central to the role of research conducted along this line in the Jones Group is the identification and/or development of metal-containing precursors for the growth of new amorphous alloys. Currently work is underway to prepare (a) ruthenium-phosphine complexes which bear alternate trialkylphosphine ligands, (b) complexes analogous to **2-I** that incorporate different metal centers, and (c) ruthenium complexes that feature tunable organometallic ligands.

(a) Alternate trialkylphosphine-ruthenium complexes. As noted above, trimethylphosphine undergoes complete demethylation in the presence of ruthenium upon heating. This may be critical to the formation of Ru-P amorphous films and may even be unique to trimethylphosphine-ruthenium systems. However, investigating the use of ruthenium complexes that bear other trialkylphosphine ligands may provide valuable

information regarding the mechanism of decomposition and may even give films with different properties. The triethylphosphine analog of **2-I**, *cis*-$H_2Ru(PEt_3)_4$ (Et = C_2H_5), has been synthesized according to the literature procedure[38] and is awaiting to be tested. Upon preparation, the product was easily identified through its ^1H and ^{31}P NMR spectra, which matched the literature.

(b) Group VIII analogues. Our preliminary results deal with the generation of Ru-containing amorphous films from the precursor **2-I**; however, analogous M-P (M = Group VIII metal) containing complexes are also of interest. Such precursors may provide films which incorporate different metals, and therefore provide different film properties. Currently, efforts towards the preparation of $RhH(PMe_3)_4$,[39] *cis*-$OsH_2(PMe_3)_4$,[40] and $PtH_2(PMe_3)_2$[41] as well as first row derivatives such as $FeH_2(PMe_3)_4$, $CoH(PMe_3)_4$ and $Ni(PMe_3)_4$ are underway. These precursors may be deposited independently to produce amorphous films incorporating their respective metal with phosphorus, or may be used in conjunction with a catalytic amount of **2-I** to initiate the decomposition that produces M-P type amorphous alloys.

(c) New Classes of Precursors. Controlling the composition of a film allows for control over its chemical and physical properties. This is tremendously important for the design of materials with useful properties. The ability to exhibit such control in a predictable fashion is challenging. One interesting feature of the amorphous RuP alloys we have studied is our ability to control the P content in the grown films by variation of the growth pressure. For example, films grown at 300 °C and 200 mTorr contain approximately 15 % P while those grown at 300 mTorr have 20 % P. Preliminary

electrical conductivity measurements on these two films show remarkable differences: the 15% P film has a resistivity of 380 μΩ·cm while that for the 20% P film is 800 μΩ·cm. Thus the electrical properties of the film are dramatically affected by a difference of 5% in P concentration. Furthermore, upon annealing the 20% film to 500 °C, the film remains amorphous, yet its resistivity drops to 400 μΩ.cm. This demonstrates that we have a simple, yet very effective way of tuning the properties of these films.

2.3.4. Related Ruthenium Chemistry

In addition to varying the growth parameters, designing and testing new volatile precursors for CVD growth should allow for control over the composition of the films. Based on our results with **2-I** it seems reasonable to assume that other Ru complexes bearing PMe_3 could serve as CVD precursors to amorphous RuP alloys. Careful selection of ancillary ligands should provide volatile precursors with tunable properties. In this context several nitrogen based donor ligands are known which could serve to facilitate dissociative adsorption of the molecule on the growing surface and also provide sufficient volatility and stability to the precursor. We are currently investigating the synthesis of Ru complexes which feature PMe_3 in addition to selected pyrazolate, amidinate, and β-

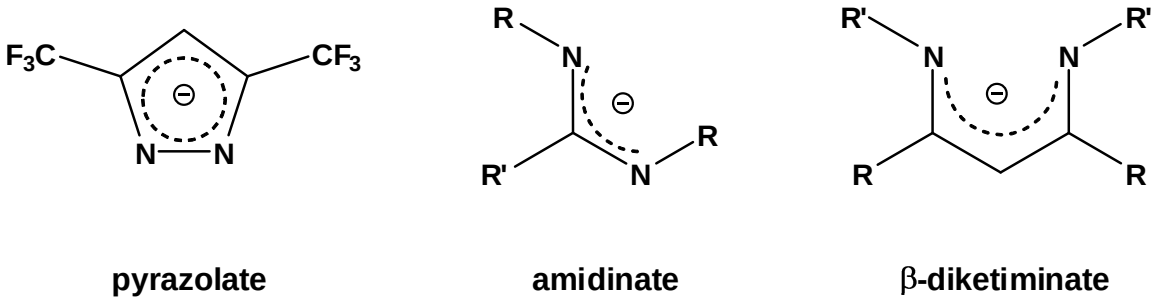

pyrazolate **amidinate** **β-diketiminate**

Scheme 2.1. Nitrogen based ligands for CVD precursor development.

diketiminates ligands (Scheme 2.1). For example, reaction of **2-I** with 3,5-bis(trifluoromethyl)pyrazole (PzH) should result in the liberation of H_2 and the formation of a new Ru-Pz complex, *i.e.*

$$\textit{cis}\text{-}RuH_2(PMe_3)_4 + 2PzH \longrightarrow (Pz)_2Ru(PMe_3)_4 + 2H_2 \quad \textbf{(Eq.1)}$$

Although the product, $(Pz)_2Ru(PMe_3)_4$, may lose PMe_3 and dimerize *via* bridging Pz units, it should still be suitable for CVD studies. Analogous reactions with β-diketiminates and amidinates should also be explored.

For the sake of completeness it should also be noted that several ruthenium-pyrazolate complexes including **2-II** – **2-V** have been prepared in our lab *via* ligand substitution reactions of lithium 3,5-bis(trifluoromethyl)pyrazolate with various chloride and triflate containing ruthenium organometallic compounds (Fig. 2.5).[42] Although the new compounds do not seem volatile enough for CVD processes in general, their isolation and characterization has helped to develop the chemistry of the Pz/Ru system in general and this work may be of use in further attempts to obtain viable precursors.

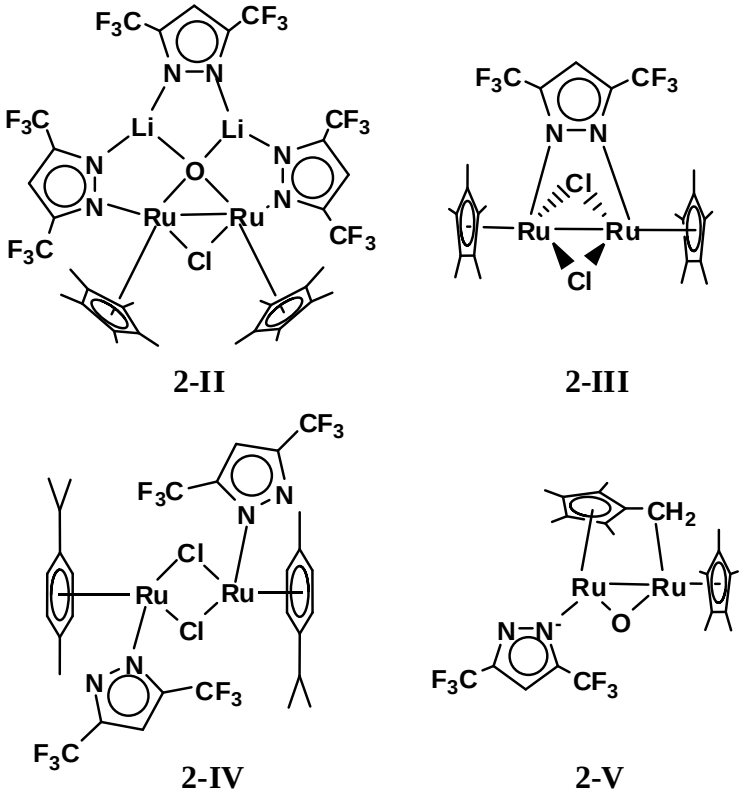

Figure 2.5. 3,5-bis(trifluoromethyl)pyrazolate derivatives **2-II** - **2-V**.

2.3.5. Ruthenium Azide Derivative

Since phosphorus and nitrogen are in the same group (group 15) we were naturally interested to see if analogous amorphous alloys of Ru_xN_y , or even $Ru_xP_yN_z$, could be formed. A suitable precursor for this kind of material is the bis azide ruthenium complex *trans*-$(N_3)_2Ru(PMe_3)_4$, which can be conveniently prepared from $RuCl_2(PMe_3)_4$.[43] This compound proved to be unsatisfactory for CVD studies due to low volatility. However, it was employed as a starting material for a potential *pyrazolate* based complex since the azides are relatively basic and could undergo a simple acid/base

reaction with PzH, like **2-I**, *i.e.*

$$\textit{trans}\text{-}(N_3)_2Ru(PMe_3)_4 \;+\; 2PzH \;\longrightarrow\; (Pz)_2Ru(PMe_3)_4 \;+\; 2\,HN_3 \quad \textbf{(Eq.2)}$$

Accordingly, one mole of *trans*-$(N_3)_2Ru(PMe_3)_4$ was mixed with two moles of 3,5-bis(trifluoromethyl)pyrazole in toluene at reflux. Surprisingly, the expected product from ligand substitution was not the major product. Rather, the interesting dinuclear tris "one-end" azide bridged structure $\{(Me_3)P_3Ru]_2(\mu_1\text{-}N_3)_3\}\cdot 3[(3,5\text{-}CF_3)_2PzH]$, **2-VI,** was obtained (Scheme 2.2). In the solid state the dinuclear Ru_2^{3+} moiety cocrystallizes with three neutral $(3,5\text{-}CF_3)_2PzH$ molecules. Reddish brown crystals **2-VI** were obtained upon

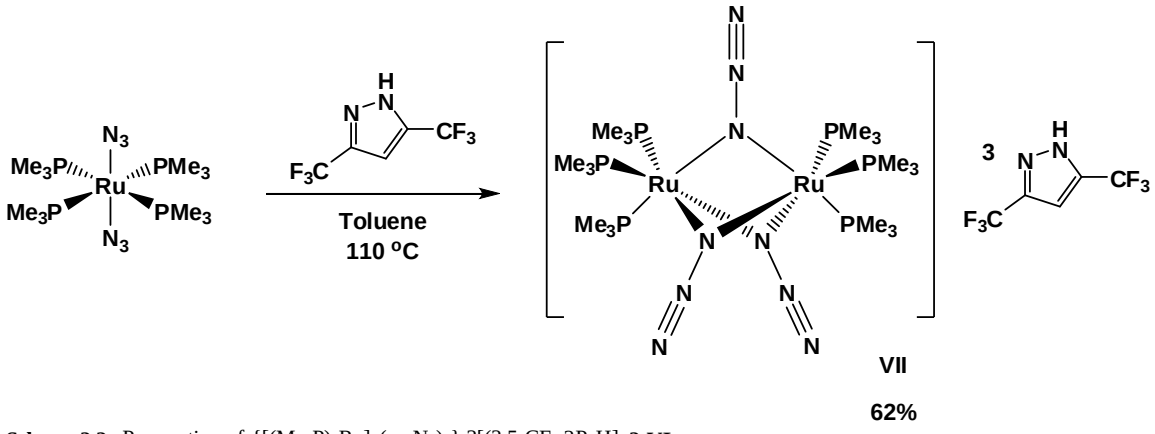

Scheme 2.2. Preparation of $\{[(Me_3P)_3Ru]_2(\mu_1\text{-}N_3)_3\}\cdot 3[(3,5\text{-}CF_3)2PzH]$, **2-VI**.

cooling the reaction mixture at -60 ºC for 24 h. Although dinuclear "one-end" azide bridged complexes of transition metals such as rhenium, manganese and copper are known,[44] no examples of such dinuclear ruthenium complexes have been reported to our knowledge. The structure of **2-VI** was determined by X-ray diffraction which clearly

shows the $Ru_2(N_3)_3$ core (Fig. 2.6). Compound **2-VI** crystallizes in the triclinic space group P1 with two independent molecules per unit cell. Each Ru atom resides an a distorted octahedral environment surrounded by three PMe_e ligands and three bridging azide ligands. The Ru-Ru distance was found to be 3.17 Å. Each azide ligand is fairly symmetric with average bond distances of 1.19 Å between the metal-bound and central nitrogen atoms and 1.15 Å between the middle and terminal nitrogen atoms. The Ru-N-Ru bond angles are all comparable and average to 91.5 º, as are the N-Ru-N bond angles which average to 74.3º. Crystallographic data is presented in Table 2.1 and selected bond lengths and angles for **2-VI** are provided in Table 2.2. The ^1H NMR spectrum of **2-VI** exhibits a sharp singlet at 6.99 and a broad singlet centered at 6.00 ppm corresponding to the C- and N-bound protons of the pyrazolate moieties, respectively, and a multiplet at 1.62 ppm corresponding to the protons of the six equivalent PMe_3 ligands. One intense singlet at 19.77 ppm in the $^{31}P\{^1H\}$ NMR spectrum further confirms the symmetry of the complex. The IR spectrum shows bands at 2059 and 1364 cm^{-1} associated to the asymmetric and symmetric stretches, respectively, of the bridging azide groups. Further

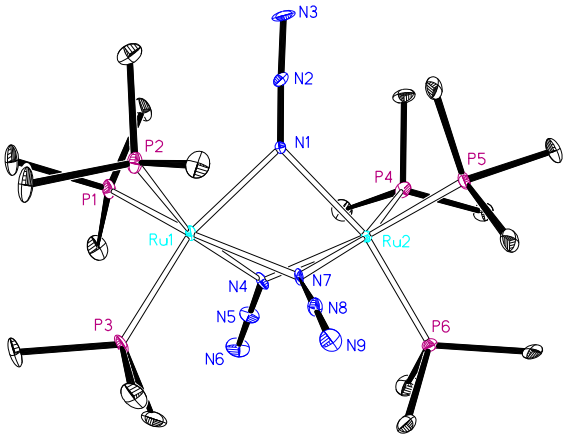

Figure 2.6. ORTEP view ofthe dinuclear ruthenium moiety of $\{[(Me_3P)_3Ru]_2(\mu_1\text{-}N_3)_3\}3[(3,5\text{-}CF_3)_2PzH]$, **2-VI**, with the numbering scheme. Ellipsoids are drawn at 25% robability level. Hydrogen atoms are omitted for clarity.

studies of ruthenium azide complexes are described in Chapter 3.

2.3.6. Conclusions

To summarize, the use of a single source precursor for the CVD growth of ultra-thin films of amorphous RuP alloys has been described. Significantly, the chemical composition of the precursor has a direct influence on both the elemental composition and morphology of the grown films. To the best of our knowledge these films are the first CVD grown binary transition metal phosphorus amorphous alloys. Further studies on the mode of decomposition of **2-I** and properties of the new films are in progress. The use of a catalytic quantity of **2-I** to promote decomposition of analogous M-P containing complexes will be explored. Finally, work towards the discovery of synthetic routes that would unveil new classes of precursors for the CVD of amorphous metal-metalloid alloys is in progress.

2.3.7. Experimental

Methods. Film Growth. This was carried out in the Ekerdt laboratories in a deposition and analysis facility consisting of a vacuum sample transfer system, load lock, X-ray photoelectron spectroscopy (XPS) system (Physical Electronics 3057; Mg Kα), CVD chamber, and a PVD chamber equipped with DC magnetron sputtering. The stainless steel CVD chamber is a cold-wall vessel (base pressure 5×10^{-8} Torr) and the SiO_2/Si(100) substrates were heated radiatively from below. Thermally grown SiO_2 (100 nm)/Si(100) 200 mm wafers were supplied by Sematech. The wafers were cut into 20 x 20 mm pieces and heated to the growth temperature under vacuum. *cis*-$RuH_2(PMe_3)_4$ was synthesized according to procedures described below; the solid compound was sublimed at 80 °C to

obtain sufficient vapor pressure and delivered to the CVD chamber using flowing Ar through a heated gas line and shower head. The deposition was carried out at ~ 200 mTorr. *Ex situ* XPS chemical state analysis was performed with a Physical Electronics 5500, which is fitted with a monochromatic Mg Kα source. Crystallinity is established using grazing angle (2º) X-ray diffraction (XRD) (Bruker-Nonius D8), cross section transmission electron microscopy (TEM) (JOEL 2010F operated at 200 keV) and selected area diffraction (SAD). The precursor, *cis*-$RuH_2(PMe_3)_4$, was prepared by a modification of the published procedure from *trans*-$RuCl_2(PMe_3)_4$ and the intermediate borohydride derivative.[30b,30c]

General. Synthesis. All reactions were performed under a dry, oxygen-free nitrogen atmosphere or under vacuum using standard Schlenk line and dry box techniques. Solvents, methanol and benzene, were dried prior to use by distillation from magnesium and CaH_2 respectively. The solvents diethyl ether and hexane were dried over sodium and freshly distilled from sodium benzophenone ketyl anion under nitrogen before use. The compounds 3,5-bis(trifluoromethyl)pyrazole,[45] $[Cp^*RuCl_2]_n$,[46] $[RuCl_2(\eta^6\text{-}1,4\text{-}Me,iPrC_6H_4)]_2$,[47] and *trans*-diazidotetrakis(trimethylphosphine)ruthenium (II) ($(Me_3P)_4Ru(N_3)_2$)[43] were prepared as previously described. Sodium borohydride was purchased from FisherScientific and dried under vacuum overnight prior to use. Trimethylphosphine (97%) was purchased from Aldrich and used without further purification.

Instrumental Details. NMR spectra were recorded on a Varian 300 Unity Plus spectrometer (^1H, 300 MHz; F^{19}, 282 MHz, P^{31}, 121 MHz) at 25 °C. ^1H NMR signals are

reported relative to residual proton resonances in deuterated solvents. Electrospray Ionization (EI) and Fast Atom Bombardment (FAB) mass spectra were recorded on a Finnigan MAT TSQ 700. Infrared spectra were recorded using a Nicolet IR 200 FTIR spectrometer and analyzed as Nujol Mulls. Microanalytical data (C, H, N) on all compounds fell within expected limits. Melting points were obtained in sealed glass capillaries under dinitrogen and are uncorrected.

X-Ray Crystallography. Details of crystallographic parameters, data collection and refinements are listed in Table 2.1. Selected bond lengths (Å) and angles (°) for **2-VI** are listed in Table 2.2. Data were collected on a Nonius Kappa CCD diffractometer with graphite monochromated Mo-Kα radiation (λ = 0.71073 Å) at 153 K. Absorption corrections were applied using GAUSSIAN. The structures were solved by direct methods and refined anisotropically using full-matrix least-squares methods with the SHELX 97 program package.[48] The coordinates of the non-hydrogen atoms were refined anisotropically, while hydrogen atoms were included in the calculation isotropically but not refined. Neutral atom scattering factors were taken from Cromer and Waber.[49]

Computational Details. The MD simulations in the canonical ensemble were carried out in the Hwang laboratories and performed within the generalized gradient approximation (PW91)[50] to density functional theory using the Vienna *ab initio* Simulation Package.[51] The $Ru_{80}P_{20}$ alloy, with 115 Ru and 29 P atoms in a periodic supercell of volume 2 nm^3, was melted at 3500 K for 3 ps with a time step of 1 fs, and then quenched to 500 K at a rate of 1.5 K/fs, followed by static structural optimization. The structural model based on melt-quenching simulations might differ from that in

experimental samples, which could also be determined by CVD kinetics. Nonetheless the MD simulation results sufficiently provide insight into the nature of local packing in Ru-P amorphous structures.

***trans*-$\mathbf{RuCl_2(PMe_3)_4}$.** To a stirred solution of $RuCl_3 \cdot xH_2O$ (2.7 g, 13 mmol) in methanol (30 mL) at 25 °C was added trimethylphosphine (4.5 g, 60 mmol). The mixture was stirred for 18 h at 25 °C during which time a yellow precipitate had formed. The greenish yellow solid was isolated by filtration, then dried under vacuum, and used in the next step without further purification. Isolated: *trans*-$RuCl_2(PMe_3)_4$, 3.8 g, 81%; m.p. 230-237 °C, (dec. 189-193 °C).

***mer*-$\mathbf{(PMe_3)_3RuH(\eta^2\text{-}H_2BH_2)}$.** To a stirred mixture of *trans*-$RuCl_2(PMe_3)_4$ (1.1 g, 2.3 mmol) and sodium borohydride (730 mg, 19 mmol) in benzene (70 mL) at 25 °C was added methanol (1.0 – 1.5 mL) dropwise and slowly until violent gas evolution was observed. The mixture was stirred for 2 h at 25°C, then the solvent was removed under vacuum. The brown residue was extracted with hexanes, and then filtered through a short bed of Celite. The filtrate was evaporated to dryness under vacuum to give a bright yellow solid. Isolated: *mer*-$(PMe_3)_3RuH(\eta^2\text{-}H_2BH_2)$, 650 mg, 82%; m.p. 105-108 °C.

***cis*-$\mathbf{RuH_2(PMe_3)_4}$ (2-I).** To a stirred solution of *mer*-$(PMe_3)_3RuH(\eta^2\text{-}H_2BH_2)$ (1.04 g, 3 mmol) in benzene (80 mL) at 25 °C was added trimethylphosphine (460 mg, 6 mmol) dropwise. The yellow mixture was stirred at 25 °C until it was nearly colorless (faintly

brown after 1 h), then the solvent was removed under vacuum. The crude, light brown solid was sublimed (80 °C, 10^{-2} Torr) onto a -78 °C cold probe. Isolated: **2-I**, 740 mg, 86% as a white solid.

[(Cp*RuLi)$_2$(μ$_4$-O)(μ$_2$-Cl)(μ-3,5-(CF$_3$)$_2$Pz)$_3$] (2-II). To a solution of 3,5-(CF$_3$)$_2$PzH (1.6 g, 7.84 mmol) in diethyl ether (30 mL) at -78 °C was added dropwise a solution of *n*-butyl-lithium (5.5 mL, 1.6 M in hexane). The light yellow solution was stirred for 30 min and then added dropwise to a solution of [RuCl$_2$(η^5-C$_5$Me$_5$)]$_n$ (1.0 g, 3.3 mmol) in diethyl ether (15 mL) at -78 °C. The resulting mixture was allowed to warm to room temperature and stirred for 10 h. The reaction mixture was then filtered through a short bed of Celite and the filtrate evaporated to dryness under vacuum. The solid residue was extracted with hexane (2 x 20 mL) and the filtrates combined. The volume of the filtrate was reduced under vacuum to ~5 mL. Cooling for 5 days (-60 °C) gave dark brown crystals which were collected and dried under vacuum. Isolated: **2-II**, 3.18g, 75 %; m.p. 147-150 °C; ^{1}H NMR (300 MHz, CDCl$_3$): δ 1.2 (s, 30 H, -*CH$_3$*), 1.62-1.66 (br m, 3H, 3,5-(CF$_3$)$_2$*Pz*); ^{19}F NMR: (282 MHz, CDCl$_3$): δ -54.52, -56.36, -63.70, -63.14; FTIR (Nujol, cm^{-1}): 2431 s, 2065 b, 1865 s, 1506 b; FAB/MS *m/e*: 1146 [M$^+$], 977 [M$^+$ - (C$_5$Me$_5$ + Cl)], 775 [(M$^+$ - 2Ru)], 573 [M$^+$ - 3,5-(CF$_3$)$_2$Pz].

[Cp*Ru(μ-Cl)]$_2$(μ-3,5-(CF$_3$)$_2$Pz) (2-III). To a solution of 3,5-(CF$_3$)$_2$PzH (0.67 g, 3.3 mmol) in diethyl ether (10 mL) at -78 °C was added dropwise a solution of *n*-butyl-lithium (2.3 mL, 1.6 M in hexane). The solution was stirred for 30 min and then added

dropwise to a solution of $[RuCl_2(\eta^5\text{-}C_5Me_5)]_n$ (1.0 g, 3.3 mmol) in diethyl ether (15 mL) at -78 °C. The mixture was allowed to warm to room temperature and stirred for 10 h. The solution was then filtered through a short bed of Celite and the filtrate evaporated to dryness under vacuum. The solid was extracted with hexane (2 x 10 mL), the filtrates combined and the volume reduced to ~5 mL. Cooling (-60 °C) gave dark green crystals of **2-III** after one week. They were collected and dried under vacuum. Isolated: **2-III**, 1.52g, 57 %; m.p. 92-102 °C; ^{1}H NMR (300 MHz, $CDCl_3$): δ 1.10 (t, 30 H, -*CH*$_3$); 6.40 (br. s, 1H, 3,5-$(CF_3)_2$*Pz*). ^{19}F NMR: (282 MHz, $CDCl_3$): δ -57.70, -56.06, -58.43, -59.82, -60.71, 60.88; FTIR (Nujol, cm^{-1}): 2231 (s), 2156 (b), 1735 (s), 1356 (b); FAB/MS *m/e*: 948 [M^+], 877 [M^+ -Cl_2], 775 [M^+ - Ru], 745 [M^+ - CF], 641 [M^+ - Ru].

$[RuCl(\eta^6\text{-}1,4\text{-}Me,iPrC_6H_4)(\mu\text{-}3,5\text{-}(CF_3)_2Pz)]_2$ (2-IV). To a solution of 3,5-$(CF_3)_2$PzH (0.1 g, 0.5 mmol) in diethyl ether (10 mL) at -78 °C was added dropwise a solution of *n*-butyl-lithium (0.5 mL, 1.6 M in hexane). The solution was stirred for 30 min and added dropwise to a solution of $[RuCl_2(\eta^6\text{-}1,4\text{-}Me,iPrC_6H_4)]_2$ (0.15 g, 0.25 mmol) in diethyl ether (10 mL) at -78 °C. The solution was allowed to warm to room temperature and stirred for 10 h. The solution was then filtered through a short bed of Celite and the filtrate evaporated to dryness under vacuum. The solid was extracted with hexane (2 x 10 mL), the filtrates combined and reduced in volume under vacuum to ~5 mL. Cooling (-60 °C) gave reddish brown crystals of **2-IV** after one week. Isolated: **2-IV**, 161 mg, 65 %; m.p. 165-173 °C; ^{1}H NMR (300 MHz, $CDCl_3$): δ 1.22 (d, 6H, *J* = 7.5 Hz, *i-Pr*), 2.15 (s, 3 H, -*CH*$_3$), 2.90 (septet, 1H, *J* = 7.5 Hz, *i-Pr*), 5.49, 5.36 (dd, 4H ($H_{AA'}$/$H_{BB'}$ *J* = 5.5 Hz),

7.05 (s, 1H, 3,5-$(CF_3)_2Pz$), ^{19}F NMR: (282 MHz, $CDCl_3$): δ -56.34, -58.33, -61.11; FTIR (Nujol, cm^{-1}): 2231 (s), 2156 (b), 1735 (s), 1356 (b); FAB/MS *m/e*: 726 [M^+], 707 [M^+ - F].

[Cp*Ru(μ-O)(μ-η^5,η^1-$C_5Me_4CH_2$)Ru(η^1-3,5-$(CF_3)_2$Pz)] (2-V). To a solution of 3,5-$(CF_3)_2$PzH (0.12 g, 0.59 mmol) in diethyl ether (10 mL) at -78 °C was added dropwise a solution of *n*-butyl-lithium (0.5 mL, 1.6 M in hexane). The solution was stirred for 30 min and added dropwise to a solution of $[Ru(CF_3SO_3)_3(\eta^5\text{-}C_5Me_5)]_n$ (0.15 g, 0.28 mmol) in diethyl ether (10 mL) at -78 °C. The resulting mixture was allowed to warm to room temperature and stirred for 10 h. The solution was filtered through a short bed of Celite. The filtrate was evaporated to dryness under vacuum and the residue extracted with hexane (2 x 20 mL). The filtrates were combined and the volume reduced to ~5 mL under vacuum. Cooling (-60 °C) gave dark brown crystals of **2-V** after 5 days. They were collected and dried under vacuum. Isolated: **2-V**, 158 mg, 75 %; m.p. 109-111 °C; ^{1}H NMR (300 MHz, $CDCl_3$): δ 0.95 (s, 15H, C_5Me_5), 1.3-1.9 (br m, 14 H, $C_5Me_4CH_2$), 6.80 (s, 1H, 3,5-$(CF_3)_2Pz$); ^{19}F NMR (282 MHz, $CDCl_3$): δ -59.43, -61.21; FTIR (Nujol, cm^{-1}): 2371 (s), 2156 (b), 1945 (b), 1627 (s), 1405 (b), 1165 (s); FAB/MS *m/e*: 691 [M^+], 675 [M^+ - O].

{$(Me_3)P_3Ru]_2(\mu_1\text{-}N_3)_3$}·3[(3,5-$(CF_3)_2$PzH] (2-VI). To a solution of $(Me_3P)_4Ru(N_3)_2$ (0.100 g, 0.2 mmol) in toluene (2 mL) was added 3,5-$(CF_3)_2$PzH (0.083 g, 0.4 mmol). The mixture was heated to reflux and stirred for 4 h. Cooling (-60 °C) gave reddish

brown crystals of **2-VI** after 1 day. They were collected and dried under vacuum. Isolated: **2-VI**, 172 mg, 62 %; m.p. 130-134 °C; ^{1}H NMR (300 MHz, $(CD_3)_2CO$): δ 6.99 (s, 3H, Pz,CH), 6.00 (br s, 3H, Pz,NH), 1.62 (m, 54H, P*Me*$_3$); ^{31}P{^{1}H} NMR (121 MHz, $(CD_3)_2CO$): δ 19.77; FTIR (Nujol, cm^{-1}): 3007 (w), 2059 (m), 1364 (s), 1221 (s), 535 (m); MS (chemical ionization, $CHCl_3$) *m/z* 786 [M^+-3Pz], 702 [M^+- 2N_3].

Table 2.1. Crystal data and structure refinement for **2-VI**.

	2-VI
Formula	$C_{33}H_{60}F_{18}N_{15}P_6Ru_2$
Fw	1396.92
Cryst syst.	triclinic
Space group	P1
a, Å	9.993(2)
b, Å	15.835(3)
c, Å	18.863(4)
α, deg	94.07(3)
β, deg	94.76(3)
γ, deg	106.87(3)
V, Å^3	2832.4(10)
Z	2
D_{calc}, g cm^{-3}	1.638
temp, K	153(1)
F(000)	1406
μ, mm^{-1}	0.803
θ rang, deg	3.01-25.00
reflns meads	15736
reflns used	9751
params	667
R[a] ($I > 2\sigma(I)$)	R1 = 0.1283
	wR2 = 0.3035
R[a] (all data)	R1 = 0.1314
	wR2 = 0.3047
S	1.128

[a] $R1 = \Sigma||F_o| - |F_c||/\Sigma|F_o|$. $wR2 = [\Sigma w[(F_o^2 - F_c^2)^2]/\Sigma|[w(F_o^2)^2]]^{1/2}$. $w=1/[\sigma^2(F_o^2)+(0.075P)^2]$, where $P = [\max(F_o^2,0)+2F_c^2]/3$.

Table 2.2. Selected Bond Lengths (Å) and Angles (°) for **2-VI**.

Ru(1)-N(4)	2.181(12)	P(1)-Ru(1)-P(3)	94.68(15)
Ru(1)-N(1)	2.225(11)	N(4)-Ru(1)-P(2)	166.4(3)
Ru(1)-N(7)	2.230(11)	N(1)-Ru(1)-P(2)	94.1(3)
Ru(1)-P(1)	2.264(4)	N(7)-Ru(1)-P(2)	96.5(3)
Ru(1)-P(3)	2.271(4)	P(1)-Ru(1)-P(2)	94.13(16)
Ru(1)-P(2)	2.274(4)	P(3)-Ru(1)-P(2)	94.50(17)
Ru(2)-N(4)	2.198(11)	N(4)-Ru(2)-N(1)	74.2(4)
Ru(2)-N(1)	2.215(11)	N(4)-Ru(2)-N(7)	73.7(4)
Ru(2)-N(7)	2.221(11)	N(1)-Ru(2)-N(7)	75.1(4)
Ru(2)-P(4)	2.265(4)	N(4)-Ru(2)-P(4)	97.0(3)
Ru(2)-P(5)	2.271(4)	N(1)-Ru(2)-P(4)	93.7(3)
Ru(2)-P(6)	2.279(4)	N(7)-Ru(2)-P(4)	166.9(3)
N(4)-Ru(1)-N(1)	74.3(4)	N(4)-Ru(2)-P(5)	165.4(3)
N(4)-Ru(1)-N(7)	73.8(4)	N(1)-Ru(2)-P(5)	96.2(3)
N(1)-Ru(1)-N(7)	74.8(4)	N(7)-Ru(2)-P(5)	93.4(3)
N(4)-Ru(1)-P(1)	94.2(3)	P(4)-Ru(2)-P(5)	94.63(16)
N(1)-Ru(1)-P(1)	96.0(3)	N(4)-Ru(2)-P(6)	93.7(3)
N(7)-Ru(1)-P(1)	166.4(3)	N(1)-Ru(2)-P(6)	166.5(3)
N(4)-Ru(1)-P(3)	95.6(3)	N(7)-Ru(2)-P(6)	95.9(3)
N(1)-Ru(1)-P(3)	165.8(3)	P(4)-Ru(2)-P(6)	93.83(15)
N(7)-Ru(1)-P(3)	93.0(3)	P(5)-Ru(2)-P(6)	94.37(15)

2.4. References

[1] Rees, W. S. Jr.. *CVD of Nonmetals*. VCH, Weinheim, **1996**.

[2] Baker, A. G.; Moris, W. C. *Rev. Sci. Int.* **1961**, *32*, 458.

[3] Sterlin, H.F; Swann, R. C. G. Belgian Patent *663, 511*, November 8, **1965**; C.A. *65: 348d*, **1966**.

[4] Nail, J. W. Ph.D. Dissertation: *Single-Source Precursors for the III/V Semiconducting Materials: From Design to Deposition*. University of Texas at Austin, **1992**.

[5] Dickinson, P. H.; Collman, J. P. "Chemical Vapor Deposition of $YBa_2Cu_3O_{7-x}$ Superconducting Films", *J. Appl. Phys.* **1999**, *66*, 444.

[6] Yavari, A. R. "A new order for metallic glasses" *Nature*. **2006**, *439*, 405.

[7] Dubey, R.; Gupta, A; Pivin, J. C. "Amorphization in iron nitride thin films prepared by reactive ion-beam sputtering" *Phys. Rev. B.* **2006**, *74*, 214110.

[8] (a) Guo, F. Q.; Poon, S. J.; Shiflet, G. J. "CaAl-based bulk metallic glasses with high thermal stability" *Appl. Phys. Lett.* **2004**, ***84***, 37; (b) Wang, D.; Li, Y.; Sun, B. B.; Sui, M. L.; Lu, K.; Ma, E. "Bulk metallic glass formation in the binary Cu–Zr system" *Appl. Phys. Lett.* **2004**, *84*, 4029; (c) Xu, D. H.; Lohwongwatana, B.; Duan, G.; Johnson, W. L.; Garland, C. "Bulk metallic glass formation in binary Cu-rich alloy series – $Cu_{100-x}Zr_x$ (x=34, 36, 38.2, 40 at.%) and mechanical properties of bulk $Cu_{64}Zr_{36}$ glass" *Acta Mater.* **2004**, *52*, 2621.

[9] (a) Mukherjee, S; Schroers, J; Johnson, W. L.; Rhim, W. K. "Influence of Kinetic and Thermodynamic Factors on the Glass-Forming Ability of Zirconium-Based Bulk Amorphous Alloys" *Phys. Rev. Lett.* **2005**, *94*, 245501; (b) W. L. Johnson, "Bulk Amorphous Metal: An Emerging Engineering Material" *JOM.* **2002**, *54*, 3, 40; (c) Inoue, A. "Stabilization of metallic supercooled liquid and bulk amorphous alloys" *Acta Mater.* **2000**, *48*, 279; (d) Johnson, W. L. "Fundamental Aspects of Bulk Metallic Glass Formation in Multicomponent Alloys " *Mater. Sci. Forum.* **1996**, *225*, 35; (d) Miracle, D. B.; Sanders, W. S.; Senkov, O. N. "The influence of efficient atomic packing on the constitution of metallic glasses" *Philos. Mag.* **2003**, *83*, 2409.

[10] Ahn, K; Louca, D.; Poon, S. J; Shiflet, G. J. "Topological and chemical ordering induced by Ni and Nd in $Al_{87}Ni_7Nd_6$ metallic glass" *Phys. Rev. B.* **2004**, *70*, 224103 .

[11] Turnbull, D. *Contemp. Phys.* **1969**, *10*, 473.

[12] Z. P. Lu and C. T. Liu, "Glass Formation Criterion for Various Glass-Forming Systems" *Phys. Rev. Lett.* **2003**, *91*, 115505.

[13] (a) Klement, W.; Willens, R. H.; Duwez, P. *Nature*. **1960**, *187*, 869; (b) Sheng, H. W; Luo, W. K; Alamgir, F. M; Bai, J. M; Ma, E. "Atomic packing and short-to-medium range order in metallic glasses," *Nature*, **2006**, *439*, 419; (c) Busch, R.; Hufnagel, T. C.; Eckert, J.; Inoue, A.; Johnson, W. L.; Yavari, A. R. "Amorphous and Nanocrystalline Metals," *Materials Research Society Symposium Proceedings*, **2004**, *806*.

[14] Kohn, A; Eizenberg, M; Shacham-Diamond, Y. "Structure of electroless deposited $Co_{0.9}W_{0.02}P_{0.08}$ thin films and their evolution with thermal annealing:" *J. Appl. Phys.* **2003**, *94*, 3810.

[15] Kelsey, J. E.; Goldberg, C.; Nuesca, G.; Peterson, G.; Kaloyeros, A. E.; Arkles, B. "Low temperature metal-organic chemical vapor deposition of tungsten nitride as diffusion barrier for copper metallization" *J. Vac. Sci. Tech. B*, **1999**, *17*, 1101.

[16] Han, C-H.; Cho, K-N.; Oh, J-E.; Paek, S-H.; Park, C-S, Lee, S-I, Lee, M. Y.; Lee, J. G. "Barrier Metal Properties of Amorphous Tantalum Nitride Thin Films between Platinum and Silicon deposited using Remote Plasma Metal Organic Chemical Vapor Method" *Jap. J. Appl. Phys. Pt 1*, **1998**, *37*, 2646.

[17] Tenhover, M. "CVD of Refractory Amorphous Metal Alloys" *Mat. Res. Soc. Symp. Proc.* **1995**, *363*, 257.

[18] Jun, C-S.; Fehlner, T. P.; Long, G. L. "Binary Thin Films from Molecular Precursors. Role of Precursor Structure in the Formation of Amorphous and Crystalline Iiron Boride (FeB)" *Chem. Mater*. **1992**, *4*, 440.

[19] Mullendore, A. W. "Formation of Amorphous Metal Alloys by Chemical Vapor Deposition," *U. S. Pat. Appl*. **1989**, 170228.

[20] Alloca, C. M.; Williams, W. S.; Kaloyeros, A. E. "Electrochemical Characteristics of Amorphous Titanium Carbide Films Produced by Low-Temperature Metalorganic Chemical Vapor Deposition (MOCVD)" *J. Electrochem. Soc*. **1987**, *134*, 3170.

[21] Czekaj, C. L.; Geoffroy, G. L. "Chemical Vapor Deposition of Iron-Cobalt ($FeCo_x$) and Iron Cobalt Oxide ($FeCo_xO_y$) Thin Films from Iron Cobalt Carbonyl Clusters" *Inorg. Chem.*, **1988**, *27*, 8.

[22] Kaloyeros, A.; Chen, X.; Kumar, K.; Seo, S.; Peterson, G.; Frisch, H.; Arkles, B.; Sullivan, J. *J. Electrochem. Soc.* **1999**, *146*, 170.

[23] Rossnagel, S.; Kim, H. *Proceedings of the IEEE 2001 International Interconnect Technology conference* (IEEE, Piscataway, PA 2001) p.3.

[24] Kim, H.; Cabral, C.; Lavoie, C.; Rossnagel, S. M. *J. Vac. Sci. Technol. B.* **2002**, *20*, 1321.

[25] Kim, S.; Oh, S.; Kim, H.; Kang, D.; Kim, K.; Li, W.; Haukka, S.; Tuominen, M. "Characterization of Atomic Layer Deposited WN*x*C*y* Thin Film as a Diffusion Barrier for Copper Metallization", *J. Electrochem. Soc.* **2004**, *151*, C272.

[26] (a) Goswami, I.; Laxman, R. *Semiconductor International.* **2004**, *27*, 49; (b) Wang, Q.; Ekerdt, J. G.; Gay, D.; Sun, Y.; White, J. M. *Appl. Phys. Letters*. **2004**, *84*, 1380; (c) Green, M.; Gross, M.; Papa, L.; Schnoes, K.; Brasen, D. *J. Electrochem. Soc.* **1985**, *132*, 2677; (d) Matsui, Y.; Hiratani, M.; Nabatame, T.; Shimamoto, Y.; Kimura, S. *Electrochem. Solid State Lett.* **2002**, *5*, C18; (e) Lashdaf, M.; Hatanpää, T.; Krause, A. O. I.; Lahtinen, J.; Lindblad, M.; Tiitta, M. *Applied Catalysis A.* **2003**, *241*, 51.

[27] (a) Chan, R.; Arunagiri, T. N.; Zhang, Y.; Chyan, O.; Wallace, R. M.; Kim, M. J.; Hurd, T. Q.; *Electrochem. Solid-State Lett.* **2004**, *7*, G154; (b) Tan, J.; Qu, X.; Xie, Q.; Zhou, Y.; Ru, G. *Thin Solid Films*. **2006**, *504*, 231.

[28] Lin, J.; Lee, C. "Grain Boundary Diffusion of Copper in Tantalum Nitride Thin Films" *J. Electrochem. Soc.* **1999**, *146*, 3466.

[29] (a) Jones, R. A.; Wilkinson, G.; Colquohoun, I. J.; McFarlane, W.; A. M. R. Galas, A. M. R.; M. B. Hursthouse, M. B. "Trimethylphosphine Hydrido- and Hydroxo-Complexes of Ruthenium. Multinuclear Magnetic Resonance Studies on μ-Hydrido-μ-hydroxo-hexakis(trimethylphosphine) diruthenium(I). Crystal Structures of Di-μ-hydrido-dihydrido hexakis(trimethylphosphine) diruthenium(II) and Tri-μ-hydrido-hexakis(trimethylphosphine)diruthenium (II) tetrafluoroborate," *J. Chem. Soc., Dalton Trans*., **1980**, 2480; (b) Schmidbauer, H.; Blaschke, G. "An Ylide Complex of Ruthenium with Three- and Four-Membered Metallocycles" *Z. Naturforsh.* **1980**, *35b*, 584; (c) Kohlmann, W.; Werner, H. "Synthesis and Reactions of Octahedral Boranatoruthenium(II) Complexes' *Z. Naturforsch.* **1993**, *48b*, 1499.

[30] (a) Shin, J.; Waheed, A.; Agapiou, K; Winkenwerder, W. A.; Kim, H.-W.; Jones, R. A.; Hwang, G. S.; Ekerdt, J. G. "Growth of Ultra-thin Films of Amorphous Ruthenium-Phosphorus Alloys Using a Single Source CVD Precursor," *J. Am. Chem. Soc.* **2006**, *128*, 51, 16510; (b) Shin, J.; Waheed, A.; Winkenwerder, W. A.; Kim, H.-W.; Agapiou, K; Jones, R. A.; Hwang, G. S.; Ekerdt, J. G. "Chemical vapor deposition of amorphous ruthenium–phosphorus alloy films" *Thin Solid Films.* **2007**, *515*, 5298.

[31] Tao, H.-S.; Diebold, U.; Shinn, N. D.; Madey, T. E. "Decomposition of $P(CH_3)_3$ on Ru(0001): Comparison with PH_3 and PCl_3**,"** *Surf. Sci*. **1997**, *375*, 257.

[32] Li, H.; Dai, W.; Wang, W.; Fang, Z.; Deng, J. "XPS studies on surface electronic characteristics of Ni–B and Ni–P amorphous alloy and its correlation to their catalytic properties," *Appl. Surf. Sci*., **1999**, *152*, 25.

[33] Wells, A. F. *Structural Inorganic Chemistry, 5th Edition*, Oxford University Press, **1986**, 840-841.

[34] Kohn, A; Eizenberg, M; Shacham-Diamond, Y. "Structure of electroless deposited $Co_{0.9}W_{0.02}P_{0.08}$ thin films and their evolution with thermal annealing," *J. Appl. Phys.*, **2003**, *94*, 3810.

[35] Park, S; Lim, S; Choi, H. "Chemical Vapor Deposition of Iron and Iron Oxide Thin Films from Fe(II) Dihydride Complexes," *Chem. Mater.*, **2006,** *18,* 5150.

[36] Park, S; Choi, H. "Liquid Cobalt (I) Hydride Complexes as Precursors for Chemical Vapor Deposition," *Chem. Mater.*, **2003,** *15*, 3121.

[37] Choi, H; Park, S; Kim, T.H. "Novel Nickel Precursors for Chemical Vapor Deposition," *Chem. Mater.*, **2003,** *15*, 3735.

[38] Gusev, D.G.; Hubener, R.; Burger, P.; Orama, O.; Berke, H. "Synthesis, Structural Diversity, Dynamics, and Acidity of M(II) and M(IV) Complexes $[MH_3(PR_3)_4]$ (M = Fe, Ru, Os; R = Me, Et)" *J. Am. Chem. Soc.* **1997**, *119*, 3716.

[39] Jones, R. A.; Mayor Real, F.; Wilkinson, G.; Galas, A. M. R.; Hursthouse, M. B. "Further chemistry of trimethylphosphine complexes of rhodium(I): X-ray crystal structures of dodeca(trimethylphosphine)tetrarhodiumhexamercury, $Hg_6Rh_4(PMe_3)_{12}$, and trans-chlorobis(trimethylphosphine)(triphenyl-phosphine) rhodium(I)," *J. Chem. Soc. Dalton*, **1981**, *1*, 126.

[40] Werner, H.; Gotzig, J. "Synthesis of $OsH(\eta^2\text{-}CH_2PMe_2)(PMe_3)_3$ and of the Basic Dihydridoosmium Complex *cis*-$OsH_2(PMe_3)_4$," *Organometallics*, **1983**, *2*, 547.

[41] Paonessa, R. S.; Trogler, W. C. "Preparation and Properties of Sterically Unhindered Cis and Trans Dihydrides of Platinum(II)," *J. Am. Chem. Soc.*, **1982**, *104*, 1138.

[42] Waheed, A.; Jones, R. A.; Agapiou, K.; Yang, X.; Moore, J. A.; Ekerdt, J. G. "Synthesis and Structures of Dinulear 3,5-Bis(trifluoromethyl)pyrazolate Complexes of Ruthenium" *Organometallics.* In press.

[43] Siebald, H. G. L. "Preparation and Crystal Structure of *Trans*-Diazidotetrakis-(trimethylphosphine) Ruthenium (II)" *Polyhedron*. **1996**, *15*, 23, 4221.

[44] Mason, R.; Rusholme, G. A. "Preparation and Crystal Structure of Tris-m-azido-hexacarbonyldimanganate (I) Anion, $[(CO)_3Mn(N_3)_3Mn(CO)_3]^-$, and of Related Complexes" *Chem. Comm.* **1971**, 496.

[45] (a) Threadgill, M. D; Heer, A. K.; Jones, B. G. "The reaction of 1,1,1,5,5,5-hexafluoropentane-2,4-dione with hydrazines: a re-investigation" *J. Fluorine Chem.* **1993**, *65*, 21. (b) Claire, P. P. K.; Coe, P. L.; Jones, C. J.; McCleverty, J. A. "3,5-Bis(trifluoromethyl)pyrazole and some N-substituted derivatives " *J. Fluorine Chem.* **1991**, *51*, 283. (c) Renn, O.; Venanzi, L. M. "High-Yield Syntheses of Sodium, Potassium, and Thallium Hydrotris[3,5-bis(trifluoromethyl)pyrazolyl]borates and the X-Ray Crystal Structure of {Hydrotris[3,5-Bis(trifluoromethyl)pyrazolyl]borato}-thallium (I)" *Helv. Chim. Acta*. **1995,** *78*, 993.

[46] (a) Tilley, T. D.; Grubbs, R. H.; Bercaw, J. E. "Halide, hydride, and alkyl derivatives of (pentamethylcyclopentadienyl)bis(trimethylphosphine)ruthenium "*Organometallics*, **1984**, *3*, 274. (b) Oshima, N.; Suzuki, H.; Moro-oka, Y. "Synthesis and Some Reactions of Dichloro(pentamethyl-cyclopentadienyl) Ruthenium (III) Oligomer" *Chem. Lett*. **1980**, 1161.

[47] Bennett, M. A.; Huang, T-N.; Matheson, T. W.; Smith, A. K. "(η^6-Hexamethylbenzene)ruthenium Complexes", *Inorg. Syn*. **1982**, *21*, 74.

[48] Sheldrick, G. M. SHELX 97, *A software package for the solution and refinement of X-ray data*; University of Göttingen: Göttingen, Germany (**1997**).

[49] Cromer, D. T.; Waber, J. T. *International Tables for X-Ray Crystallography*, Kynoch Press, Birmingham, vol. 4 (**1974**), Table 2.2A.

[50] Perdew, J. P.; Chevary, J, A.; Vosko, S. H.; Jackson, K. A.; Pederson, M. R.; Singh, D. J.; Fiolhais, C. "Atoms, molecules, solids, and surfaces: Applications of the generalized gradient approximation for exchange and correlation," *Phys. Rev. B*, **1992**, *46*, 6671.

[51] Kresse, G.; Furthmüller, J. "Efficient iterative schemes for *ab initio* total-energy calculations using a plane-wave basis set," *Phys. Rev. B*, **1996**, *54*, 11169.

Chapter 3: Triazolato Ruthenium Complexes from Metal Azide Alkyne Cycloaddition

3.1. Introduction

The 1,3-dipolar cycloaddition of organic azides and alkynes proposed by Huisgen is the most straightforward method to prepare 1,2,3-triazoles.[1] Due to the high activation energy, however, these cycloadditions often proceed very slowly even under forcing conditions and give regioisomeric mixtures (Scheme 3.1). A significant advancement

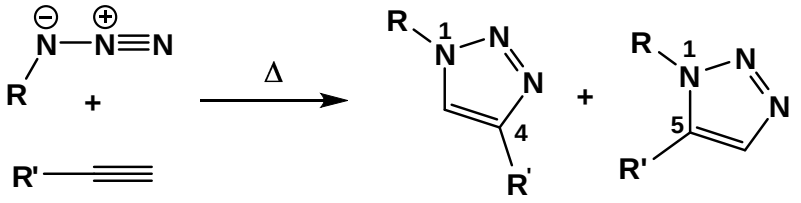

Scheme 3.1. 1,3-dipolar cycloaddition of organic azides with alkynes leading to 1,4- and 1,5-disubstituted 1,2,3-triazoles.

came with the discovery that Cu(I) efficiently facilitates the union of terminal alkynes and azides under mild conditions with high levels of regioselectivity. [2] This has led the Cu(I)-catalyzed azide-alkyne cycloaddition to become perhaps the most powerful "click" reaction known, and its utility has been demonstrated through many applications in chemistry, biology and materials science. Not only has this useful reaction manifold been extended to ruthenium catalysis[3], which allows cycloadditions with internal alkynes and provides exclusively 1,5-disubstituted-1,2,3-triazoles, but also to the use of metal-azido complexes as reaction partners. Reactions between metal-coordinated azides and

electron-deficient alkynes have been shown for several transition metals, most often Pd, Pt, Rh or Co.[4] Reactions involving Ta, Fe, Ru, Au and Ni have also been reported, but are less common.[5] With this in mind, the ruthenium complex diazidotetrakis(trimethylphosphine) ruthenium (II)[6], **3-I**, was prepared and screened in reactions with terminal and internal electron-deficient alkynes. While terminal alkynes gave alkynyl-ruthenium products resulting from deprotonation at the acetylenic hydrogen followed by ligand exchange at the ruthenium center, reaction with the internal alkyne diethyl acetylenedicarboxylate provided the desired bis-triazolato-ruthenium complex.

Interestingly, while cycloadditions with metal-coordinated azides typically furnish N2-bound triazolato species, presumably due to a combination of steric and electronic effects, the reaction of **3-I** with diethylacetylene dicarboxylate gives both N2- and N1-bound triazolato ligands coordinated to the same ruthenium nucleus. This suggests that a kinetic trapping of N1-triazolato-ligated ruthenium has been demonstrated. Further studies will be conducted to extend the class of reacting partners as well as exploit this type of reactivity with bis-alkynyl containing dipolarophiles. It is envisioned that products obtained form such cycloadditions may provide metal-containing oligomeric and/or polymeric species with interesting properties.

3.2. Results and Discussion

The ruthenium diazide complex **3-I** was synthesized in a two step procedure starting from $RuCl_3 \cdot xH_2O$ (Scheme 3.2). Thus, $RuCl_3 \cdot xH_2O$ was reacted with PMe_3 in methanol at 25 ºC for 12 h to provide the yellowish green *trans*-dichlorotetrakis(trimethylphosphine) ruthenium (II)[7] complex in good yield. After

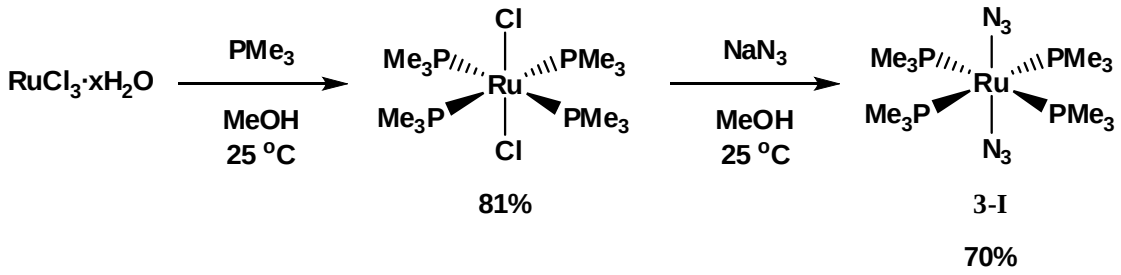

Scheme 3.2. Synthetic route to diazidotetrakis(trimethylphosphine)ruthenium(II), **3-I**.

addition of sodium azide to a solution of the dichloride in methanol the reaction was stirred at 25 ºC for 6 h. Orange crystals of **3-I** precipitated from the mixture upon standing for ~ 48 h in the dark. Complex **3-I** was found to react with terminal and internal electron deficient alkynes to give mixed azido-alkynyl, bis-alkynyl and bis-triazolato species of ruthenium. An interesting "end-to-end" azide-bridged dinuclear ruthenium complex has also been isolated from these experiments.

3.2.1. Reactions with Terminal Alkynes

Terminal alkynes have been shown to undergo reaction with metal-mono-azides to afford triazoloto species – most recently with gold and ruthenium mono-azido complexes.[5d,5c] Accordingly, the bis-azide **3-I** was reacted with phenylacetylene and trimethylsilylacetylene in an attempt to generate the respective phenyl-and trimethylsilyl-substituted triazolato complexes. It was found, however, that alkynyl substituted ruthenium species were produced by ligand substitution of the resulting phenyl- and/or trimethylsilylacetylide for either one or both of the azide ligands. This is consistent with previous reports that terminal alkynes react as CH acids and participate in ligand substitution with liberation of HN_3 rather than a 1,3-dipolar cylcoaddition with cobalt

complexes.[4a]

$(Me_3P)_4Ru(N_3)(C{\equiv}CC_6H_5)$ (3-II). Reaction of **3-I** with phenylacetylene a 1:2.5 mole ratio in refluxing toluene gave the azido-alkynyl substituted ruthenium complex

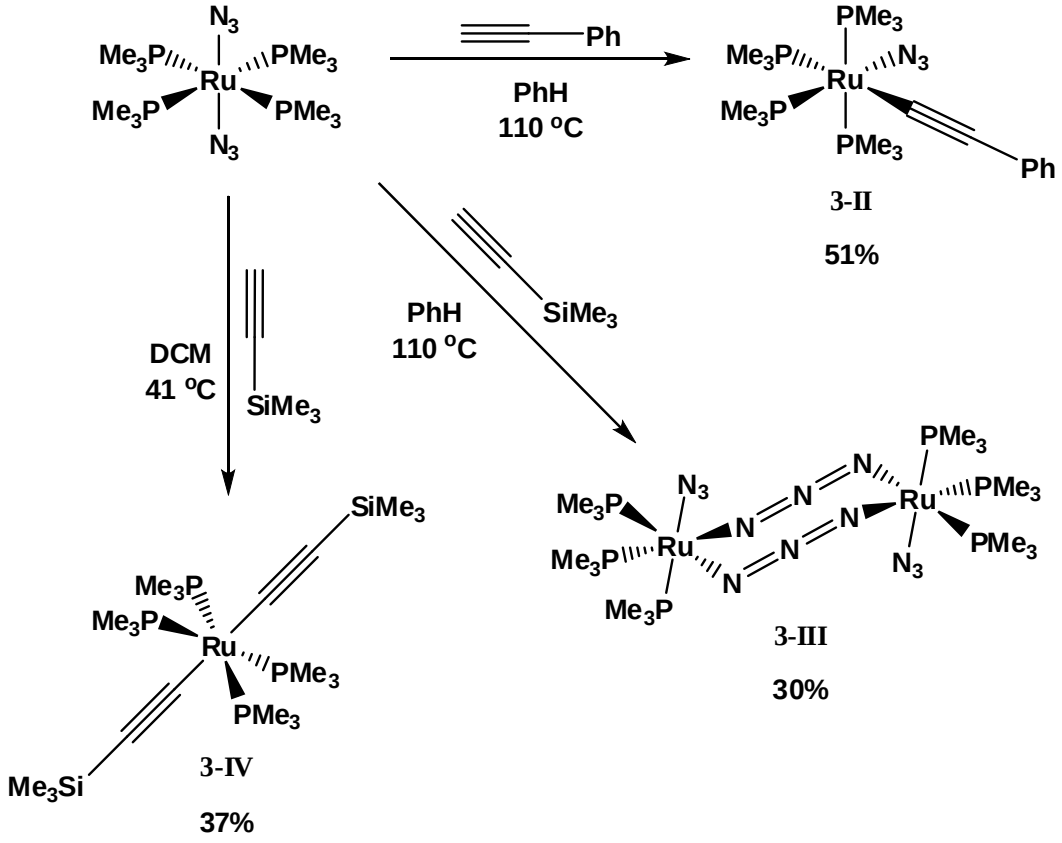

Scheme 3.3. Preparation of azido-alkynyl- (**3-II)**, azide-bridged- (**3-III)**, and bis-alkynyl-ruthenium (**3-IV**) complexes from the reaction of **3-I** with terminal alkynes.

3-II in moderate yield (Scheme 3.3). Attempts to form the bis-acetylide using excess phenylacetylene were unsuccessful. However, the bis-trimethylsilyl acetylide complex **3-IV** could be isolated using trimethylsilylacetylene. Brown crystals of **3-II** precipitated

from the reaction mixture upon cooling to room temperature. Compound **3-II** crystallizes in the triclinic P1 space group with two independent molecules per unit cell (Fig. 3.1). Crystallographic details are given in Table 3.1 and selected bond lengths and angles for **3-II** in Table 3.2. X-ray diffraction studies revealed a distorted octahedral structure for **3-II.** The azide ligand is fairly symmetric with a N(1)-N(2) bond distance of 1.19 Å and the N(2)-N(3) distance found to be 1.16 Å. The Ru-N(1)-N(2) bond angle of 127.2º falls within the expected range for coordinated azides. The C(1)-C(2) bond length in the alkynyl group was in agreement with the normal value for a carbon-carbon triple bond at 1.21 Å. The ^{1}H NMR spectrum of **3-II** taken in $CDCl_3$ showed resonances in the range of 6.95 to 7.29 ppm corresponding to the aryl protons of the phenyl-substituted alkynyl ligand. Peaks were also observed at 1.52, 1.37 and 1.31 ppm in 2:1:1 ratio resulting from two equivalent PMe_3 ligands and two non-equivalent PMe_3 ligands on ruthenium. This supports the observed *cis* relationship of the azide and phenylacetylide ligands. A *trans* relationship would give a more simplified spectrum due to four equivalent PMe_3 ligands as is the case with the starting *trans*-diazide **3-I**. The ^{31}P {^{1}H} NMR spectrum in $CDCl_3$

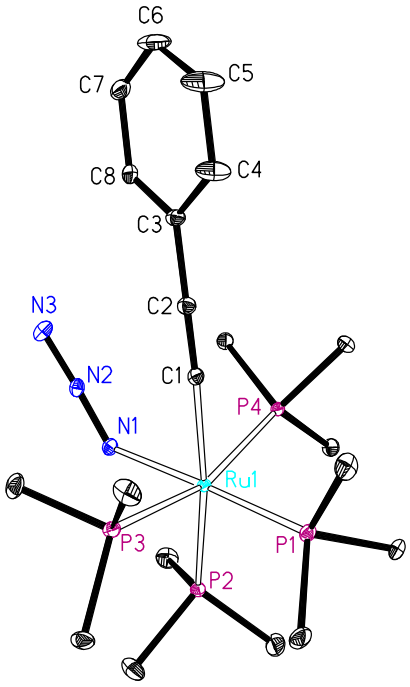

Figure 3.1. ORTEP view of **3-II** with atom numbering scheme. Ellipsoids are drawn at 25% probability level. Hydrogen atoms are omitted for clarity.

has three distinct resonances at 10.96 (dt), -2.40 (dd) and -10.91 (dt) ppm in a 1:2:1 ratio confirming that the *cis* configuration is retained in solution. The IR spectrum displays bands at 2080, 2041 and 1365 cm^{-1} corresponding to alkyne and azide stretching frequencies.

$[(Me_3P)_3(N_3)Ru]_2(\mu_{1,3}\text{-}N_3)_2$ (3-III). Surprisingly, reaction of trimethylsilylacetylene with **3-I** in refluxing toluene, under similar conditions used for the preparation of **3-II**, resulted in the formation of an unusual bis "end-to-end" azide bridged dinuclear ruthenium complex **3-III** as light brown crystals in 30% yield (Scheme 3.3). The molecular structure of **3-III** was determined by X-ray diffraction (Fig. 3.2a).

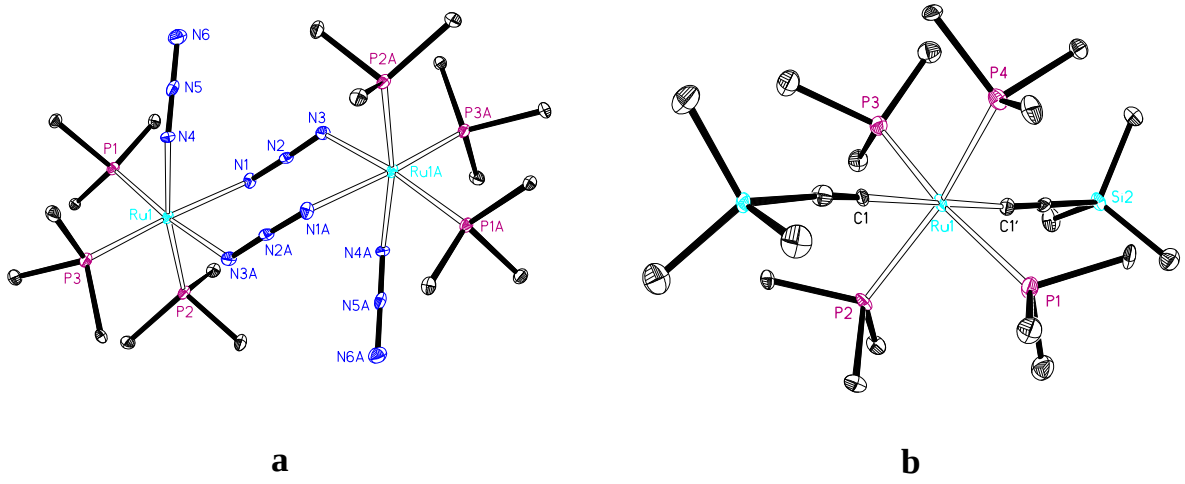

Figure 3.2. ORTEP views of (a) **3-III** and (b) **3-IV** with atom numbering schemes. Ellipsoids are drawn at 25% probability level. Hydrogens are omitted for clarity.

Compound **3-III** crystallizes in the orthorhombic Pcab space group with four independent molecules per unit cell. Crystallographic details are given in Table 3.1 and

selected bond lengths and angles for **3-III** in Table 3.3. The structure shows an eight-membered Ru_2N_6 ring core with pseudo-octahedral geometry linked by two bridging azide moieties. Such "end-to-end" azide bridging modes have been described for some dinuclear transition metal complexes[8], however, to our knowledge, examples of dinuclear ruthenium complexes bearing this type of bridging have not been reported. The eight-membered heteroatom ring is clearly nonplanar with both azide groups lying parallel and the two ruthenium atoms tilted at an angle of 70.4º with respect to one another. The bridging azide groups are nearly symmetric. Thus N(1)-N(2) and N(1A)-N(2A) bond distances are each 1.19 Å while the N(2)-N(3) and N(2A)-N(3A) bond distances are slightly shorter at 1.16 Å each. The distance between the ruthenium atoms in the chelate ring is 5.30 Å. Each ruthenium atom bears a terminal azide ligand, and they are in an *anti* relationship relative to one another. The terminal azide ligands are less symmetric then their bridging counterparts exhibiting distances of 1.13 Å between the metal-bound nitrogens and the center nitrogens and 1.20 Å between the middle nitrogens and the terminal nitrogens. The Ru-N_3 bond angle is 124.9º, which is within the expected range. The ^{1}H NMR in $CDCl_3$ spectrum of **3-III** clearly showed two distinct resonances representing two non-equivalent sets of PMe_3 ligands which are related by a C_2-axis of symmetry. A multiplet at 1.50 ppm corresponds to the methyl protons of the four equivalent PMe_3 ligands, P(2), P(3), P(2A), and P(3A) (Figure 3.2a). The other set of two equivalent PMe_3 ligands, P(1) and P(1A) (Figure 3.2a) give rise to the triplet at 1.39 ppm. The peaks at 1.50 and 1.39 ppm are in a 2:1 ratio as expected for this structure. In contrast, the ^{31}P {^{1}H} NMR spectrum in $CDCl_3$ is complex and suggests that a mixture of

isomers is present in solution. Determining the degree of coordination of the azide ligand, either monocoordinate or bridging, is often difficult to determine solely from IR data.[9] However, the presence of both bridging and terminal azides in a single binuclear complex can be confirmed by the observation of two asymmetric stretching frequencies.[9] Thus, the IR spectrum of **3-III** exhibits bands at 2042 and 2030 cm^{-1} corresponding to the terminal and bridging azides.

***trans*-$(Me_3P)_4Ru[C{\equiv}C(SiMe_3)]_2$ (3-IV).** The boiling point of trimethylsilyacetylene is 53 ºC and it is possible that it is too readily displaced from refluxing toluene to react with **3-I**. This would explain the formation of **3-III**, above. Therefore the diazide **3-I** was also reacted with trimethylsilylacetylene at lower temperature in dichlormethane. This resulted in the formation of the *trans* dialkyne-substituted ruthenium complex **3-IV** (Scheme 3.3). It has been shown that **3-IV** can be synthesized from the analogous ruthenium dihydrides.[10] However, no reports of dialkynyl-substituted ruthenium complexes prepared from the corresponding azides exist to our knowledge. Light brown crystals of **3-IV** were isolated upon cooling the concentrated reaction filtrate for 24 h. This compound has been reported by Rappert and Yamamoto, however, the structure in the solid state does not appear to have been described.[10] The structure of **3-IV** was determined through X-ray diffraction (Fig. 3.2b), and shows the ruthenium center in a distorted octahedral environment. Compound **3-IV** crystallizes in the triclinic P1 space group with four independent molecules per unit cell Crystallographic details are given in Table 3.1 and selected bond lengths and angles for **3-IV** in Table 3.4. The trimethylsilylacetylide units reside *trans* to one another at an

angle of 177.8º. One set of two PMe_3 ligands bends out of the octahedral plane toward one acetylide group while the other set bends out of the plane in the opposite direction toward the other acetylide group. This gives rise to two sets of P-Ru-acetylide bond angels averaging 81.3º and 98.7º. The C≡C bond lengths of 1.19 Å in the trimethylsilylacetylide groups were in the expected range. The structure of complex **3-IV** was further supported by inspection of its ^{1}H and ^{31}P NMR and IR spectra which were in agreement with reported values from the literature.[10]

3.2.3. Reactions with Internal Alkynes

$(Me_3P)_3Ru[N_3C_2\text{-}(CO_2Et)_2]_2$ (3-V). In order to circumvent the acid-base reaction that leads to products of ligand substitution, internal alkynes, which lack a labile acetylenic proton, were reacted with **3-I**. Treatment of **3-I** with diethylacetylene dicarboxylate in tetrahydrofuran at 25º for 12 h affords the bis-triazolato ruthenium complex **3-V** in 41% isolated yield (Scheme 3.4). Yellow crystals of complex **3-V** were

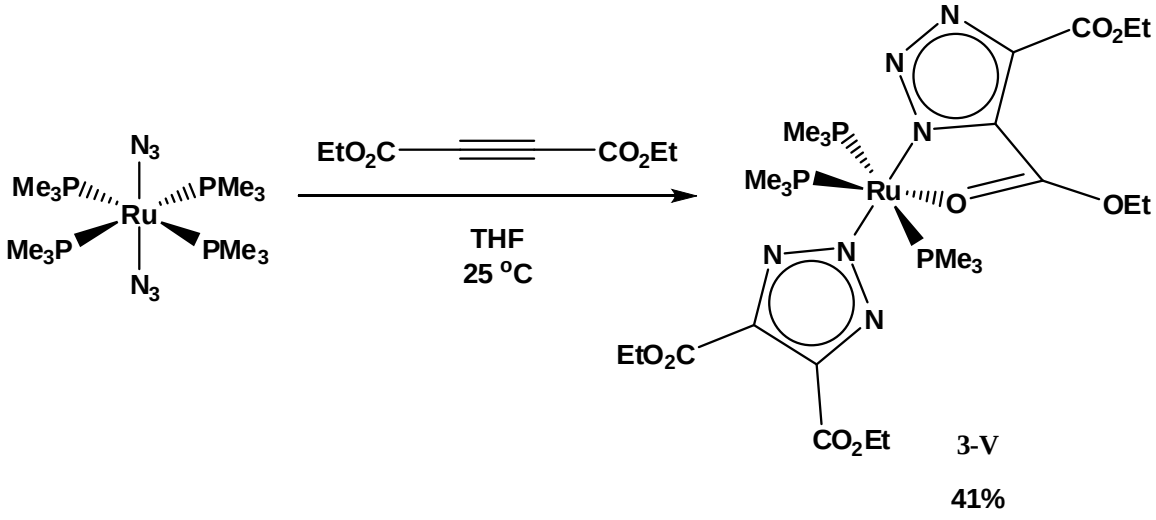

Scheme 3.4. Preparation of N1,N2-bis-triazolato ruthenium complex, **3-V**.

obtained upon cooling the concentrated reaction filtrate, and were characterized by a single-crystal X-ray diffraction analysis. Compound **3-V** crystallizes in the monoclinic P2(1)/n space group with four independent molecules per unit cell (Fig. 3.3). Crystallographic details are given in Table 3.1 and

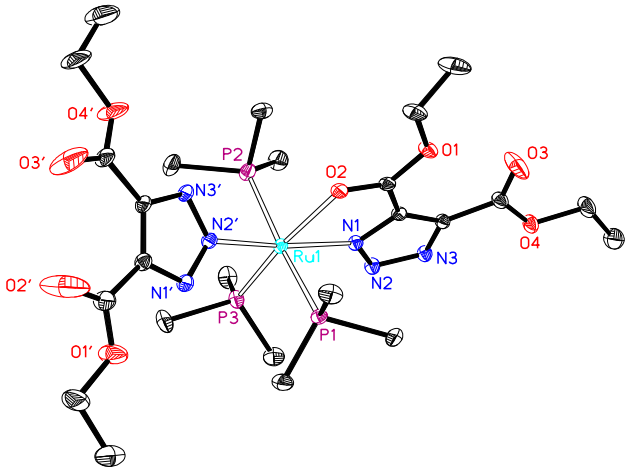

Figure 3.3 ORTEP view of **3-V** with atom numberin scheme. Ellipsoids are drawn at the 25% probabilit level. Hydrogen atoms are omitted f or clarity.

selected bond lengths and angles for **3-IV** in Table 3.5. The resulting structure shows the presence of both N1- and N2-bound triazolato ligands coordinated to the single ruthenium atom. Previous reports involving triazolato and tetrazolato complexes of Co and Ni indicate that either of the two isomers N1- and N2- are formed simultaneously, giving rise to a mixture of products, or only the N2 isomer is produced exclusively.[5c] Though the N1 isomer can be considered to be the kinetic product of these cycloadditions, the thermodynamically stable N2 isomer is more commonly isolated.[4a] Isomerization to the N2-bound product has been attributed to steric concerns, although electronic properties of the ligand environment and of the alkyne dipolarophile have also been proposed.[11] To our knowledge there are no reports of a complex bearing *both* N1- and N2-triazolato ligands coordinated to the same metal center.

The structure obtained from X-ray diffraction, shown in Figure 3.3, depicts a

ruthenium center residing in a distorted octrahedral environment. The triazolate groups are *trans* to one another at an angle of 168.4º. The five atoms of each triazolato ring are planar. Ru-triazolate bond distances are 2.06 Å and 2.08 Å for the N1- and N2-coordinated triazolato rings, respectively, and agree with reported values for ruthenium triazolato complexes.[5c] An interesting feature of **3-V** is the coordination of one of the N1-triazolato ester carbonyl oxygens to ruthenium. This coordination gives rise to a planar, five-membered metallocycle adjacent to the N1-triazolato ring, and effectively traps the triazolate group in its observed configuration. This arrangement, thus, gives **3-V** an electron count of 18.

The structure of **3-V** was further supported by its ^{1}H and ^{31}P NMR spectra taken in $CDCl_3$. Perhaps most diagnostic in the ^{1}H NMR spectrum are the resonances corresponding to the methylene ($-CH_2-$) groups of the triazolate ethyl ester moieties. Three quartets in a 1:1:2 ratio were observed at 4.52, 4.37 and 4.31 ppm, respectively. Peaks at 4.52 and 4.37 ppm are related to the two nonequivalent ethyl ester substituents of the N1-triazolato ring. The more intense quartet at 4.31 ppm can be attributed to the two equivalent ethyl ester groups of the N2-triazolato ring, which are related by rotation of the ring around the Ru(1)-N(2') bond from Figure 3. The ^{31}P NMR spectrum showed two diagnostic resonances at 30.45 and -0.08 ppm in a 1:2 ratio. The triplet at 30.45 ppm corresponds to the PMe_3 ligand *trans* to the chelating carbonyl oxygen. The doublet at -0.08 ppm can be attributed to the two equivalent PMe_3 ligands that are related by a mirror plane containing O(2)-N(1)-P(3)-N(2') from Figure 3. The bis-triazolato complex gave a characteristic IR spectrum that clearly shows the absence of the azide asymmetric

stretching frequency and the presence of C=O and C–O bands at 1777, 1730 and 1299 cm^{-1}. Triazolato ring frequencies are also observed at 1426, 862, 799 and 736 cm^{-1}.

3.2.4. Reactions with Bis-alkynyl Dipolarophiles

$(Me_3P)_4Ru(N_3)(C{\equiv}CC_6H_4C{\equiv}CH)$ (3-VI). Having identified conditions which lead to the cycloaddition product, the use of bis-alkynyl dipolarophiles was explored. Though terminal alkynes had shown to give products from ligand substitution rather than cycloaddition, 1,4-diethynylbenzene was screened first. As previously observed for reactions with terminal alkynes, the reaction of **3-I** with 1,4-diethynylbenzene in tetrahydrofuran at 25 ºC for 12 h gave the product from ligand substitution, **3-VI,** in 72%

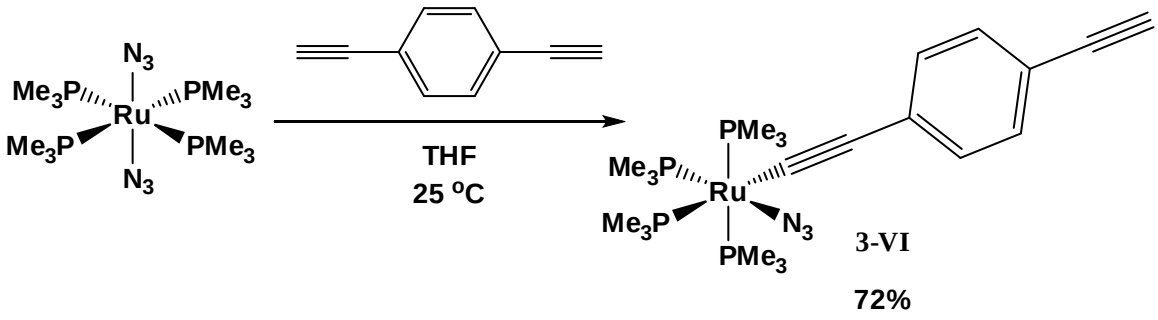

Scheme 3.5. Preparation of azide-alkynyl ruthenium complex, **3-VI**.

yield (Scheme 3.5). Azide-alkynyl ruthenium complex **3-VI** crystallized as orange needles after cooling the reaction filtrate for 5 d. X-ray diffraction studies of these needles gave the structure of **3-VI** and clearly shows the ruthenium center residing in a distorted octahedral environment with the azide and (4-ethynyl)phenyl-acetylide ligands in a *cis* relationship (Fig. 3.4). Compound **3-VI** crystallizes in the rhombohedral R3 space group with eighteen independent molecules per unit cell. Crystallographic details

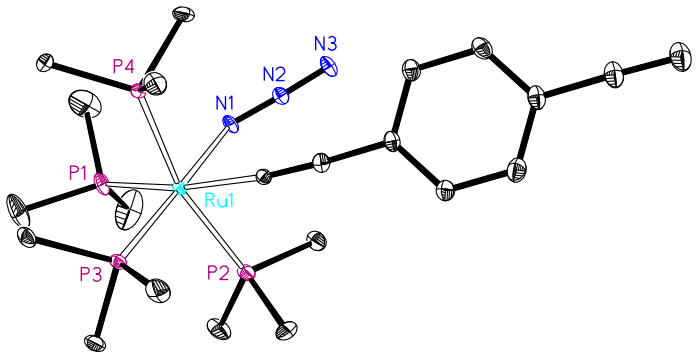

Figure 3.4. ORTEP views of **3-VI** with atom numbering scheme. Ellipsoids are drawn at 25% probability level. Hydrogen atoms are omitted for clarity.

are given in Table 3.1 and selected bond lengths and angles for **3-IV** in Table 3.6. The Ru-azide bond angle is 126.9º and falls within the expected range.[9] The azide group is nearly symmetric with N-N bond distances of 1.20 and 1.17 Å. The Ru-acetylide bond angle is 167.8º reflecting a deviation from linear geometry at the metal-coordinated sp^3 hybridized carbon. The C≡C bond lengths of 1.22 and 1.20 Å are within the expected range, with the coordinated alkynyl moiety being slightly longer that the terminal unit. The ^{1}H NMR spectrum of **3-VI** taken in d^6-acetone showed aryl signals at 7.23 ppm, and a singlet at 2.84 ppm corresponding to the terminal acetylenic proton. Peaks were also observed at 1.56, 1.48 and 1.39 ppm in 2:1:1 ratio resulting from a set of two equivalent PMe_3 ligands and two non-equivalent PMe_3 ligands on ruthenium. This supports the observed *cis* relationship of the azide and (4-ethynyl)phenylacetylide ligands. ^{31}P {^{1}H} NMR in d^6-acetone gave a spectrum for **3-VI** exhibiting three distinct resonances at 11.03 (dt), -2.21 (dd) and -10.72 (dt) ppm in a 1:2:1 ratio which are consistent with the *cis*

structure observed in the solid state. The IR spectrum displays bands at 2108, 2080, 2041 and 1365 cm^{-1} corresponding to two alkyne units (coordinating and terminal) and azide stretching frequencies.

3.3. Future Studies

Further studies should be carried out to explore the viability of bis-alkynyl reacting partners. Such dipolarophiles, when reacted with diazide **3-I**, may give rise to interesting metal-containing oligomeric or polymeric materials upon cycloaddition (Scheme 3.6). Reek and coworkers have shown that 1,4-Diethynylbenzene participates in

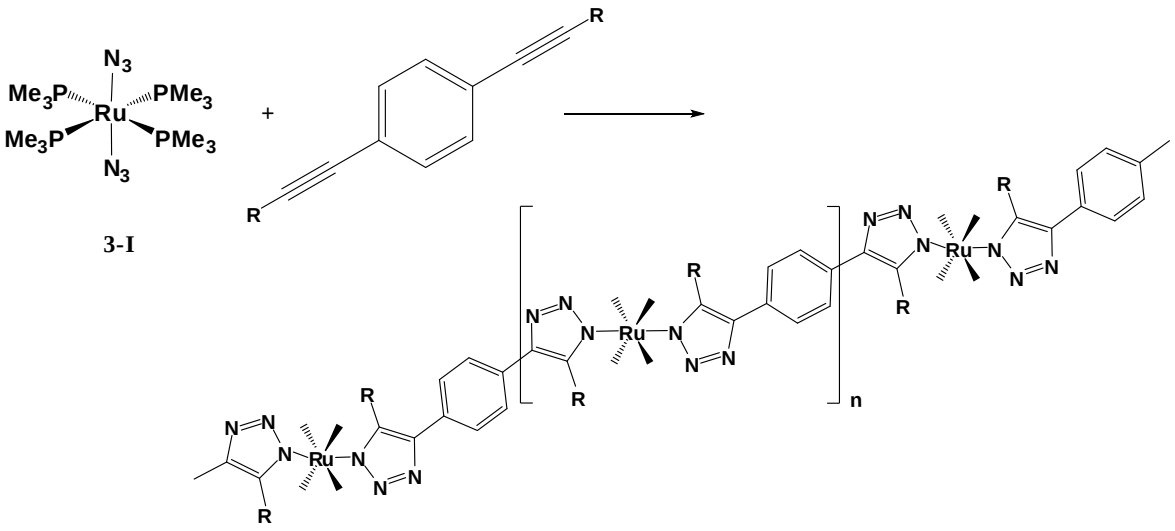

Scheme 3.6. Envisioned Ru-triazolato conjugated system from the cycloaddition of diazide **3-I** and 1,4-diethynylbenzene derivatives. PMe_3 groups in the product have been omitted for clarity.

Cu catalyzed 1,3-dipolar cycloadditions with organic bis-azides to give triazolate-containing conjugated polymers.[12] Similar products should be obtained by employing bis-azido metal complexes. Whereas terminal alkyne dipolarophiles give rise to products of ligand substitution when reacted with azido metal complexes such as **3-I**, internal alkynes

have been shown to provide triazolato ruthenium complexes through cycloaddition. One possibility, since 1,4-diethynylbenzene reacts to provide alkynyl-substituted products, would be to use 1,4-bis(bromoethynyl)benzene, **3-VII** (Scheme 3.7). Bis-bromoalkyne

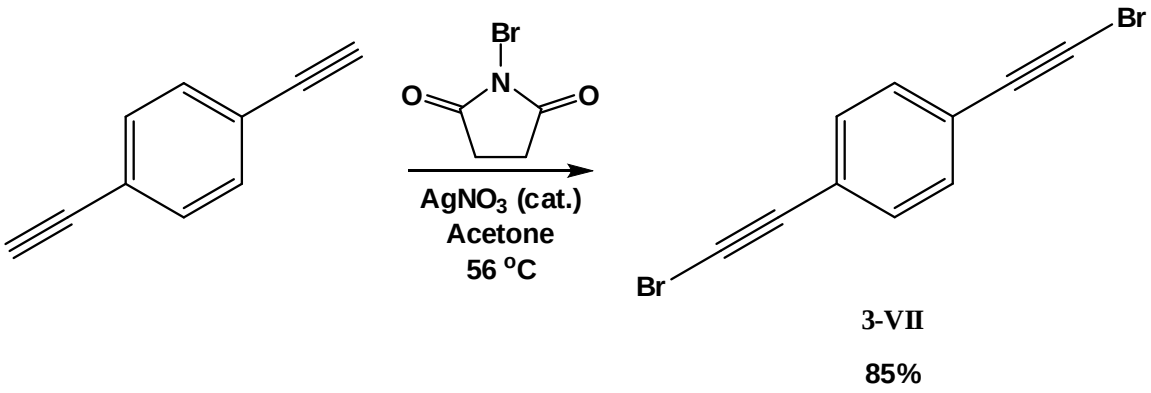

3-VII

85%

Scheme 3.7 Preparation of 1,4-bis(bromoethynyl)benzene, **3-VII**.

3-VII has been reported previously[13], although a detailed experimental procedure and complete characterization was not included. A synthetic procedure for this compound is therefore included in the experimental section. Incorporation of the terminal bromine substituents would exclude the possibility of acid-base chemistry taking place at the acetylenic proton. Additionally, **3-VII** may be converted to terminal aryl and/or alkenyl containing bis-alkynyl dipolarophiles through synthetic means. This is of great utility since it is recognized that haloalkynes such as **3-VII** can participate in alternate chemical processes such as oxidative addition across the carbon-halogen bond giving rise to undesired byproducts.

In addition to alkynes, a number of other dipolarophiles are available for

cycloadditions.[11] Electron-deficient nitriles and isonitriles may be employed to give metal-nitrogen- and metal-carbon-bonded tetrazolates, respectively. Reactions with heterocumulene dipolarophiles such as carbon disulfide and phenyl isothiocyanates afford 1,2,3,4-thiatriazole-5-thiolate and 1-phenyltetrazolate-5-thione complexes, respectively. All of the proposed dipolarophiles provide a means to access extended metal-containing conjugated structures upon cycloaddition.

Finally, optimization of the azido ruthenium participant may facilitate the cycloaddition pathway leading to desired products. Subtle modifications to the phophine ligand system may alter the reactivity of the metal center and, consequently, the complex as a whole. Exchanging the PMe_3 ligands for bidentate bis-phosphine groups such as 1,2-bis(diethylphosphino)ethane (depe) can impart greater reactivity to the azido-ruthenium complex. The analogous depe containing bis[1,2-bis(diethylphosphino)ethane]-bis(azido)ruthenium(II) has been reported.[14] The increased steric requirement of the depe ligand compared with PMe_3 may make depe a more labile ligand which facilitates the cycloaddition reaction.

3.4. Conclusion

In summary, it was shown that diazidotetrakis(trimethylphosphine)ruthenium(II), **3-I**, undergoes reactions with electron deficient terminal and internal alkynes to provide alkynyl-azido, bis-alkynyl, bridged azido and triazolato ruthenium species. A unique complex exhibiting both N1- and N2-triazolato ligands coordinated to a single ruthenium center has been shown, demonstrating a kinetic trapping of the N1-bound triazolate ring.

The alkynyl-azido complexes obtained may be tested to see if they can undergo homo cycloadditions to give ruthenium-triazolato systems. Also, the bis-alkynyl product obtained may be reacted with **3-I** to give products from hetero cycloaddition reactions. Further investigations regarding alternative dipolarophiles and modifications to the metal complex reacting partner should be performed as well as the pursuit of suitable conditions to promote the cycloaddition of **3-I** with bis-alkynyl containing dipolarophiles.

3.5. Experimental

General. Unless otherwise noted, all reactions and manipulations were carried out under a dry, oxygen-free nitrogen atmosphere using standard Schlenk techniques or in an inert atmosphere glove-box. All solvents were dried prior to use by distillation from CaH_2 (toluene, dichloromethane, tetrahydrofuran) or magnesium (methanol). The following chemicals were used as received: phenylacetylene (Aldrich), trimethylsilylacetylene (Aldrich), diethyl acetylenedicarboxylate (Aldrich), 1,4-diethynylbenzene (TCI America). *Trans*-diazidotetrakis(trimethylphosphine)ruthenium (II) was prepared as described in the literature.[6]

Instrumental Details. NMR spectra were recorded on a Mercury 400 MHz spectrometer and/or Varian 300 Unity Plus 300 MHz spectrometer at 25 °C. ^{1}H NMR signals are reported relative to residual proton resonances in deuterated solvents. ^{31}P NMR signals are reported relative to an external phosphoric acid standard. Electrospray ionization (ESI) and fast atom bombardment (FAB) mass spectra were recorded on a Finnigan MAT TSQ 700. High-resolution mass spectra (HRMS) were obtained on a VG Analytical

ZAB-VE sector instrument and are reported as *m/z* (relative intensity). Low-resolution chemical ionization (CI) mass spectra were collected on a Micromass Autospec Ultima mass spectrometer. Infrared spectra were recorded using a Nicolet IR 200 FTIR spectrometer. Melting points were obtained in sealed glass capillaries under dinitrogen and are uncorrected.

X-Ray Crystallography. The crystallographic data and structure refinement for complexes **3-II** – **3-VI** are listed in Table 3.1. Selected bond lengths (Å) and angles (°) for **3-II, 3-III, 3-IV, 3-V** and **3-VI** are given in Tables 3.2, 3.3, 3.4, 3.5 and 3.6, respectively. Data were collected on a Nonius Kappa CCD diffractometer with graphite monochromated Mo-Kα radiation (λ = 0.71073 Å) at 153 K. Absorption corrections were applied using GAUSSIAN. The structures were solved by direct methods and refined anisotropically using full-matrix least-squares methods with the SHELX 97 program package.15 The coordinates of the non-hydrogen atoms were refined anisotropically, while hydrogen atoms were included in the calculation isotropically but not refined. Neutral atom scattering factors were taken from Cromer and Waber.16

$(Me_3P)_4Ru(N_3)(C{\equiv}CC_6H_5)$ (3-II). To a solution of $(Me_3P)_4Ru(N_3)_2$ (0.100 g, 0.2 mmol) in toluene (2 mL) was added phenylacetylene (0.052 g, 0.51 mmol). The mixture was heated to reflux and stirred for 3 h. Upon cooling to room temperature brown crystals of **3-II** precipitated from the reaction mixture. They were collected and dried under vacuum. Isolated: **3-II**, 0.056g, 51 %; m.p. 176-180 °C. ^{1}H NMR (400 MHz, $CDCl_3$): δ 7.29 (br m, Ar *H*, 2H), 7.10 (t, Ar *H*, 2H, *J* = 7.8 Hz), 6.95 (t, Ar *H*, 1H, *J* = 8 Hz), 1.52 (t, P*Me*$_3$,

18H, *J* = 2.8 Hz), 1.37 (d, P*Me*$_3$, 9H, *J* = 7.6 Hz), 1.31 (d, P*Me*$_3$, 9H, *J* = 6.4 Hz); ^{31}P {^{1}H}NMR (121 MHz, $CDCl_3$): δ 10.96, -2.40, -10.91; FTIR (Nujol, cm^{-1}): 3150 (w), 2252 (s), 2116 (m), 2080 (m), 2041 (m), 1716 (s), 1424 (m), 1365 (m), 1246 (s), 690 (m); MS (chemical ionization, $CHCl_3$) *m/z* 550 [M^+], 508 [M^+- N_3].

[(Me$_3$P)$_3$(N$_3$)Ru]$_2$($\mu_{1,3}$-N$_3$)$_2$ (3-III). To a solution of $(Me_3P)_4Ru(N_3)_2$ (0.100 g, 0.2 mmol) in toluene (2 mL) was added trimethylsilylacetylene (0.050 g, 0.51 mmol). The mixture was heated to reflux and stirred for 3 h. After cooling to room temperature, the reaction mixture was filtered. The filtrate was concentrated under vacuum to ~1 mL. Cooling (-30 °C) gave **3-III** as yellow crystals after 5 days. Crystals suitable for XRD were also obtained by evaporation from a solution of **3-III** in $CDCl_3$. Isolated: **3-III**, 0.050g, 30 %; m.p. 220-222 °C; ^{1}H NMR (300 MHz, $CDCl_3$): δ 1.50 (t, P*Me*$_3$, 36H, *J* = 3.1 Hz), 1.39 (t, P*Me*$_3$, 18H, *J* = 4.0 Hz); FTIR (Nujol, cm^{-1}): 3407 (s), 2966 (m), 2043 (m), 2030 (m), 1642 (s), 1413 (m), 1306 (w), 1262 (m), 1098 (s), 1017 (s), 947 (m), 800 (s); MS (chemical ionization, $CHCl_3$) *m/z* 826 [M^+].

***trans*-(Me$_3$P)$_4$Ru[C≡C(SiMe$_3$)]$_2$ (3-IV).** To a solution of $(Me_3P)_4Ru(N_3)_2$ (0.100 g, 0.2 mmol) in dichloromethane (2 mL) was added trimethylsilylacetylene (0.050 g, 0.51 mmol). The mixture was heated to reflux and stirred for 3 h. After cooling to room temperature, the reaction mixture was filtered. The filtrate was concentrated under vacuum to ~1 mL. Cooling (-30 °C) gave **3-IV** as light brown crystals after 24 h. They were collected and dried under vacuum. Isolated: **3-IV**, 0.044 g, 37%; ^{1}H NMR (400

MHz, $CDCl_3$): δ 1.52 (m, P*Me*$_3$, 36H), 0.12 (s, Si*Me*$_3$, 18H); ^{31}P {^{1}H}NMR (121 MHz, $CDCl_3$): δ -7.83; FTIR (Nujol, cm^{-1}): 2963 (s), 1985 (m), 1431 (m), 1368 (m).

$(Me_3P)_3Ru[N_3C_2$-$(CO_2Et)_2]_2$ (3-V). To a solution of $(Me_3P)_4Ru(N_3)_2$ (0.100 g, 0.2 mmol) in tetrahydrofuran (10 mL) was added diethyl acetylenedicarboxylate (0.102 g, 0.6 mmol). The mixture was stirred for 12 h at 25 °C, and then filtered. The filtrate was concentrated under vacuum to ~ 3 mL. Cooling (-30 °C) gave **3-V** as yellow crystals which were suitable for x-ray diffraction. Isolated: **3-V**, 0.062g, 41%; mp 156-160 °C; ^{1}H NMR (400 MHz, $CDCl_3$): δ 4.52 (q, *CH*$_2$CH$_3$, 2H, *J* = 7.2 Hz), 4.37 (q, *CH*$_2$CH$_3$, 2H, *J* = 7.2 Hz), 4.31 (q, *CH*$_2$CH$_3$, 4H, *J* = 7.2 Hz), 1.52-1.43 (m, -*CH*$_3$, 30H), 1.40 (t, CH$_2$*CH*$_3$, 3H, *J* = 7.2 Hz), 1.32 (t, CH$_2$*CH*$_3$, 6H, *J* = 7.2 Hz), 1.46 (s, -*CH*$_3$, 6H), 1.43 (s, -*CH*$_3$, 4H), 1.40 (t, -*CH*$_3$, 8H, *J* = 7.2 Hz), 1.32 (t, -*CH*$_3$, 6H, *J* = 7.2 Hz), 1.10 (t, -*CH*$_3$, 15H, *J* = 3.2 Hz); ^{31}P {^{1}H}NMR (121 MHz, $CDCl_3$): 30.45, -0.08; FTIR (Nujol, cm^{-1}): 2968 (s), 2914 (m), 1777 (m), 1730 (s), 1426 (s), 1299 (m), 1261 (s), 862 (s), 799 (m), 736 (m); HRMS (chemical ionization, CH_2Cl_2): *m/z* calcd for $C_{25}H_{48}N_6O_8P_3{}^{96}Ru$ 749.1822 (M^+), found 749.1829.

$(Me_3P)_4Ru(N_3)(C{\equiv}CC_6H_4C{\equiv}CH)$ (3-VI). To a solution of $(Me_3P)_4Ru(N_3)_2$ (0.100 g, 0.2 mmol) in tetrahydrofuran (10 mL) was added 1,4-diethynylbenzene (0.028 g, 0.22 mmol). The mixture was stirred for 12 h at 25 ºC. The mixture was filtered, and the filtrate placed in the freezer. Cooling (-30 ºC) gave **3-VI** as orange needles after 5 days. They were collected and dried under vacuum. Isolated: **3-VI**, 0.041g, 72 %; m.p. 162-166

°C, (dec 180-184 °C); ^{1}H NMR (300 MHz, $(CD_3)_2CO$): δ 7.23 (d, Ar *H*, 4H, *J* = 2.7 Hz), 2.84 (s, ≡C*H*, 1H), 1.56(t, P*Me*$_3$, 18H, *J* = 3.3 Hz), 1.48 (d, P*Me*$_3$, 9H, *J* = 8.2 Hz), 1.39 (d, P*Me*$_3$, 9H, *J* = 6.9 Hz); ^{31}P {^{1}H}NMR (121 MHz, $CDCl_3$): δ 11.03, -2.21, -10.72; FTIR (Nujol, cm^{-1}): 3395 (s), 3150 (w), 2255 (s), 2116 (m), 2079 (m), 2042 (m), 1715 (s), 1426 (m), 1364 (m), 1246 (s), 960 (s), 890 (s), 690 (m); MS (chemical ionization, $CHCl_3$) *m/z* 573 [M^+], 543 [M^+- N_2].

1,4-Bis(bromoethynyl)benzene (3-VII). A mixture of 1,4-diethynylbenzene (0.500 g, 4 mmol), N-bromosuccinimide (1.55 g, 8.7 mmol), and silver nitrate (0.068 g, 0.4 mmol) in acetone was stirred at reflux for 16 h. Upon cooling to room temperature the reaction mixture was filtered. The filtrate was concentrated under vaccum to give an orange solid. Recrystallization from acetone gave **3-VII** as yellowish orange crystals. Isolated: **3-VII**, 0.966 g, 85%; mp 148-150 ºC; ^{1}H NMR (300 MHz, $CDCl_3$): δ 7.36 (s, Ar *H*, 4H); ^{13}C NMR (100 MHz, $CDCl_3$): δ 131.8, 122.9, 79.5, 52.2; FTIR (Nujol, cm^{-1}): 2986 (s), 2083 (m), 853 (m), 792 (m), 637 (s), 612 (s); HRMS (chemical ionization, CH_2Cl_2): *m/z* calcd for $C_{10}H_4Br_2$ 282.8758 (M^+), found 282.8758.

Table 3.1. Crystal data and structure refinement for complexes **3-II, 3-III, 3-IV, 3-V** and **3-VI**.

	3-II	**3-III**	**3-IV**	**3-V**	**3-VI**
Formula	$C_{20}H_{41}N_3P_4Ru$	$C_{22}H_{58}Cl_{12}N_{12}P_6Ru_2$	$C_{22}H_{54}P_4Si_2Ru$	$C_{25}H_{47}N_6O_8P_3Ru$	$C_{22}H_{40}N_3P_4Ru$
Fw	548.51	1304.16	599.78	753.67	571.52
Cryst syst.	triclinic	orthorhombic	triclinic	monoclinic	rhombohedral
Space group	P-1	Pcab	P1	P2(1)/n	R-3
a, Å	9.1742(18)	12.6525(2)	10.605(2)	8.8536(2)	40.991(6)
b, Å	9.7212(19)	16.9803(2)	16.140(3)	11.9100(2)	40.991(6)
c, Å	15.539(3)	24.2552(3)	20.919 (4)	34.322(2)	10.097(2)
α, deg	73.16(3)	90	111.57(3)	90	90
β, deg	87.18(3)	90	89.99(3)	95.814(2)	90
γ, deg	86.97(3)	90	90.01(3)	90	120
V, Å^3	1323.7(5)	5211.07(12)	3330.1(11)	3600.5(3)	14693(4)
Z	2	4	4	4	18
D_{calc}, g cm^{-3}	1.376	1.662	1.196	1.390	1.163
temp, K	153(1)	153(1)	153(1)	153(1)	153(1)
F(000)	572	2624	1272	1568	5346
μ, mm^{-1}	0.845	1.412	0.743	0.618	0.688
θ rang, deg	2.98-25.00	3.01-25.00	2.93-25.00	2.94-25.00	2.98-25.00
reflns meads	7220	8341	14090	10872	27661
reflns used	4600	4498	14090	6281	5746
params	253	245	1040	261	271
R^a ($I > 2\sigma(I)$)	R1 = 0.0224	R1 = 0.0866	R1 = 0.0897	R1 = 0.0497	R1 = 0.0438
	wR2 = 0.0814	wR2 = 0.2156	wR2 = 0.2305	wR2 = 0.1448	wR2 = 0.1270
R^a (all data)	R1 = 0.0236	R1 = 0.1235	R1 = 0.1494	R1 = 0.0580	R1 = 0.0599
	wR2 = 0.0822	wR2 = 0.2302	wR2 = 0.2905	wR2 = 0.1542	wR2 = 0.1385
S	1.283	1.127	1.011	1.146	1.117

[a] $R1 = \Sigma||F_o| - |F_c||\Sigma|F_o|$. $wR2 = [\Sigma w[(F_o^2 - F_c^2)^2]/\Sigma|[w(F_o^2)^2]]^{1/2}$. $w=1/[\sigma^2(F_o^2)+(0.075P)^2]$, where $P = [\max(F_o^2,0)+2F_c^2]/3$.

Table 3.2. Selected Bond Lengths (Å) and Angles (°) for **3-II**.

Ru(1)-C(1)	2.046(2)	P(1)-Ru(1)-P(4)	92.69(4)
Ru(1)-N(1)	2.182(2)	C(1)-Ru(1)-P(2)	167.69(7)
Ru(1)-P(1)	2.2724(10)	N(1)-Ru(1)-P(2)	81.84(6)
Ru(1)-P(4)	2.3548(9)	P(1)-Ru(1)-P(2)	96.55(3)
Ru(1)-P(2)	2.3685(9)	P(4)-Ru(1)-P(2)	95.01(4)
Ru(1)-P(3)	2.3708(10)	C(1)-Ru(1)-P(3)	82.69(7)
C(1)-Ru(1)-N(1)	86.55(8)	N(1)-Ru(1)-P(3)	86.12(6)
C(1)-Ru(1)-P(1)	95.15(7)	P(1)-Ru(1)-P(3)	92.98(4)
N(1)-Ru(1)-P(1)	177.97(5)	P(4)-Ru(1)-P(3)	162.76(2)
C(1)-Ru(1)-P(4)	80.59(7)	P(2)-Ru(1)-P(3)	100.49(3)
N(1)-Ru(1)-P(4)	88.68(6)		

Table 3.3. Selected Bond Lengths (Å) and Angles (°) for **3-III**.

Ru(1)-N(3)#1	2.203(10)	N(1)-Ru(1)-P(3)	171.8(3)
Ru(1)-N(4)	2.205(9)	N(3)#1-Ru(1)-P(1)	173.7(3)
Ru(1)-N(1)	2.215(10)	N(4)-Ru(1)-P(1)	90.4(3)
Ru(1)-P(3)	2.260(4)	N(1)-Ru(1)-P(1)	92.8(3)
Ru(1)-P(1)	2.271(3)	P(3)-Ru(1)-P(1)	94.84(12)
Ru(1)-P(2)	2.274(3)	N(3)#1-Ru(1)-P(2)	90.4(3)
N(3)#1-Ru(1)-N(4)	83.7(4)	N(4)-Ru(1)-P(2)	170.2(3)
N(3)#1-Ru(1)-N(1)	84.3(4)	N(1)-Ru(1)-P(2)	86.4(3)
N(4)-Ru(1)-N(1)	85.2(4)	P(3)-Ru(1)-P(2)	95.86(12)
N(3)#1-Ru(1)-P(3)	87.9(3)	P(1)-Ru(1)-P(2)	95.08(11)
N(4)-Ru(1)-P(3)	91.7(3)		

Table 3.4. Selected Bond Lengths (Å) and Angles (°) for **3-IV**.

Ru(1)-C(1)	2.05(3)	P(2)-Ru(1)-P(1)	92.0(3)
Ru(1)-C(6)	2.04(3)	C(1)-Ru(1)-P(3)	79.7(8)
Ru(1)-P(2)	2.319(11)	C(6)-Ru(1)-P(3)	98.7(9)
Ru(1)-P(1)	2.323(7)	P(2)-Ru(1)-P(3)	90.2(4)
Ru(1)-P(3)	2.331(9)	P(1)-Ru(1)-P(3)	162.6(3)
Ru(1)-P(4)	2.345(9)	C(1)-Ru(1)-P(4)	101.1(9)
C(1)-Ru(1)-C(6)	176.9(15)	C(6)-Ru(1)-P(4)	81.6(11)
C(1)-Ru(1)-P(2)	95.5(9)	P(2)-Ru(1)-P(4)	163.3(3)
C(6)-Ru(1)-P(2)	81.8(11)	P(1)-Ru(1)-P(4)	91.9(3)
C(1)-Ru(1)-P(1)	82.9(8)	P(3)-Ru(1)-P(4)	91.0(3)
C(6)-Ru(1)-P(1)	98.7(9)		

Table 3.5. Selected Bond Lengths (Å) and Angles (°) for **3-V**.

Ru(1)-N(1)	2.056(4)	O(2)-Ru(1)-P(3)	171.52(9)
Ru(1)-N(2')	2.079(4)	N(1)-Ru(1)-P(2)	91.09(13)
Ru(1)-O(2)	2.247(3)	N(2')-Ru(1)-P(2)	89.65(13)
Ru(1)-P(3)	2.2501(15)	O(2)-Ru(1)-P(2)	85.81(10)
Ru(1)-P(2)	2.3674(17)	P(3)-Ru(1)-P(2)	94.93(7)
Ru(1)-P(1)	2.3879(15)	N(1)-Ru(1)-P(1)	90.87(13)
N(1)-Ru(1)-N(2')	168.41(17)	N(2')-Ru(1)-P(1)	86.66(13)
N(1)-Ru(1)-O(2)	75.35(14)	O(2)-Ru(1)-P(1)	86.15(10)
N(2')-Ru(1)-O(2)	93.18(15)	P(3)-Ru(1)-P(1)	93.63(6)
N(1)-Ru(1)-P(3)	96.18(12)	P(2)-Ru(1)-P(1)	170.95(6)
N(2')-Ru(1)-P(3)	95.27(13)		

Table 3.6. Selected Bond Lengths (Å) and Angles (°) for **3-VI**.

Ru(1)-C(10)	1.996(4)	P(3)-Ru(1)-P(4)	92.60(5)
Ru(1)-N(1)	2.186(4)	C(10)-Ru(1)-P(2)	80.86(14)
Ru(1)-P(3)	2.2711(12)	N(1)-Ru(1)-P(2)	88.00(12)
Ru(1)-P(4)	2.3459(13)	P(3)-Ru(1)-P(2)	91.97(5)
Ru(1)-P(2)	2.3644(14)	P(4)-Ru(1)-P(2)	163.59(5)
Ru(1)-P(1)	2.3708(14)	C(10)-Ru(1)-P(1)	167.24(13)
C(10)-Ru(1)-N(1)	86.24(16)	N(1)-Ru(1)-P(1)	81.01(11)
C(10)-Ru(1)-P(3)	96.03(13)	P(3)-Ru(1)-P(1)	96.72(5)
N(1)-Ru(1)-P(3)	177.70(11)	P(4)-Ru(1)-P(1)	96.02(6)
C(10)-Ru(1)-P(4)	82.99(14)	P(2)-Ru(1)-P(1)	99.08(6)
N(1)-Ru(1)-P(4)	88.05(12)		

3.6. References

[1] (a) Huisgen, R.; Szeimies, G.; Mobius, L. *Chem. Ber.* **1967**, *100*, 2494; (b) Tome, A. C. From *Science of Synthesis*; Thieme: Stuttgart, **2004**, Vol. 13, 415; (c) Huisgen, R. From *1,3-Dipolar Cycloaddition Chemistry*; Padwa, A., Ed.; Wiley: New York, **1984**.

[2] (a) Rostpvtsev. V. V.; Green, L.G.; Fokin, V. V.; Sharpless, K. B. *Angew. Chem. Int. Ed.* **2002**, *41*, 2596; (b) Tornoe, C. W.; Christensen, C.; Meldal, M. *J. Org. Chem.* **2002**, *67*, 3057.

[3] (a) Zhang, L.; Chen, X.; Xue, P.; Sun, H. H. Y.; Williams, I. D.; Sharpless, K. B.; Fokin, V. V.; Jia, G. *J. Am. Chem. Soc.* **2005**, *127*, 15998. (b) Majireck, M. M.; Weinreb, S. M. *J. Org. Chem.* **2006**, *45*, 3143.

[4] (a) Kemmerich, T. ; Nelson, J. H.; Takach, N. E.; Boehme, H.; Jablonski, B.; Beck, W. *Inorg. Chem.* **1982**, *21*, 1226; (b) Hsieh, B. T.; Nelson, J. H.; Milosavljevic, E. B.; Beck, W.; Kemmerich, T. *Inorg. Chim. Acta* **1987**, *133*, 267; (c) Moore, D. S.; Robinson, S. D. From *Advances in Inorganic Chemistry*; Sykes, A. G., Ed.; Academic Press: San Diego, **1988**, Vol. 32, 171.

[5] (a) Herberhold, M.; Goller, A.; Milius, W. Z. *Anorg. Aalg. Chem.* **2003**, *629*, 1162; (b) Busetto, L.; Marchetti, F.; Zacchini, S.; Zanotti, V. *Inorg. Chim. Acta* **2005**, *358*, 1204; (c) Chang, C. W.; Lee, G. H. *Organometallics* **2003**, *22*, 3107; (d) Partyka, D. V.; Updegraff, J. B., III; Zeller, M.; Hunter, A. D.; Gray, T. G. *Organometallics* **2007,** *26*, 183; (e) Paul, P.; Nag, K. *Inorg. Chem.* **1987**, *26*, 2969.

[6] Siebald, H. G. L.; Fabre, P.-L.; Dartiguenave, M.; Dartiguenave, Y.; Simard, M.; Beauchamp, A. L. "Preparation and Crystal Structure of *Trans*-Diazidotetrakis(trimethylphosphine)ruthenium(II)", *Polyhedron*, **1996**, *15*, 4221.

[7] (a) Schmidbauer, H.; Blaschke, G. "An Ylide Complex of Ruthenium with Three- and Four-Membered Metallocycles" *Z. Naturforsh.* **1980**, *35b*, 584; (b) Kohlmann, W.; Werner, H. "Synthesis and Reactions of Octahedral Boranatoruthenium(II) Complexes' *Z. Naturforsch.* **1993**, *48b*, 1499.

[8] Selected examples: (a) Palenik, G. H. *Acta Crystallogr.* **1964**, *17*, 360; (b) Abu-Youssef, M. A. M.; Mautner, F. A.; Vicente, R. *Inorg. Chem*, **2007**, *46*, 4654; (c) Song, X.; Xu, Y.; Li, L.; Jiang, Z.; Liao, D. *Inorg. Chem. Comm.* **2006**, *9*, 1212; (d) Meyer, F.; Kircher, P.; Pritzkow, H. *Chem. Commun.* **2003**, 774.

[9] Dori, Z.; Ziolo, R. F. "The Chemistry of Coordinated Azides", *Chem. Rev.* **1973**, *73*, 247.

[10] Rappert, T.; Yamamoto, A. *Organometallics* **1994**,*13*, 4984.

[11] Frühauf, H.-W. *Chem. Rev.* **1997**, *97*, 523.

[12] van Steenis, D. J. V. C.; David, O. R. P.; van Strijdonck, G. P. F.; van Maarseveen, J. H.; Reek, J. N. H. *Chem. Comm.* **2005**, 4333.

[13] Collins, S. K.; Yap, G. P. A.; Fallis, A. G. *Org. Lett.* **2000**, *2*, 3189.

[14] Buys, I. E.; Field, L. D.; George, A. V.; Hambley, T. W.; Purches, G. R. *Aust. J. Chem.* **1995**, *48*, 27.

[15] Sheldrick, G. M. SHELX 97, *A software package for the solution and refinement of X-ray data*; University of Göttingen: Göttingen, Germany, **1997**.

[16] Cromer, D. T.; Waber, J. T. *International Tables for X-Ray Crystallography*, Kynoch Press, Birmingham, vol. 4, **1974**, Table 2.2A.

Vita

Kyriacos Agapiou was born in Englewood, New Jersey on April 27, 1978, the son of Agapios and Ana Agapiou and brother of Teresa Agapiou. Kyriacos was raised in Humble, TX on the Northeast side of the greater Houston area. After completing his work at Humble High School in 1996, he entered Trinity University in San Antonio. He received the degree of Bachelor of Science in Chemistry in May of 2000. In August 2000, Kyriacos entered the graduate school of the Department of Chemistry and Biochemistry at the University of Texas at Austin. After receiving the degree of Master of Arts from The University in May 2003, he began working in the laboratory of Prof. Richard A. Jones toward the completion of his Ph.D.

Permanent Address: 19911 Seventeenth Green Ct., Humble, TX 77346

This dissertation was typed by the author.